

Radiochromic film dosimetry system:
from calibration to *in vivo* measurements
and IMRT quality assurance
measurements

Patrick Delage

Master of Science

Department of Medical Physics

McGill University

Montréal, Québec

January 26, 2011

A thesis submitted to McGill University in partial fulfilment of the requirements of
the degree of Masters in Medical Physics.

©Patrick Delage 2010

ACKNOWLEDGEMENTS

For her constant support throughout the writing of this document, I would like to thank my girlfriend who was kind enough to encourage and motivate me when needed. I would also like to thank Dr. Slobodan Devic who was of great help throughout all the work associated with the completion of this document. I would also like to thank my colleagues from Centre Hospitalier Universitaire de Sherbrooke: Nicolas M. Tremblay, Vincent Hubert Tremblay, Charles Lavoie, Stéphane Mercure and Luc Ouellet. I would also like to warmly thank Dr. Ervin Podgorsak who gave me the chance to discover the wonderful world of medical physics.

ABSTRACT

A radiochromic film dosimetry system is presented for the radiochromic film model EBT-2 using a flatbed document scanner, the Epson Expression 10000XL model, as a densitometer. The author presents the protocol for radiochromic film dose measurements along with the characterization of the radiochromic film dosimetry system. Results from the measurements taken to characterize the system are presented as well as other typical clinical measurements such as quality assurance measurements and skin dose measurements. Finally intensity modulated radiation therapy (IMRT) quality assurance measurements are presented and compared with the MatriXX ionization chamber array system.

ABRÉGÉ

Un système de dosimétrie de films radiochromiques est présenté pour le modèle de film radiochromique EBT-2 et utilisant un numériseur de photographies, Epson Expression 10000XL, comme densitomètre. L'auteur présente le protocole pour les mesures de dose utilisant les films radiochromiques ainsi que la caractérisation du système de dosimétrie de films radiochromiques. Les résultats des mesures caractérisant le système sont présentés ainsi que d'autres mesures cliniques typiques telles que des mesures d'assurance qualité et des mesures de dose la peau. Enfin des mesures d'assurance qualité pour la radiothérapie par intensité modulée (IMRT) sont présentées et comparées aux mesures de la matrice de chambre à ionisation MatriXX.

TABLE OF CONTENTS

ACKNOWLEDGEMENTS		ii
ABSTRACT		iii
ABRÉGÉ		iv
LIST OF TABLES		viii
LIST OF FIGURES		x
1	Introduction	1
	1.1	2
	1.2	3
	1.2.1	5
	1.2.2	5
	1.2.3	6
	1.2.4	8
	1.2.5	9
2	Theory	11
	2.1	11
	2.1.1	12
	2.2	12
	2.3	16
	2.3.1	17
	2.3.2	19
	2.3.3	20
	2.3.4	22
	2.3.5	25
	2.4	27
	2.4.1	27
	2.4.2	27

	2.4.3	Absorbed dose	28
2.5		Ionizing radiation production in the (modern) medical world	28
2.6		Dose measurement and important concepts in radiation therapy	30
	2.6.1	Charged particle equilibrium	32
	2.6.2	Bragg-Gray and Spencer-Attix cavity theory	33
	2.6.3	Dosimeters	34
	2.6.4	Measurements performed by a medical physicist	39
3		Film dosimetry system	42
3.1		Film dosimetry system	42
	3.1.1	Film	43
	3.1.2	Film readout system	43
3.2		Radiochromic films: how do they work?	45
	3.2.1	Constitution	46
	3.2.2	Absorption spectrum	47
	3.2.3	Post-irradiation coloration of radiochromic films	49
	3.2.4	Linearity	49
	3.2.5	Energy dependance	51
	3.2.6	Dose-rate dependence	52
	3.2.7	Film non-uniformity	52
3.3		Uncertainties in radiochromic film dosimetry systems	54
3.4		Protocols	58
	3.4.1	Film preparation	59
	3.4.2	Control film piece	59
	3.4.3	Film scanning	60
	3.4.4	Calibration curve of the radiochromic film dosimetry system	61
	3.4.5	Handling precautions and other corrections	67
	3.4.6	Summary of radiochromic film measurement protocol	67
3.5		Software for analysis of films	69
	3.5.1	Film co-registration	69
	3.5.2	Applied corrections	70
4		Results	71
4.1		Radiochromic film dosimetry system	71
	4.1.1	Calibration curve	71
	4.1.2	Uncertainty analysis	75
	4.1.3	Scanner corrections	77

4.2	Linear accelerator and other equipment QA	80
4.3	Percent depth dose of a 6 MV photon beam	85
4.4	<i>In vivo</i> measurements	87
	4.4.1 Seminoma of the testis	87
	4.4.2 Skin dose measurement	90
4.5	IMRT plan QA measurements	92
4.6	GammaKnife QA measurements	99
	4.6.1 Profile measurements	100
	4.6.2 Treatment plan validation and patient positioning system verification	101
5	Conclusion	105
	REFERENCES	108

LIST OF TABLES

<u>Table</u>	<u>page</u>	
1-1	Composition of radiochromic films. Note that the surface layer contains about 15 % moisture and gelatin which makes the composition vary from batch to batch because of their organic composition. The composition of the transparent and yellow polyester, the adhesive, and the opaque white polyester is derived from calculations.	7
1-2	Characteristics of the different radiochromic film models. Note that the active layer thickness is the total thickness from all the active layers if more than one layer is present in a particular film model. Note that the missing values were not provided by the manufacturer.	9
3-1	The chemical composition of the different layers of the radiochromic EBT-2 film model. Note that the active layer contains trace of nitrogen (N), potassium (K), bromine (B), and sulfur (S).	47
3-2	Sources of uncertainties for radiochromic film dosimetry systems	55
4-1	Measurements performed for the calibration curve.	72
4-2	Difference between the value obtained for a film piece irradiated to 200 cGy and scanned using the same time interval as with the different calibration curves and the value obtained for the film piece used to build the calibration curve.	73
4-3	Profile data for different cylinder sizes of the orthovoltage unit. The measured profile have an uncertainty of ± 0.2 mm. The delivered dose is 1.60 Gy.	84
4-4	Results of skin dose measurements for different bolus thicknesses and the electron beam.	91
4-5	Gamma function results for the different IMRT QA measurements performed with radiochromic films and compared with the MatriXX ionization chambers array.	98

4-6	Profile data from the 4 collimator sizes of the Gammaknife. The uncertainty on the profile measurement is ± 0.2 mm.	100
4-7	Patient positioning system verification.	103

LIST OF FIGURES

<u>Figure</u>	<u>page</u>
1-1 Absorption spectra for the different radiochromic film models for the specified dose. The curves for all the film models except EBT-2 represent net absorbance (film absorbance prior to irradiation subtracted from the measured absorbance post-irradiation) whereas the curve for EBT-2 represents the absorption spectrum of this film model.	4
2-1 Schematic of the different interactions between an electron with an absorbing atom. (a) Shows a hard collision i.e. when the impact parameter b is comparable to the atomic radius a , (b) shows a soft collision i.e. when the impact parameter b is (much) greater than the atomic radius a , and (c) shows a radiative collision i.e. when the impact parameter b is (much) smaller than the atomic radius a . Figure from [66] on page 142.	13
2-2 The regions where the different photon processes dominate as shown for photon energy $h\nu$ with respect to atomic number of an absorber Z . The solid lines represent the regions where the atomic cross sections for the different processes are equal to one another. Figure from [65] page 246.	17
2-3 Schematic diagram of a Compton scattering event.	18
2-4 A schematic diagram showing the photoelectric interaction.	20
2-5 A schematic diagram of (a) the pair production process (in the Coulomb field of an atom) and (b) the triplet production process (in the Coulomb field of an orbital electron). Both figures from [66] on page 228.	23
2-6 The mass attenuation coefficient with respect to photon energy for lead (figure from [42]).	25

2-7	A linear accelerator from the company Elekta [1]. On this picture one can see the treatment table, the accelerator gantry, the portal imaging flat-panel, and a cone-beam x-ray imaging device.	29
2-8	The GammaKnife at the CHUS.	31
2-9	A schematic diagram of a typical cylindrical ionization chamber (figure from [65]).	35
2-10	A typical central axis percent depth dose of a photon beam.	39
2-11	A typical transverse photon beam profile.	40
3-1	The EBT-2 gafchromic film model structure (figure from [69]).	46
3-2	This figure shows the absorption spectra of the EBT and EBT-2 film model. (a) Shows the absorbance spectra of both film models prior to irradiation (subscript <i>before</i>) and post irradiation (subscript <i>after</i>) of a 1 Gy dose. (b) Shows the resultant net absorbance change of the two film models (figures from [26]).	48
3-3	Comparison of the response for the EBT film model between a spectrophotometer and a laser scanner (figure from [80]).	50
3-4	Mass collision stopping-power ratios and ratios of mass-energy absorption coefficients for the sensitive materials in radiochromic films relative to water (figure from [80]).	51
3-5	The response of the radiochromic film model MD-55-2 for different doses at different dose-rate measured at a wavelength of 670 nm (figure from [58])	53
3-6	A typical calibration curve for the EBT film model (data from [31]).	62
3-7	The experimental setup for obtaining the calibration curve of the radiochromic film dosimetry system. (a) Shows the positioning of the film pieces under a reference beam with the monitor chamber below the film while (b) shows the regions of interest (ROI) on both an irradiated film piece and the control film piece (before and after irradiation, the top film pair being the irradiated film piece and the bottom film pair being the control film piece).	64

4-1	The calibration curves for GAFCHROMIC EBT-2 lot # A041510-01B. (a) Shows the most used and recommended calibration curve that is the one for a 24h waiting period between irradiation and digitization. (b) Shows the variation in the calibration curves for different waiting periods between irradiation and digitization. . . .	74
4-2	The electron beam profile used for the irradiation of the film pieces for the lateral correction measurements.	77
4-3	Profile of the film irradiated to a dose of 200 cGy and the resulting mathematical fit as ratio of the value for the middle of the scanner bed.	78
4-4	Profiles for all the films along the scanner bed with their respective mathematical fit.	79
4-5	Coincidence between the a $10 \times 10 \text{ cm}^2$ light field displayed by the linac versus its measured $10 \times 10 \text{ cm}^2$ radiation field.	81
4-6	Measurement of two virtual filter fields delivery (45 degrees and 60 degrees) using a Siemens Oncor Impression linear accelerator. . . .	82
4-7	Measurement of the profile for the cylinders of an orthovoltage unit. (a) Shows the film taken for the 5 cm cylinder at an energy of 150 kVp and (b) shows the dose profile of this cylinder.	84
4-8	Experimental setup for the percent depth dose film measurement. The film is setup parallel to the direction of the beam using a plexiglass film holder.	85
4-9	Percent depth dose of a 6 MV photon beam in water. Comparison between film measurement and ionization chamber measurement. The ionization chamber used is an Exradin A12 Farmer type and the Percent depth dose curve was shifted 18.3 mm according to the method explained in [3] (chamber shifting technique).	86
4-10	Gonodal shielding setup and results: (a) shows the placement of the films in the gonodal shield prior to each treatment fraction, (b) shows the unexposed films scanned before the first treatment fraction, and (c) shows the exposed films scanned after the last treatment fraction.	88

4–11 Dose measurement for the scrotal shielding as function of the fraction number for the anterior and posterior film.	89
4–12 Skin dose measurement films. (a) Shows the film for the treatment with 10 mm bolus and (b) shows the electron beam skin dose measurement (no bolus added).	91
4–13 IMRT QA film measurements. (a) Shows a film taken for a single incidence of an IMRT treatment plan. (b) Shows a sum plan, that is the sum of all incidences, of an IMRT QA measurement.	93
4–14 Typical IMRT QA results using radiochromic films. (a) Shows the dose map measured using the radiographic film and (b) shows the expected dose map as extracted from the treatment planning software (TPS). Note that the film is rotated compared to the TPS image and that the scaling is not the same.	95
4–15 Same IMRT QA measurement than as in figure 4–14 but performed using the MatriXX ionization chambers array. (a) Shows the dose map measured using the MatriXX system and (b) shows the gamma function results of the dose map measured with the MatriXX compared to the expected dose map from the treatment planning software.	96
4–16 Comparison of the gamma function results for the MatriXX ionization chambers array and the radiochromic film. (a) Shows the gamma function results for the MatriXX system and (b) shows the gamma function results for the film. Both dose maps are compared to the treatment planning software expected dose map and converted to the same dose grid.	97
4–17 Profile of the (a) 4 mm collimator and (b) 18 mm collimator both in the x direction for the Gammaknife 4C.	99
4–18 Treatment plan validation and patient positioning system validation. (a) Shows the treatment plan as planned with the software for the Gammaknife <i>GammaPlan version 8.3.1</i> , (b) shows the verification film converted to dose and (c) shows the dose profile through the middle of the two 4 mm irradiations (called shots).	102

CHAPTER 1

Introduction

The applications of physics to the medical world have grown to tremendous importance over the last few decades. The range of applications goes from imaging with applications such as diagnostic radiology, nuclear medicine, magnetic resonance imaging, to treatment of disease with applications such as radiation therapy, hyperthermia, and laser surgery. These are only a few examples from an ever growing range of applications that help diagnose and treat a wide range of diseases. Many of these applications were developed in the research world, that is outside of the everyday reality of hospitals and clinics. The medical physicist is the perfect candidate to assist in developing these technologies and bring them to functionality in the medical world. According to the Canadian Organization of Medical Physicists, “medical physicists are health care professionals with specialized training in the medical applications of physics”. [62] The work of the medical physicist typically involves clinical service, radiation safety, research and development, and/or teaching. Most medical physicists have complex clinical service duties which involve working in the area of radiation therapy and diagnostic imaging. An example of an indispensable task that is asked of medical physicists in the clinic is the accurate measurement of the radiation output from radiation sources employed in cancer therapy (radiation dosimetry). To accomplish this task,

the medical physicist employs a variety of tools and instruments such as ionization chambers or films.

1.1 Films for imaging and dosimetry purposes

Films used in imaging and dosimetry can be put in the general category of coloration detectors i.e. media that change color when irradiated. Many detectors fall into that category ranging as far back as conventional silver halide photographic media which aided Röntgen in the discovery of x-rays. An early unit of radiation exposure is also based on a coloration detector, the human skin. When exposed to radiation it will redden, a phenomenon known as erythema, giving rise to what is known as the erythema dose. Other materials which change color upon irradiation have been discovered over the years. However many of these were not optimized for use in imaging and dosimetry because of their relatively low sensitivity.

Radiographic film is an exception: having a very high sensitivity at low energy beam qualities makes it an ideal candidate for imaging applications. However this type of film requires development which makes it complicated to use, process requiring a darkroom and various chemicals. Furthermore the randomness associated with the development process makes this type of film only an average candidate for precise dosimetry purposes, but it has been successfully used for many years with good results. [63] In film dosimetry the measured quantity is light transmission: the more radiation delivered to the film the darker it becomes.

Recently, interest has grown tremendously over a different type of film, radiochromic film, which requires no post-irradiation development; radiochromic film.

It combines all the advantages of the radiographic films without many of their disadvantages. The fact that they require no development makes radiochromic films an ideal candidate for replacing radiographic films in cancer clinics as many centers are currently becoming filmless. Radiochromic film also becomes darker as it receives radiation but does not require chemical development procedures. The dye creation occurs through a polymerisation process during which energy is transferred from an energetic particle to the receptive part of the colorless photo monomer molecule. The coloration of the film due to radiation is therefore instantaneously visible to the naked eye above a certain dose threshold. Radiochromic films are the main topic of this thesis and a complete discussion of their characteristics is available in chapter 3. The core design of these films is an emulsion layer (active layer) where the dye formation takes place, sandwiched between adhesive and protective layers. The main manufacturer of radiochromic film, International Specialty Products (ISP) Wayne, NJ, manufactures radiochromic film models under the brand name GAFCHROMIC.

1.2 Evolution of radiochromic films

Radiochromic films have evolved greatly over the last few decades from the first models used mainly in industrial processes which were designed to detect doses from several grays up to hundreds of grays. The following sections describe the evolution of radiochromic films used for dosimetry purposes. Figure 1–1 shows the evolution of the absorption spectra of the different models of radiochromic

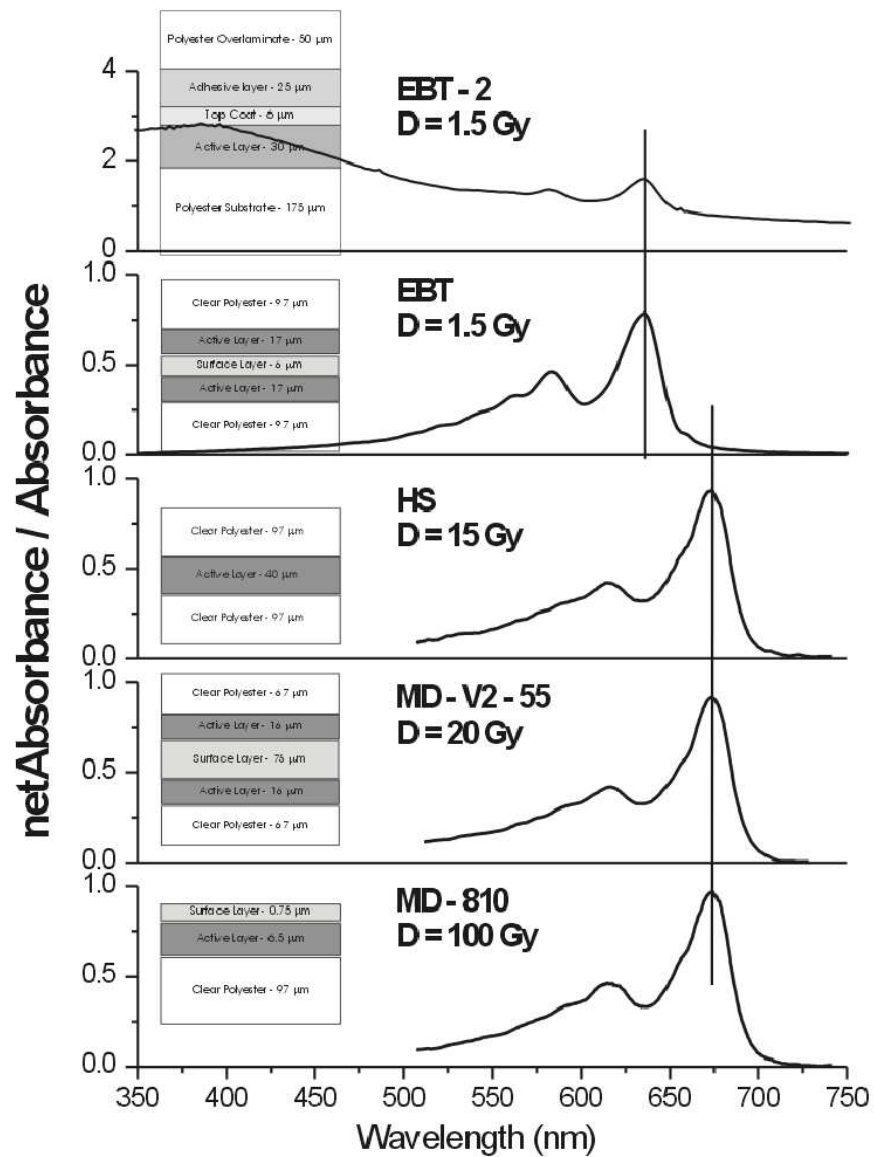


Figure 1-1: Absorption spectra for the different radiochromic film models for the specified dose. The curves for all the film models except EBT-2 represent net absorbance (film absorbance prior to irradiation subtracted from the measured absorbance post-irradiation) whereas the curve for EBT-2 represents the absorption spectrum of this film model.

films¹. The active layer chemical composition has been constant through the film models up to the most recent models (EBT and EBT-2). One can see this on figure 1–1, where the most sensitive wavelength was 673 nm for earlier film models and shifts to 635 nm for the most recent film models.

1.2.1 HD-810 model

Initially commercialised under the model name DM-1260, the film model HD-810 was the first model suitable for dosimetry purposes [59, 79] even though it was mainly designed for industrial purposes [60, 78]. This film has a thin emulsion layer of $6.5 \mu\text{m}$ which makes it relatively insensitive for most clinical applications but has the advantages of specifying the position of the dose measurement rather accurately. It is effectively the dosimeter with the shallowest effective point of measurement amongst all the available dosimeters today [27]. A dose of about 30 Gy is required to produce an optical density (OD) of 1 absorbance unit (AU) and it can measure up to 2500 Gy. It also has a very thin protective layer of $0.75 \mu\text{m}$ which makes it hard to manipulate without damaging the active layer. This model is still commercially available. [70]

1.2.2 MD-55 model

The MD-55 model was not only made with a significant increase in the thickness of the active layer (now $16 \mu\text{m}$ thick) but also introduced a transparent polyester on top of the active layer to protect it. The first model of this series is MD-55-1 and its design was an active layer sandwiched between two polyester

¹ Figure used with permission from Dr. Slobodan Devic, McGill University.

protective layers of $67\ \mu\text{m}$ each. This model is suitable for use in the dose range from 10 Gy to 100 Gy. It was however replaced with the MD-55-2 model which has two active layers with $16\ \mu\text{m}$ thickness each and also sandwiched between two polyester protective layers. The two active layers are separated by a transparent polyester layer ($25\ \mu\text{m}$ thick) and two adhesive layers (about $20\ \mu\text{m}$ thick each) for a total thickness of $231\ \mu\text{m}$. According to the manufacturer this film model can be used in the dose range of 1 Gy to 100 Gy. This film has two main advantages over the HD-810 model; increased sensitivity and the fact that it can be used in water due to the protective layers. It has also been replaced by an improved version called MD-V2-55, which has an increased protective layer thickness ($91\ \mu\text{m}$) and improved coating uniformity. This model is much more suitable for dosimetry applications than its predecessor. [16, 64] However, the dose response was non-uniform so a model similar to MD-55-1 was released with a sensitive layer thickness of $38\ \mu\text{m}$. This model is the HS model and has a higher sensitivity and better uniformity than its predecessors. The increase in sensitivity for early models is most likely due to an increase in the thickness of the active layer in the film. [71]

1.2.3 EBT and EBT-2 models

The EBT (external beam therapy) and EBT-2 models are the most recent models and are designed specifically for radiotherapy purposes. The EBT model consists of two emulsion layers ($17\ \mu\text{m}$ thick) sandwiched between two polyester layers ($97\ \mu\text{m}$ thick) and separated by a surface layer ($6\ \mu\text{m}$ thick). The emulsion material (active layer) composition has changed from early models (see table 1-1) making this model effectively water equivalent. This feature is very important for

Table 1–1: Composition of radiochromic films. Note that the surface layer contains about 15 % moisture and gelatin which makes the composition vary from batch to batch because of their organic composition. The composition of the transparent and yellow polyester, the adhesive, and the opaque white polyester is derived from calculations.

Material	Density (g/cm ³)	Effective Z	N _e (10 ²⁷ /m ³)	Elemental composition (percentage by mass)				
				H	C	N	O	Other
Early models emulsion	1.08	6.27	328	9.3	56.6	15.7	18.4	
EBT emulsion	1.1	7.05	328	9.4	57.4	13.2	16.4	0.8 Li; 2.9 Cl
XRQA emulsion	1.2	32.6	303	6.4	38.1	5.5	13.8	0.4 Li; 13.4 Br; 22.3 Cs
Surface layer	1.2	9.90	317	6.5	32.3	21.6	20.5	2.3 Li; 16.8 Cl
Transparent and yellow polyester	1.35	6.64	313	4.2	62.5		33.3	
Adhesive	1.2	6.26	329	9.4	65.6		24.9	3.5 S; 15.1 Ba
Opaque white polyester	1.6	27.6	302	3.1	46.6		31.7	
Water	1.00	7.42	334	11.2			88.8	

a dosimeter as water is considered the reference material in which radiotherapy devices are calibrated according to the accepted dosimetry calibration protocols [3]. This model is also more suitable for dosimetry as it shows an increase in sensitivity of an order of magnitude larger than previous models covering a dose range of 0.05 Gy to 8 Gy according to the manufacturer. However this is only when using only a single color channel (red) on a flatbed document scanner. When all three color channels are used (red, green, and blue), it has been shown that the dynamic range of the EBT film model can be extended to well over 100 Gy [31]. Recent investigation testing the limit of achievable accuracy with radiochromic film dosimetry systems employing the EBT film model have shown that a remaining 2% level of the dose measurement uncertainty is mostly attributed to the non-uniformity of the sensitive layer of the film. [92] To improve this the manufacturer

decided to incorporate a yellow dye in the active layer of the film. This dye is incorporated in order to correct for subtle differences in the thickness of the sensitive layer assuming that the marker dye is uniformly distributed throughout the sensitive layer and that change in the optical density of the film when exposed to radiation is not affected by the presence of this marker dye. [68] This led to the development of the most recent model of radiochromic film (EBT-2). In this model, the active layer chemical composition remains the same as in the EBT model. However the structure has gone from two active layers to one. It now consists of a polyester overlamine of 50 μm thick, an adhesive layer of 25 μm thick, a topcoat layer of 5 μm thick, an active layer of 30 μm thick, and finally a polyester substrate of 175 μm thick for a total thickness of 285 μm (see top part of figure 1-1). By examining figure 1-1, one can see that the film models EBT and EBT-2 experience the same change in absorbance upon dose deposition. However the sensitivity of the most recent model EBT-2 is slightly lower than that of the model EBT. This is due to the fact that the sensitive layer is slightly thinner in the EBT-2 model than the thickness of the EBT model (total sensitive layer thickness of 30 μm versus 34 μm). [69] Also the manufacturer's hypothesis that the addition of the yellow marker dye not affecting the dosimetric properties of the latest film model was recently confirmed. [26]

1.2.4 XR models

The XR emulsion based model is a type of film that was developed in order to provide additional sensitivity for the low-energy photon beams used in diagnostic radiology. Several models are available depending on the desired application for

the film. The most general is the XR-RV2 model. Other models were developed for quality assurance (QA) of specific applications: the XR-CT model for computed tomography QA; the XR-M for mammography unit QA; and the XR-QA for general radiology QA. These film models have an opaque backing and thus must be digitized in reflection mode when using a flatbed document scanner. The manufacturer added high atomic number components in their active layer for increased photon detection efficiency. However as one can see from table 1-1 this makes this film model less water equivalent. [72]

Table 1-2: Characteristics of the different radiochromic film models. Note that the active layer thickness is the total thickness from all the active layers if more than one layer is present in a particular film model. Note that the missing values were not provided by the manufacturer.

Film model	Active layer thickness (μm)	Sensitivity (mAU/Gy)	Dose range (Gy)
HD-810	6.5	3	10–100
MD-V2-55	32	20	1–100
HS	38	35	0.5–50
EBT	34	400 to 800	0.05–100
EBT-2	30	400 to 800	0.01–100
XR-V2	17	(-)	0.01–5
XR-QA	50	0.001–0.2	(-)

1.2.5 Applications of radiochromic films

The most recent models of radiochromic film EBT and EBT-2 were designed for intensity-modulated radiotherapy (IMRT) quality assurance measurements. However over the years they have been used for a wide variety of applications

such as skin dose measurements and superficial build-up region measurements [10, 19, 20, 27], brachytherapy [21, 33, 49, 67], stereotactic radiotherapy [82, 90, 91], total body irradiation (TBI) [84], electron therapy [39, 83], total skin electron therapy (TSET) [13, 50], dosimetry characterization of proton therapy beams [24, 88, 94], and dose verification of cell irradiation in radiobiological experiments [86]. They also show great potential for two dimensional clinical dosimetry of electron beams and dose measurement in nonstandard fields [23]. In addition, XR emulsion films can be used to measure dose within diagnostic energy range during diagnostic CT scans [73] and CBCT acquisitions [85]. Radiochromic films are also being used for a wide variety of quality assurance applications including commissioning of dynamic wedge in treatment planning system [36], transmission and beam penumbra measurements of multileaf collimators [38], and IMRT QA measurements [6, 32, 87, 89, 93].

CHAPTER 2

Theory

The following chapter unveils the most important concepts and theories related to dose deposition mechanisms. The references for this part are mainly from Ervin B. Podgorsak [66, 65] and Jan P. F. Seuntjens [65] whom I was lucky enough to have as teachers, and from inescapable references in the medical physics world that are Harold E. Johns and John R. Cunningham [44], Faiz M. Khan [46], and Frank H. Attix [4].

2.1 Ionizing radiation

Radiation can be classified in two categories: ionizing radiation and non-ionizing radiation. Radiation can ionize matter if its energy is higher than the ionization potential of matter. Ionizing radiation can be split in two categories which are directly ionizing radiation (charged particles such as electrons, protons, etc.) and indirectly ionizing radiation (neutral particles such as photons and neutrons). Deposition of energy in the medium is done through direct Coulomb interactions between a charged particle and orbital electrons of atoms in the medium. Thus directly ionizing radiation deposits its energy directly to the medium and indirectly ionizing radiation has to first transfer its energy to a light charged particle (electron or positron) in the medium to deposit its energy in the medium. The measure of energy deposited in the medium through ionizing

radiation is dose and it is measured as the energy deposited per unit mass of medium (J/kg), or Gray (Gy) in the International System of Units (SI) [25].

2.1.1 Cross section

The process of dose deposition in a medium requires an interaction between two particles. The concept of cross section, typically denoted σ , represents the probability of interaction between particles and is represented in units of area (typically cm^2 or barn (b)). It can be thought of as an area surrounding the target particles that a photon or incoming particle sees when traveling towards the target particle. All the different interactions have a specific cross section and the sum of all the cross sections represents the total cross section. Note that the cross section for photons is smaller than the cross section for charged particles.

2.2 Electron interactions

Electrons (as well as other charged particles) interact with the medium while traveling through it. They can interact through Coulomb interactions with the atomic nuclei or the orbital electrons of the absorber. These interactions can be elastic, that is the electron is scattered and no energy is transferred to the medium, or inelastic, that is the electron is scattered and energy is transferred to the medium's orbital electron (nucleus) or the energy is radiated in the form of Bremsstrahlung. As shown in figure 2-1, depending on how close the electron passes to the atom (impact parameter, b) with respect to the radius of the atom (a), there are three types of collision possible. If $b \gg a$, a soft collision between the incoming electron and the whole atom will occur and a small amount of energy will be transferred to the orbital electrons. If $b \simeq a$, a hard collision

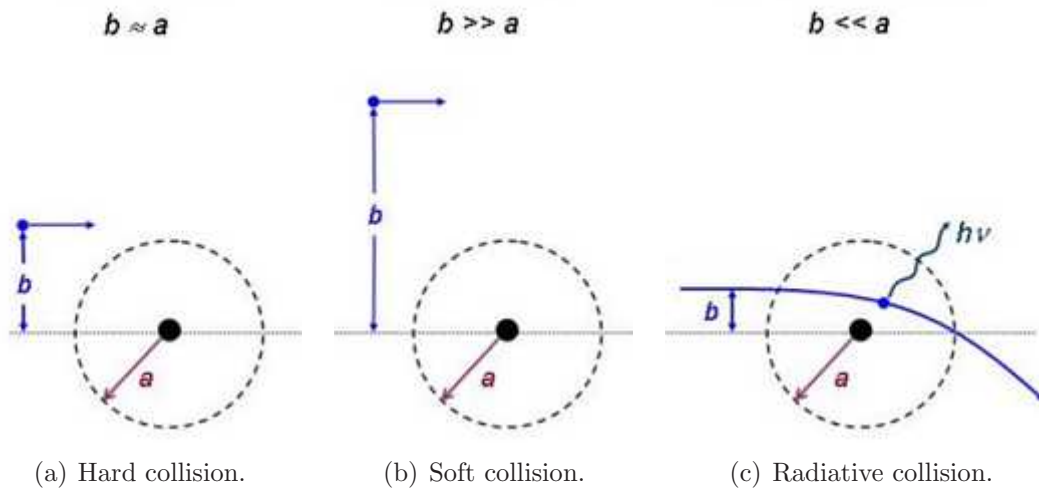


Figure 2-1: Schematic of the different interactions between an electron with an absorbing atom. (a) Shows a hard collision i.e. when the impact parameter b is comparable to the atomic radius a , (b) shows a soft collision i.e. when the impact parameter b is (much) greater than the atomic radius a , and (c) shows a radiative collision i.e. when the impact parameter b is (much) smaller than the atomic radius a . Figure from [66] on page 142.

between the electron and an atomic electron occurs and an important fraction of the electron's kinetic energy is transferred to the orbital electron. Finally, if $b \ll a$, a radiative interaction between the incoming electron and the nucleus occurs and a fraction (or all) of the kinetic energy of the electron is emitted as a Bremsstrahlung photon. For the case of the electron-orbital electron interaction, it results in either an ionization which results in an ejection of an orbital electron from the absorber atom, or an excitation of the absorber atom which results in a transfer of an electron from a higher orbit to the vacant shell with the difference in energy released in the form of a photon. These types of energy losses are described using the collisional stopping power. For the case of electron-nucleus

interaction, it results in the electron being scattered and the energy loss is through Bremsstrahlung radiation. This is characterized by the radiative stopping power. Note that the energy loss by radiation increases directly with the absorber atomic number and incoming electron kinetic energy. The stopping power describes these losses of energy. It is usually split in two components: the radiative stopping power for radiative collisions and the collisional stopping power for hard and soft collisions.

Total (mass) stopping power

The total stopping power is simply the sum of the radiative and collisional stopping power. It is most often expressed as the total mass stopping power in which the density of the medium divides the stopping power. Since the stopping power describes the kinetic energy loss by the charged particle per unit path length, it can be written as follows:

$$\frac{S_{\text{tot}}}{\rho} = \frac{1}{\rho} \frac{dE_K}{dx} = \frac{S_{\text{col}}}{\rho} + \frac{S_{\text{rad}}}{\rho} \quad (2.1)$$

where S represents the stopping power and ρ represents the density. Note that the collisional stopping power has a very important role in dosimetry as the dose (D in [Gy]) in a medium may be expressed as

$$D = \phi \frac{S_{\text{col}}}{\rho} \quad (2.2)$$

where ϕ is the electron fluence.

Bremsstrahlung yield

The bremsstrahlung (or radiative) yield, denoted $B(E_{K_0})$, is defined for a charged particle with kinetic energy E_{K_0} that strikes an absorber medium. It is the fraction of initial kinetic energy that is emitted as bremsstrahlung radiation (radiative collisions) as the charged particle slows down within the medium. For heavy charged particles the bremsstrahlung yield is negligible, i.e. $B(E_{K_0}) \approx 0$. For light charged particles such as electrons and positrons, the bremsstrahlung yield is obtained using:

$$B(E_{K_0}) = \frac{1}{E_{K_0}} \int_0^{E_{K_0}} \frac{S_{\text{rad}}(E)}{S_{\text{tot}}(E)} dE \quad (2.3)$$

where S represents the stopping power. Note that during in-flight annihilation of positrons, the photon production is usually ignored from the calculation of the bremsstrahlung yield. The radiative fraction (\bar{g}) is an average value of the bremsstrahlung yield for light charged particles of various initial energies, E_{K_i} , present in the spectrum of light charged particles produced in a medium by impinging photons.

Range of charged particles

The range (R [cm]) of charged particles in a particular medium is an experimental concept that measures the thickness (mean path length) that the charged particles can penetrate in the medium before being put to a complete stop. Heavy charged particles experience negligible radiative losses and transfer only a small amount of energy in collisions with orbital electrons, thus they mainly suffer small angle deflections in elastic collisions. Their journey through the medium is rather linear and their range large, making their range more or less equivalent

to the mean path length. Light charged particles on the other hand can lose a large amount of their energy in collisions with orbital electrons and in radiative collisions, making their scattering angle larger and their path through the medium more tortuous thus their range is smaller than the mean path length in most cases. The mean path length (R_{CSDA} [cm]) can be calculated using the continuous slowing down approximation (CSDA) as follows:

$$R_{\text{CSDA}} = \int_0^{E_{\text{K}_0}} \frac{dE}{S_{\text{tot}}(E)} \quad (2.4)$$

where E_{K_0} is the initial kinetic energy of the charged particle.

2.3 Photon interactions

As mentioned earlier photons are indirectly ionizing radiation and they deposit their energy in the absorbing media through a two-step process. Not all the photon interactions are relevant in medical physics. We will focus our efforts on the important processes that play a fundamental role in imaging, radiotherapy and radiation dosimetry. The cross section for a photon interaction depends on the energy of the photon, and the density and atomic number of the absorber. The outcome of the photon following an interaction with an atom is either the photon disappears, meaning that its energy is completely absorbed and transferred to particles, or it is scattered with its full energy or part of it is transferred to the particles. In an absorbing media, photons can interact directly with the nucleus or its electrostatic field, or they can interact with either its loosely bound electrons or tightly bound electrons. A loosely bound electron is an electron whose binding energy (E_{B}) is much smaller than the photon energy ($h\nu$), and a tightly bound

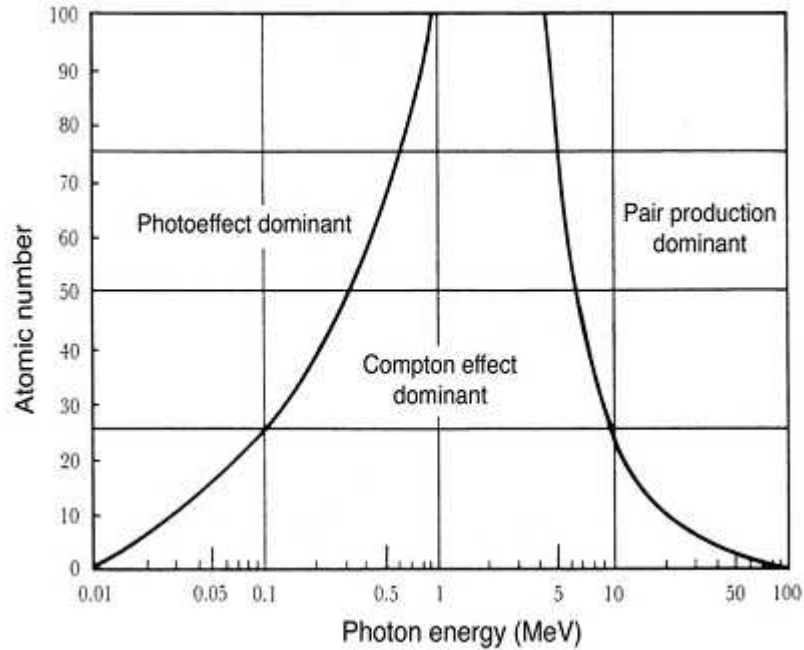


Figure 2–2: The regions where the different photon processes dominate as shown for photon energy $h\nu$ with respect to atomic number of an absorber Z . The solid lines represent the regions where the atomic cross sections for the different processes are equal to one another. Figure from [65] page 246.

electron is an electron whose binding energy is comparable too or larger than the energy of the photon. There are three main processes that dominate over a region of energies when compared to the atomic number Z of an absorber (as shown in figure 2.3): photoelectric effect, Compton effect, and pair production.

2.3.1 Compton scattering

Compton scattering is an interaction between a photon and a loosely bound orbital electron. It is also referred to as incoherent scattering. In this process, the electron is considered to be stationary and free with respect to the incoming photon. Refer to figure 2.3.1 for a schematic diagram of a Compton scattering

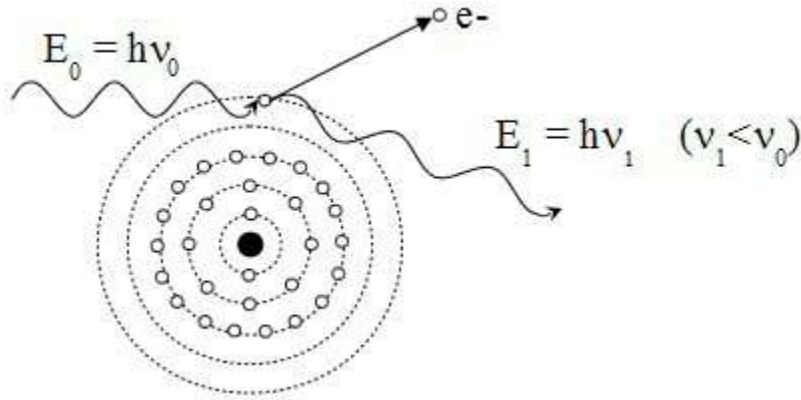


Figure 2–3: Schematic diagram of a Compton scattering event.

event. During a Compton scattering event, the incident photon ($h\nu$) is scattered by the electron which is ejected from the atom and has energy E_k . Note that the incident photon energy is often expressed as its normalized value with respect to the electron rest energy $\epsilon = h\nu/m_e c^2$. The scattered photon now has energy $h\nu'$. Using a classical picture of an elastic collision between two particles and the conservation of energy and momentum, one can find that the energy for the scattered photon and ejected electron can be expressed as follows:

$$h\nu' = h\nu \frac{1}{1 + \epsilon(1 - \cos \theta)} \quad (2.5)$$

and,

$$E_k = h\nu \frac{\epsilon(1 - \cos \theta)}{1 + \epsilon(1 - \cos \theta)} \quad (2.6)$$

where θ represents the angle between the incident and scattered photon. The relation between the scattering angle θ and the recoil electron angle ϕ can be

expressed as follows:

$$\cot \phi = (1 + \epsilon) \tan(\theta/2) \quad (2.7)$$

with ϵ as above. Note that θ ranges from 0 to π and ϕ ranges from 0 to $\pi/2$. The difference in wavelength is expressed as follows:

$$\delta\lambda = \lambda' - \lambda = \lambda_c(1 - \cos \theta) \quad (2.8)$$

where $\lambda_c = 2\pi/m_e c^2 = 0.0243 \text{ \AA}$ is the Compton wavelength of the electron.

Compton effect is the dominant interaction for photons with energy ranging from 0.2 to 10 MeV. The Compton cross section in the energy region not affected by electron binding effects is given by:

$$\sigma_c = \frac{Z N_A}{A} \rho_e \sigma_c^{\text{KN}} \approx \frac{N_A}{2} \rho_e \sigma_c^{\text{KN}} \quad (2.9)$$

where ${}_e\sigma_c^{\text{KN}}$ is the electronic Klein-Nishina cross section for Compton scattering. This approximation is valid for all elements with the exception of Hydrogen and makes the cross section independent of the atomic number Z .

2.3.2 Rayleigh scattering

Rayleigh scattering is also referred to as coherent scattering. In this photon interaction process the photons are scattered by bound atomic electrons of the absorbing medium. This process is essentially an elastic collision hence the photon is scattered at small angles and conserves its initial amount of energy. Since no energy is transferred to the absorbing medium by this process it does not contribute to the energy transfer coefficient. However it does contribute to the

attenuation coefficient. The Rayleigh atomic cross section is given by:

$${}_a\sigma_R = \pi r_e^2 \int_0^\pi \sin \theta (1 + \cos^2 \theta) [F(x, Z)] d\theta \propto \frac{Z^2}{(h\nu)^2} \quad (2.10)$$

where $F(x, Z)$ is the so-called atomic form factor, and $x = \sin(\theta/2)/\lambda$ is the momentum transfer variable. One should note that this process has a relatively small importance compared to the other interaction processes in the atomic number range of tissue and tissue-equivalent material for photon energy greater than 20 keV.

2.3.3 Photoelectric effect

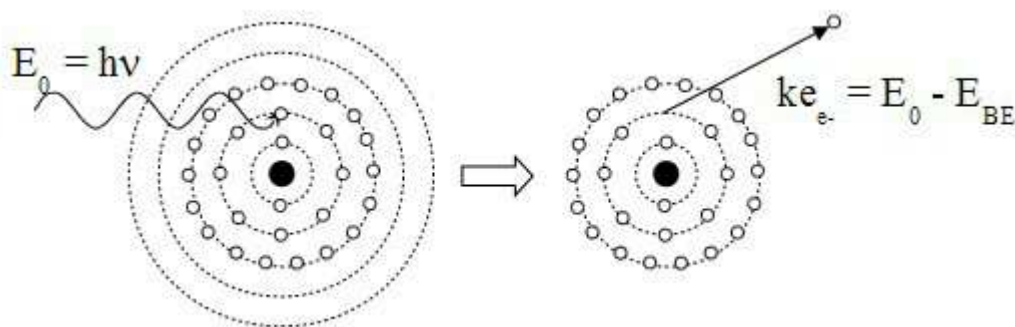


Figure 2-4: A schematic diagram showing the photoelectric interaction.

The photoelectric effect, also known as the photoeffect, is an interaction between a photon and a tightly bound orbital electron of an absorber. The process is shown graphically in figure 2-4. In this process, the photon energy is completely absorbed by the tightly bound electron which is then ejected from the atom. The electron is referred to as a photoelectron and its kinetic energy (E_k) is given by:

$$E_k = h\nu - E_B \quad (2.11)$$

where E_B is the binding energy of the electron in the atom. This creates a vacancy in the shell of the atom where the electron was ejected. This vacancy is then filled by a higher shell electron and the energy difference which is created from the transition is emitted as either a characteristic photon or as an Auger electron. Note that there is a threshold energy for this process to happen. The energy of the incoming photon has to be larger than the binding energy of the K-shell of the absorber. About 80% of all photoelectric absorptions occur with the K-shell electrons of the absorber. There are three distinct energy regions that characterize the photoelectric effect atomic cross section (${}_a\tau$). The first is the immediate vicinity of the absorption edges where predictions for ${}_a\tau$ are difficult to make and uncertain. The second is at some distance from the absorption edge where the atomic cross section for the K-shell is given by:

$${}_a\tau_K = \alpha^4 {}_e\sigma_{\text{Th}} Z^n \sqrt{\frac{32}{\epsilon^7}} \quad (2.12)$$

where $\epsilon = h\nu / (m_e c^2)$ is the normalized photon energy, α is the fine structure constant, Z is the atomic number of the absorber, ${}_e\sigma_{\text{Th}}$ is the total Thomson electronic cross section, and n is the power for the Z dependence of ${}_a\tau_K$ which range from $n = 4$ for low photon energies to $n = 4.6$ for high photon energies. Finally the third energy region is in the relativistic region far from the K absorption edge where the photoelectric atomic cross section is given as follow:

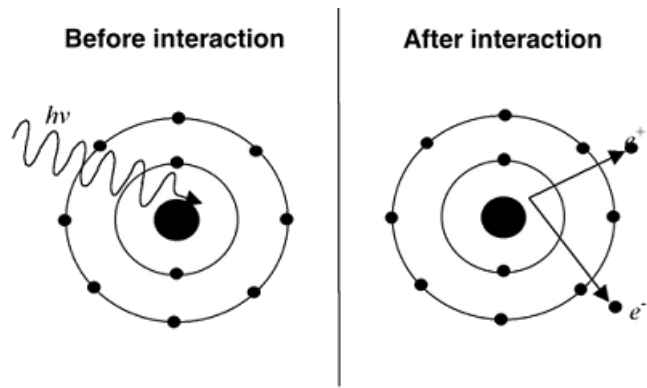
$${}_a\tau_K = \frac{1.5}{\epsilon} \alpha^4 Z^5 {}_e\sigma_{\text{Th}} \quad (2.13)$$

Overall the atomic cross section for the photoelectric effect is proportional to $Z^4/(h\nu)^3$ for low photon energies and gradually transforms to being proportional to $Z^5/(h\nu)$ for high photon energies. The steady decrease with respect to increasing photon energy is also accompanied by sharp discontinuities for photon energies equal to the binding energy of a particular shell of the absorber.

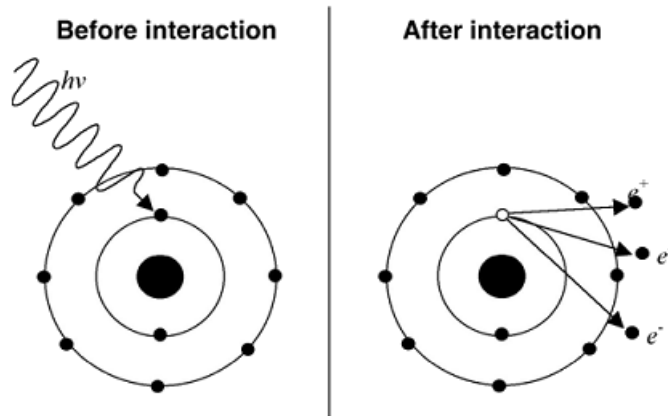
2.3.4 Pair and triplet production

The pair production process occurs in the nuclear Coulomb field. This process has an energy threshold before it can occur. The energy of the incoming photon must be greater than $2m_e c^2 = 1.022$ MeV. In this process the photon is completely absorbed and an electron-positron pair is created. A schematic diagram of the pair production process is shown in figure 2-5(a). Three quantities are conserved during this process. Energy and charge are conserved even if the interaction occurs in free-space. However, momentum conservation makes it such that the event can only occur in the Coulomb field of a nucleus (pair production) or an orbital electron (triplet production). A schematic diagram of the triplet production process is shown in figure 2-5(b). The threshold energy for the triplet production process is $4m_e c^2 = 2.04$ MeV. These threshold energies can be shown using the conservation of energy and momentum. Two charged particles are released in the pair production process (one electron and one positron) while three charged particles are released in the triplet production process (two electrons and one positron). After the interaction the electron-positron pair has kinetic energy equal to

$$E_k = h\nu - 2m_e c^2 \tag{2.14}$$



(a) Pair production process.



(b) Triplet production process.

Figure 2-5: A schematic diagram of (a) the pair production process (in the Coulomb field of an atom) and (b) the triplet production process (in the Coulomb field of an orbital electron). Both figures from [66] on page 228.

and the electrons-positron triplet has kinetic energy equal to

$$E_k = h\nu - 4m_e c^2 \quad (2.15)$$

where E_k represents the kinetic energy. Following the reaction the positron experiences collisional and radiative losses of its kinetic energy in the absorbing

medium and eventually collides and annihilates with an electron from the absorbing medium. Most probably the positron will lose all of its kinetic energy before annihilating with the electron in which case the electron-positron pair disappears creating two photons each with energy of 0.511 MeV and emitted at almost 180 degrees from one another. In the case where the positron still has kinetic energy and annihilates with a tightly bound electron (in-flight annihilation), the nucleus can pick up the recoil momentum and only one photon with energy $E_k + 2m_e c^2$ will be emitted. In the case where it annihilates with a free electron, two photons are produced one with energy $E_k + (3/2)m_e c^2$ and one with energy $(1/2)m_e c^2$ such that the momentum is conserved. The atomic cross section for the pair production process is given as follows:

$${}_a\kappa_{pp} = \alpha r_e^2 Z^2 P(\epsilon, Z) \quad (2.16)$$

where α is the fine structure constant, r_e is the classical radius of the electron, Z is the atomic number of the absorber, and $P(\epsilon, Z)$ is a function of the photon energy and atomic number of the absorber. Note that since the atomic cross section of the pair production process significantly exceeds that of the triplet production and since it can be shown that ${}_a\kappa_{pp}/{}_a\kappa_{tp} = \eta Z$ where η is a parameter depending on the incoming photon energy and Z is the atomic number of the absorber, the total atomic cross section for the pair and triplet production is given as

$${}_a\kappa = {}_a\kappa_{pp} [1 + 1/(\eta Z)] \quad (2.17)$$

with the atomic cross section for the pair production process being zero for photon energies less than $2m_e c^2$.

2.3.5 Attenuation coefficients

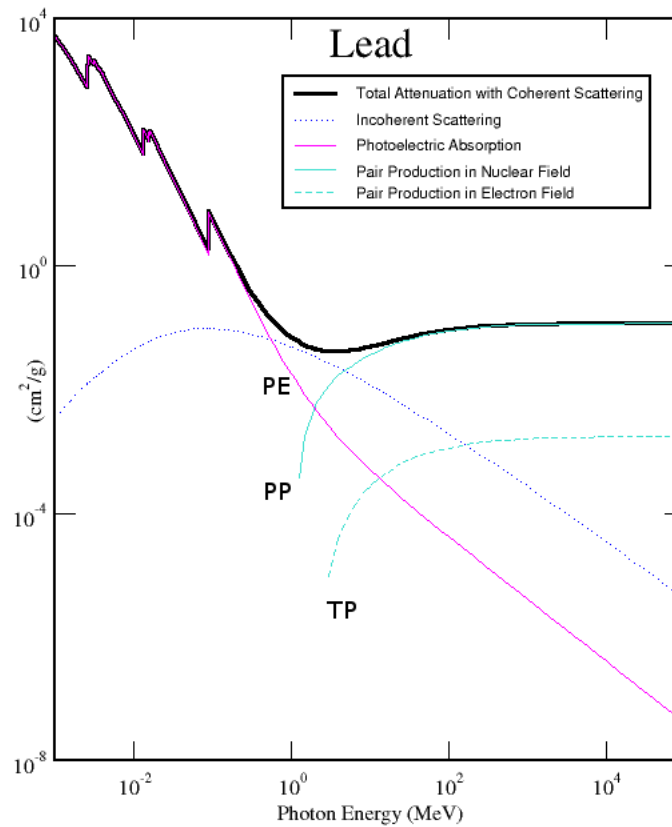


Figure 2–6: The mass attenuation coefficient with respect to photon energy for lead (figure from [42]).

The linear attenuation coefficient μ is the probability per unit path length that a photon will have an interaction with the absorbing medium. It depends on the energy of the incoming photon and the atomic number of the absorber. It is the sum of the values for all the possible different interactions:

$$\mu = \sigma_R + \sigma_c + \tau + \kappa \quad (2.18)$$

Since every cross section is dependent on the density of the absorber, the mass attenuation coefficient is often used:

$$\mu_m = \frac{\mu}{\rho} = \frac{\sigma_R}{\rho} + \frac{\sigma_c}{\rho} + \frac{\tau}{\rho} + \frac{\kappa}{\rho} \quad (2.19)$$

with ρ being the density of the absorber. The mass attenuation coefficient describes the ability of a material to attenuate the intensity of a photon beam. The mass attenuation coefficient for lead with respect to photon energy is shown in figure 2–6. As one can see the total mass attenuation coefficient curve shows the K, L, and M absorption edges from the photoelectric effect which is the dominant effect for photon energies up to 0.5 MeV, then the Compton effect dominates the behavior of the curve for energies from 0.5 MeV to 10 MeV, and pair production effect takes over for photon energies above 10 MeV.

Two other coefficients are used to describe the energy transferred from the photon to the charged particles and the energy absorbed by the medium. They are called the mass energy transfer coefficient (μ_{tr}/ρ) and the mass energy absorption coefficient (μ_{ab}/ρ) respectively and the definitions for those two coefficients are:

$$\frac{\mu_{tr}}{\rho} = \frac{\mu}{\rho} \frac{\overline{E}_{tr}}{h\nu} = \sigma_c \left[\frac{\overline{E}_{tr}^\sigma}{h\nu} \right] + \tau \left[1 - \frac{P_K \omega_K \overline{h\nu}_K}{h\nu} \right] + \kappa \left[1 - \frac{2m_e c^2}{h\nu} \right] \quad (2.20)$$

and,

$$\mu_{ab} = \mu_{tr} (1 - \overline{g}) \quad (2.21)$$

where \overline{g} is the radiative fraction, that is, the average fraction of secondary charged particle energy lost in radiative interactions (bremsstrahlung and in-flight annihilations) that they experience while travelling through the absorbing medium. For

low absorber Z and low photon energy, the radiative fraction goes to zero. For increasing Z or photon energy, the radiative fraction increases gradually. These coefficients are used to determine the outcome of an impinging photon of energy $E_{h\nu}$ on the absorbing medium.

2.4 Dosimetric basics

Directly ionizing radiation deposits energy in a medium while travelling through it. Radiation dosimetry addresses the methods to determine quantitatively this energy deposition by using different concepts and theories.

2.4.1 Kerma

Kerma (K) represents an acronym that stands for *kinetic energy released per unit mass*. It applies to indirectly ionizing types of radiation and quantifies the energy transferred from indirectly ionizing radiation (such as photons) to directly ionizing radiation (such as electrons) in the medium. It is defined as a mean energy transfer per unit mass:

$$K = \frac{d\overline{E}_{\text{tr}}}{dm} \quad (2.22)$$

Note that the energy from impinging photons is transferred to the medium in a two stage process: first the energy is transferred to directly ionizing radiation (mainly electrons) in the medium (as described by kerma) through the processes described in section 2.3, then the electrons transfer their energy to the medium through processes described in section 2.2.

2.4.2 Exposure

The exposure is a quantity that describes the amount of charges produced in a volume of air upon ionizing radiation traversing the volume. The symbol for

exposure is X and its unit is the Roentgen [R] which converted to international system units is equal to 2.58×10^{-4} C/kg. Note that exposure does not include radiative losses by the electrons created in the volume and it is only defined in air. The energy expended to produce an ion pair in dry air is denoted by $\overline{W}_{\text{air}}$ and is usually divided by the charge of an electron:

$$\frac{\overline{W}_{\text{air}}}{e} = 33.97 \pm 0.05 \text{ J/C} \quad (2.23)$$

Note that this is the currently recommended value for this quantity [12].

2.4.3 Absorbed dose

The energy imparted (ϵ) by ionizing radiation to a medium (mass m , volume V) can be calculated by summing all the radiant energy entering the volume and subtracting all the energy leaving the volume. The absorbed dose within the volume dm is defined using this quantity as:

$$D = \frac{d\bar{\epsilon}}{dm} \quad (2.24)$$

where $\bar{\epsilon}$ is the mean energy imparted. It can also be defined as a function of stopping powers as described in section 2.2. Absorbed dose is a very important quantity in radiation dosimetry since the important biological effects of ionizing radiation are directly related to the deposition of energy in the medium (e.g. human body), and therefore to the absorbed dose.

2.5 Ionizing radiation production in the (modern) medical world

The production of ionizing radiation in the medical world has greatly evolved over the last 50 years. Up to the 1950s, most of the external beam therapy was

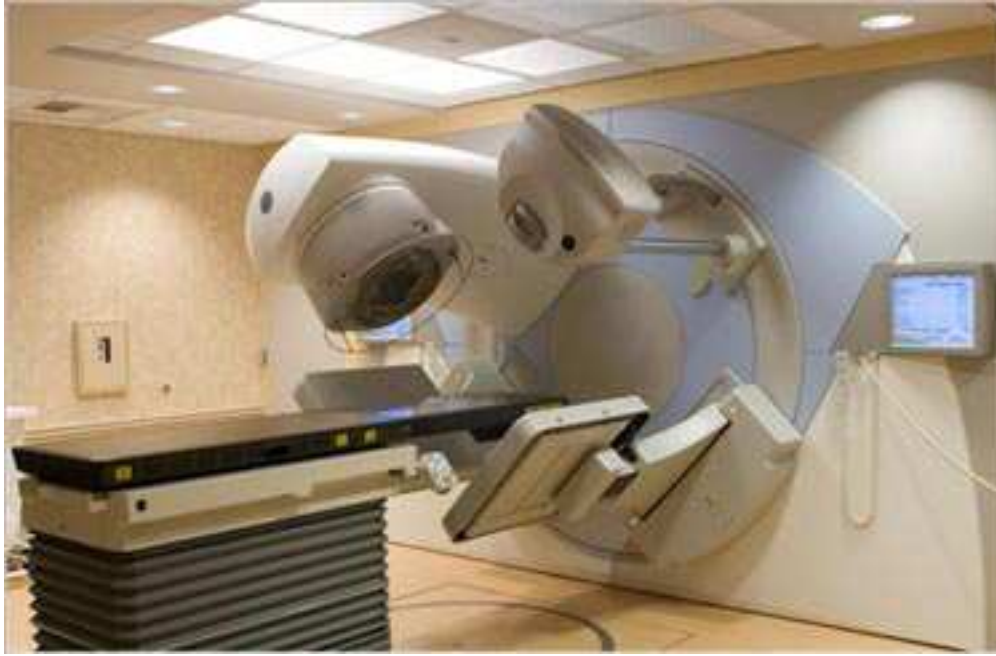


Figure 2-7: A linear accelerator from the company Elekta [1]. On this picture one can see the treatment table, the accelerator gantry, the portal imaging flat-panel, and a cone-beam x-ray imaging device.

performed using kilovoltage units capable of delivering photon beams with energies up to 300 kVp. Improved versions of these units are still used nowadays mainly for treatment of superficial skin lesions. They were gradually replaced by Co-60 teletherapy units producing monoenergetic gamma rays of 1.25 MeV by the beta-decay of the Co-60 radionuclide into Ni-60 which then emits two photons through gamma decay of energies 1.173 MeV and 1.332 MeV for an average of 1.25 MeV. This machine brought great improvements over the kilovoltage units and was widely used for radiotherapy throughout the world. They are still used nowadays but have been relegated to specialty treatment procedures such as total body irradiation. The successors of these units are linear accelerators which still

represent the golden standard of cancer care in external beam radiotherapy. Their development is now to the fifth generation. They can produce both photon and electron beams to energies of up to 25 MeV. The same machine can produce beams of different energies which makes it a very versatile machine in the clinic. See figure 2–7 for a picture of a typical modern linear accelerator.

Other types of machines for producing ionizing radiation are used for more specialized treatments such as brachytherapy and radiosurgery. In brachytherapy radiation sources are radionuclides which are put in close proximity to the treatment site through catheters inserted in the patient. The sources are either inserted for a defined period of time (high dose rate or low dose rate) or permanently. This type of treatment is standard in many clinics for treatment of gynecological tumors, prostate tumors, and breast tumors. Radiosurgery is performed either using an adapter attached to standard linear accelerators, or using specialty machines such as Gammaknife or Cyberknife. These machines can produce very small fields with high dose rates permitting delivery of high local doses.

As an example of a medium size clinic, at the Centre Hospitalier Universitaire de Sherbrooke (CHUS) there are four linear accelerators (LINACs) for external beam radiotherapy, a high dose rate brachytherapy suite, and a Gammaknife for radiosurgery. The Gammaknife of the CHUS is shown in figure 2–8.

2.6 Dose measurement and important concepts in radiation therapy

Dose measurement is of primary importance in radiation therapy. Before delivering a radiation treatment to a patient, one has to know what the treatment machine output is and how it will react in the presence of the patient. Nowadays



Figure 2–8: The GammaKnife at the CHUS.

a treatment planning software is used to produce treatment plans according to the radiation oncologist's demands. The planning software requires a set of beam data to be measured and modeled (such as beam profiles, percent depth dose curves, output factors, wedge profiles and factors, etc) so that it can calculate the dose delivered to the patient. These measurements are performed by medical physicists and are typically verified (quality assurance) at various pre-determined time intervals. Some of these tests involve the mechanical functioning of the machine while others require measuring the output of the beam (photons or charged particles) of the machine. These tests require the use of a dosimeter, which is an instrument that can measure absorbed dose. There are different dosimeters

available for the medical physicist to use and all of them have advantages and disadvantages. Typical dosimeters available in a common radiation therapy clinic are presented in section 2.6.3. Accurate dose measurement requires some conditions to be respected which are presented in the following sections. Note that dose measurement is mainly performed in water or water equivalent material. This is because the human body consists predominantly of water, and measuring the dose in water represents a good approximation of the dose eventually delivered to the patient.

2.6.1 Charged particle equilibrium

Charged particle equilibrium (CPE) is a condition that is applied to a certain finite volume (V). It exists if the amount of charged particles entering the volume is equal to the amount of charged particles leaving the volume. Typically charged particle equilibrium for high-energy photon beams (1 MeV to 20 MeV) is reached within the first few centimeters below the surface of a medium. This is because of the reduced electron fluence near the surface of the medium due to the lack of material where secondary electrons would be created. The region between the surface of the material and where charged particle equilibrium is reached is called the build-up region. Note that the point in the medium where charged particle equilibrium is reached is also the region of maximum dose and at this point collisional kerma and absorbed dose are equal. After this point attenuation by the medium decreases the photon fluence and the kerma and dose are gradually reduced at the same rate. The absorbed dose at a depth can be determined using

the following relationship between collisional kerma and dose:

$$D = \beta K_{\text{coll}} \tag{2.25}$$

where β is a factor that is energy and material dependent. For the build-up region β is smaller than 1, while for the depth of maximum dose β is equal to one. Below this depth, one assumes a transient charged particle equilibrium (TCPE) and β is again smaller than 1. This is because the beam is attenuated as it passes through the material and the photon fluence decreases. However, within a small volume CPE can be assumed. The curve of dose versus depth is often represented in the form of dose percentage (with respect to the maximum dose) as a function of depth and is called a percent depth dose curve. More information regarding percent depth dose is contained in section 2.6.4. CPE condition is required for most dosimeters to properly measure absorbed dose.

2.6.2 Bragg-Gray and Spencer-Attix cavity theory

When measuring dose to a medium, one has to put the dosimeter in the medium thus removing a part of the medium and replacing it with the dosimeter. Bragg-Gray cavity theory has been developed in order to provide a relation between the absorbed dose measured in a dosimeter and the absorbed dose in the medium. The application of this theory requires two conditions to be fulfilled. The first condition requires the cavity created by the presence of the dosimeter to be small compared to the range of the charged particle impinging on it so that it does not perturb the fluence of charged particle in the medium. The second condition is that one can assume that photon interactions within the cavity are negligible

and can be ignored so that the absorbed dose in the cavity is solely deposited by the charged particle crossing its volume. This means that no secondary electrons are produced within the cavity and that the charged particles completely cross the cavity, meaning that no charged particle stops within the cavity. The first condition is only achieved in regions where CPE or TCPE is present. In these regions the perturbation to the fluence due to the presence of the cavity can be corrected by a fluence correction factor. When the conditions for the Bragg-Gray cavity theory are met, the dose to the medium can be related to the dose to the cavity by:

$$D_{\text{med}} = D_{\text{cav}} \frac{(\overline{S}/\rho)_{\text{med}}}{(\overline{S}/\rho)_{\text{cav}}} = D_{\text{cav}} \left(\frac{\overline{S}}{\rho} \right)_{\text{cav}}^{\text{med}} \quad (2.26)$$

where \overline{S}/ρ represents the average unrestricted mass stopping power.

Spencer-Attix cavity theory is an extension of the Bragg-Gray cavity theory that takes into account the creation of secondary electrons within the volume of the cavity. It operates under the same two conditions as the Bragg-Gray theory and the secondary electrons created within the cavity are also required to fulfill those two conditions. The dose to the medium can be related to the dose to the cavity in the Spencer-Attix cavity theory by:

$$D_{\text{med}} = D_{\text{cav}} \left(\frac{s}{\rho} \right)_{\text{cav}}^{\text{med}} \quad (2.27)$$

where s/ρ represents the average restricted mass stopping power.

2.6.3 Dosimeters

A general definition for a dosimeter is any device capable of measuring quantities related to ionizing radiation such as exposure, kerma, absorbed dose,

equivalent dose, or their rate (time derivative), etc. The main criteria for evaluating a particular dosimeter are:

1. Accuracy and precision,
2. Linearity,
3. Dose rate dependence,
4. Energy dependence,
5. Directional dependence,
6. Spatial resolution and physical size,
7. Readout convenience,
8. Convenience of use.

Ionization chambers and reference dosimetry

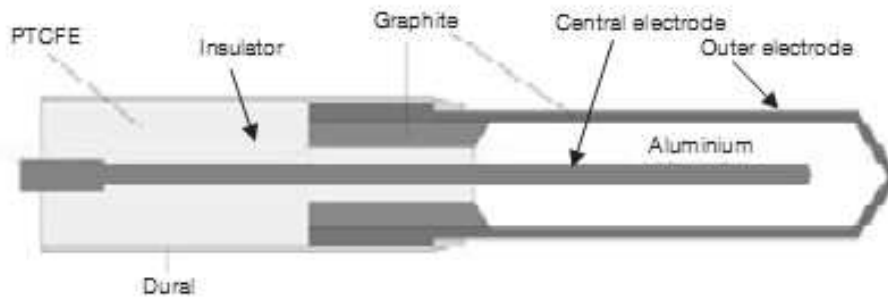


Figure 2–9: A schematic diagram of a typical cylindrical ionization chamber (figure from [65]).

Different dosimeters measure different quantities and some are more adapted to a particular measurement than others. For a desired measured quantity, choosing the appropriate dosimeter will affect the success of the experiment. In radiation therapy, beam calibration (also referred to as reference beam dosimetry)

is mainly performed using an ionization chamber dosimetry system consisting of a calibrated ionization chamber under reference conditions and an electrometer. Absolute beam dosimetry can be performed by calorimetry, Fricke dosimetry, or with free-air ionization chambers. Ionization chambers are the most practical among the three techniques from a clinical point of view. They can be used as a reference or relative dosimeter depending on what is known about the chamber. An ionization chamber is a cavity filled with gas and surrounded by a conductive outer wall (outer electrode). There is a collecting electrode and leakage current is prevented by a guard electrode (see figure 2-9).

There are many types of ionization chambers such as standard free air ionization chambers, cylindrical (thimble) ionization chambers, parallel-plate ionization chambers, pressurized well type ionization chambers, and extrapolation chambers. Standard free air ionization chambers are mainly used in national standards laboratories for low beam qualities to calibrate other types of chambers due to their limitations and size. Cylindrical ionization chambers are widely used in clinic. They have a volume varying from 0.1 to 1 cm³ and they can be used for reference dosimetry, be it in-air, in solid phantoms, and even in water if properly designed. As its name refer, they are of cylindrical shape and they can be sealed or not (in which case the temperature and pressure of air become important as the volume of air in the cavity varies with those two quantities). Parallel-plate ionization chambers are also known as plane-parallel ionization chambers. They consist of two plates, one serving as entry window and polarizing electrode and the other as back wall and collecting electrode. They are mainly

used for dosimetry of electron beams with energy below 10 MeV but can also be used for surface dose and dose measurement in the build-up region of photon beams. Ionization chambers used in brachytherapy (well type chambers) are used to measure dose from low air kerma rate sources that are used in brachytherapy. Their volume is much larger than cylindrical chambers (in the range of 250 cm³) for greater sensitivity. Extrapolation chambers have the same design as parallel-plate chambers but their sensitive volume can be varied. They are mainly used in surface dose measurements for kilovoltage and megavoltage beams. All types of chambers require knowledge of certain experimental parameters (such as pressure and temperature) or physical characteristics of the chamber and make use of many correction factors for accurate dose measurement.

Film dosimetry

Film dosimetry has evolved greatly in recent years. Radiographic films have been used in clinics for both radiography and dosimetry. Nowadays, the trend in cancer clinics is to be filmless, so that the use of silver halide films requiring development is fading quickly. However a relatively new type of film called radiochromic film has been developed and is replacing radiographic films for dosimetry in many centers. It is the main subject of this document and details regarding radiochromic film dosimetry is provided in the subsequent chapter.

Luminescence dosimetry

Luminescence dosimetry is based on a medium that upon absorption of ionizing radiation, retains some of the absorbed energy within metastable states inside energy gap that is later released in the form of ultraviolet, visible or

infrared light. This phenomenon is known as luminescence and the energy is released by either of the two processes: fluorescence in which the energy is released within 10^{-10} to 10^{-8} s and phosphorescence in which the energy is released with a time delay greater than 10^{-8} s. Phosphorescence is the process used in luminescence dosimetry and it can be accelerated using an exciting agent such as heat (thermoluminescent dosimetry or TLD) or light (optically stimulated luminescence or OSL). TLDs are used in many clinics for *in vivo* dosimetry on patients, verification of treatment techniques in various phantoms, dosimetry audits, or comparison among centers. They are somewhat tedious to use but can provide advantages over other techniques when the dosimetry system is properly implemented.

Semiconductor dosimetry

Semiconductor dosimetry is conducted using either silicon diodes or MOSFET (metal-oxide semiconductor field effect transistor) technology. Amongst silicon diodes only p-types diodes are used. They are useful for measurement of small fields or in high-dose gradients (as in radiosurgery and intensity modulated radiotherapy or IMRT) and they can also be used for depth dose measurements of electron beams. They are also used for *in vivo* dosimetry on patients. MOSFETs are of small size. They offer little attenuation to the beam and provide excellent spatial resolution. This makes them good candidates for *in vivo* dosimetry and they are also used for phantom dose measurements, brachytherapy, TBI, IMRT, intraoperative radiotherapy and radio-surgery.

Other dosimetry systems

Other dosimetry systems include gel dosimetry systems, diamond dosimeters, alanine-electron paramagnetic resonance dosimetry systems, and plastic scintillator dosimetry systems. They are mostly used as research tools but can provide valuable dose measurement results.

2.6.4 Measurements performed by a medical physicist

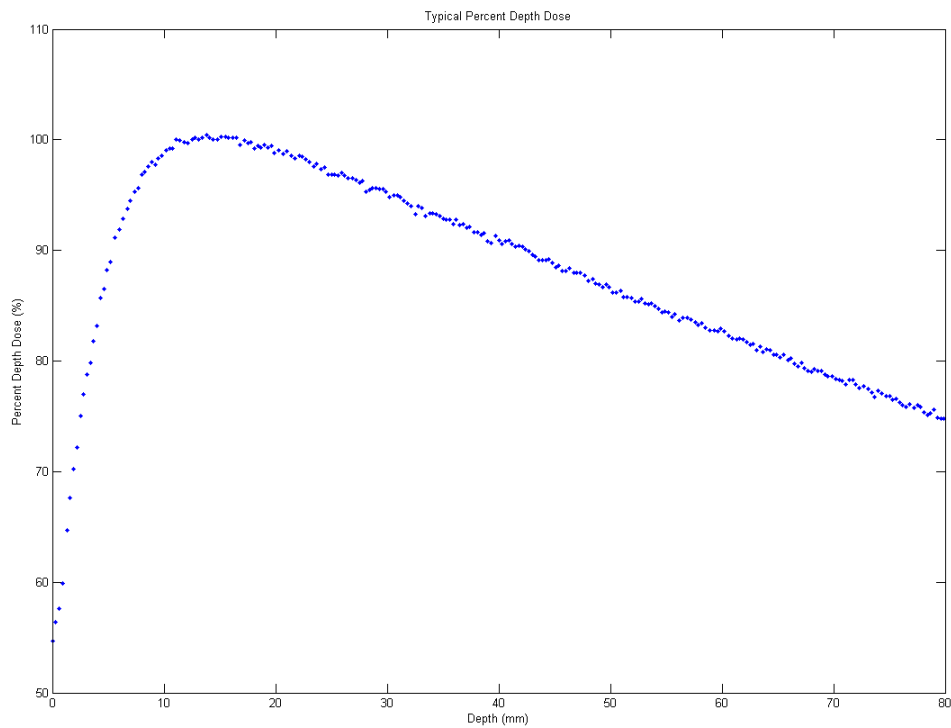


Figure 2–10: A typical central axis percent depth dose of a photon beam.

Many measurements are performed by a medical physicist on a routine basis for quality assurance or during the commissioning of a treatment machine.

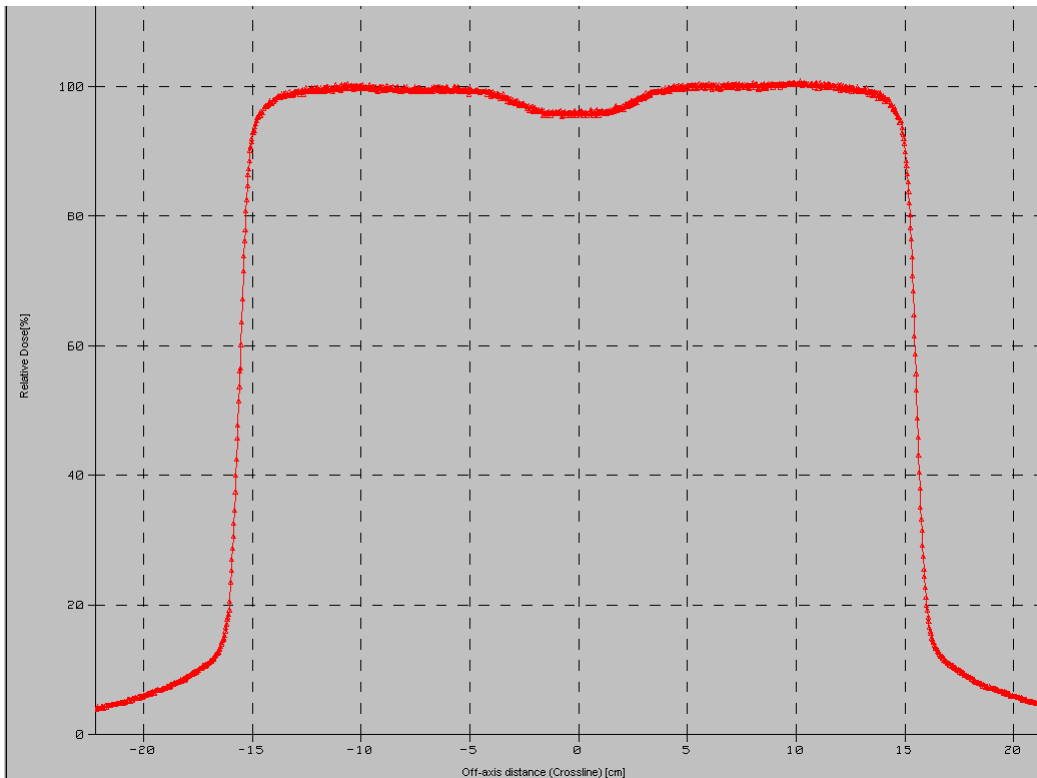


Figure 2–11: A typical transverse photon beam profile.

Amongst them, the important ones are central axis percentage depth doses (usually referred as percent depth dose or PDD) and transverse beam profiles. A typical PDD is shown in figure 2–10. It represents the variation of the dose with respect to the depth in a phantom (in the form of a percentage). They are used to determine to depth of maximum dose, or dose at any other depth, and thus act as beam quality quantifiers for both photon and electron beams. They can be measured using several dosimetry systems but ionization chambers represent the preferred method. Transverse profiles show dose variation in the lateral or

longitudinal direction with respect to the general direction of the beam. A typical transverse profile for an open photon beam is shown in figure 2-11.

CHAPTER 3

Film dosimetry system

A dosimetry system comprises the radiation sensor (dosimeter) and also the analytical methods that relate the radiation-induced signal to the absorbed dose at a location in a given medium. [57] In this chapter the radiochromic film dosimetry system that was used for this research will be described.

3.1 Film dosimetry system

A film dosimetry system consists of the particular film model used, the film readout system (densitometer), and the protocol to determine the calibration curve and dose reading from the film. This can be considered to be a reference dosimetry system when used under reference conditions and using a reference radiation beam for calibration. A reference dosimetry system, be it ion chambers, thermo-luminescent detectors, MOSFET detectors, or any other type of dosimetry system, measures absolute dose following a protocol determined at calibration under reference conditions. In our case the film model used is EBT-2 GAFCHROMIC™ (which will be referred to as EBT-2 for the rest of this text)¹ film with the Epson Expression 10000XL flatbed document scanner². A reference

¹ International Specialty Products, Wayne, NJ

² Seiko Epson Corporation, Nagano, Japan

radiation beam is a radiation beam calibrated following an accepted reference dosimetry protocol such as AAPM TG-51: Protocol for Clinical Dosimetry of High-Energy Photon and Electron Beams [3].

3.1.1 Film

The particular film model used is an essential part of the film dosimetry system. The film dosimetry system is calibrated as a whole and needs to be calibrated for every film model one wishes to use. The particular film model used is EBT-2: section 3.2 provides a more detailed review of its particularities and characteristics.

3.1.2 Film readout system

Different instruments can be used to perform two-dimensional film dosimetry such as single-point densitometer, one- or two-dimensional position sensitive light detector densitometers, and flat-bed document scanners with the option to operate in transmission mode. [28] The later has recently become more widely used as it allows significant cost reduction when compared with the more traditional laser densitometry system (single-point densitometer). The discussion will therefore be geared towards this type of film readout system.

Light source

A light source is required to read the transmission of films. Traditional scanning densitometers typically have a small diameter He-Ne laser which operates at a wavelength of 633 nm. [17] Flatbed document scanners contain a long fluorescent light source and thus emit light in a wide spectrum of wavelengths. This spectrum usually incorporates wavelengths from the UV region. For the

EBT film model, exposure to UV light was more of a problem as it was more sensitive than the EBT-2 model. It has been shown that for the EBT-2 model even the exposure to scanning light from more than a thousand scans brought no noticeable change in the optical density if the temperature of the scanner bed is kept constant. [52]

Light detection

When measuring transmission one measures the amount of light that was transmitted and compares it with the amount of light detected when the absorbing medium is not present. For laser scanning densitometers photodiodes are used as detectors and are optimized for the wavelength at which the light source emits. In a flatbed document scanner a moving CCD array is used and it moves together with the light source along the perpendicular direction of the CCD array/light source axis. One has to keep in mind that for such a system the detected signal is the value of the absorbance averaged over the wavelengths of the light source and weighted by the spectral response of the detectors. For the flatbed system the signal is also a spatial average over the area of the detector (single CCD).

Signal and spatial resolution

The spatial resolution in such a system is a quantity that can be more or less controlled by the user. For a flatbed document scanner system the user can specify the dot per inch (dpi) thereby altering the image resolution. The pixel size can be determined using the inverse of the dpi. The Epson 10000XL flatbed document scanner is capable of a maximum resolution of 2400 dpi which corresponds to 10.6 μm pixels. The output signal of the flatbed document scanner represents a

measure of the transmission. As the flatbed document scanner is connected to a computer the transmission is thus converted to a specific shade value. The more shade values in the scale, the more precise the reading will be. An 8-bit image for example has 256 shades of color intensity. Current flatbed document scanners are capable of acquiring data in 16-bit format for each of the three color channels (when acquiring in color mode) for a 48-bit color image (or 65536 shade values for each color channel). However a single color channel is typically used at a time for analysis (see section 3.2.2).

Other components

Flatbed document scanners possess a bed on which the film is positioned prior to reading. This bed is made of a clear glass plate and may contain defects. It is important to quantify the uniformity of the bed by performing regular background scans (empty bed) to identify defects to the surface that may induce error in film reading. Other components of the film dosimetry system includes phantoms, film mounting jigs and the scanner control software.

3.2 Radiochromic films: how do they work?

Radiochromic films are media that change color when irradiated. The radiochromic reaction for a particular film model (MD-55-1) has been investigated by McLaughlin *et al.* using flash photolysis and pulse radiolysis. [60] They found that the radiochromic reaction is a solid-state polymerisation in which the film undergoes progressive 1,4-*trans* additions, producing a polyconjugated polymer chain (polyacetylene dye polymers) which exhibits the blue colouration from radiation exposure. The blue coloration of the produced polymers cause the film

to absorb light preferably in the red part of the visible spectrum (see figure 1–1 on page 4). The reaction for EBT emulsion (EBT and EBT-2 film model) is a bit different in that the chromophores (the part of a molecule that is responsible for its color) are needle-like microcrystals about $1\ \mu\text{m}$ to $2\ \mu\text{m}$ in diameter and $15\ \mu\text{m}$ to $25\ \mu\text{m}$ in length. [68]

3.2.1 Constitution

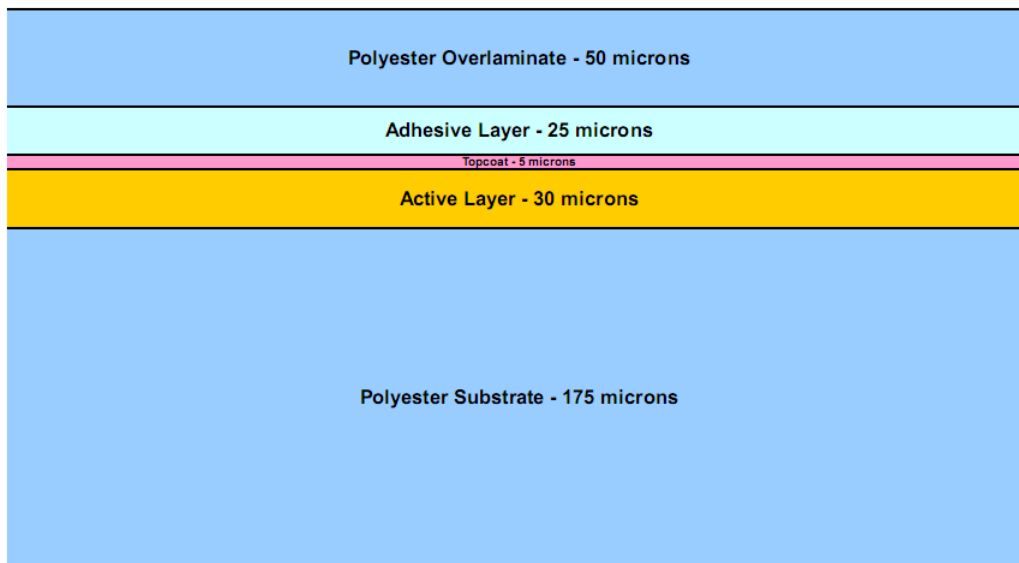


Figure 3–1: The EBT-2 gafchromic film model structure (figure from [69]).

The structure of the radiochromic film model EBT-2 can be seen in figure 3–1. As one can see it consists of a $50\ \mu\text{m}$ thick polyester overlamine, a $25\ \mu\text{m}$ thick adhesive layer, a $5\ \mu\text{m}$ thick topcoat layer (also called surface layer), a $30\ \mu\text{m}$ thick active layer, and finally a $175\ \mu\text{m}$ thick polyester substrate. The polyester overlamine and the polyester substrate are the same material but denoted differently to differentiate its position in the film structure. Note that this

Table 3–1: The chemical composition of the different layers of the radiochromic EBT-2 film model. Note that the active layer contains trace of nitrogen (N), potassium (K), bromine (B), and sulfur (S).

Layer	Thickness (μm)	Density (g/cm^2)	Compostion (% atom)				
			H	Li	C	O	Cl
Polyester film base	50	1.35	36.4	0.0	45.5	18.2	0.0
Adhesive	25	1.2	57.1	0.0	33.3	9.5	0.0
Topcoat	5	1.2	56.9	0.9	25.7	15.6	0.0
Active layer	30	1.2	58.3	0.8	29.6	10.7	0.3
Polyester film base	175	1.35	36.4	0.0	45.5	18.2	0.0
Overall composition	285	(-)	40.85	0.10	42.37	16.59	0.04

model is not symmetric, hence the need to differentiate between the *top* (polyester overlamine layer) and the *bottom* (polyester substrate layer). This can be done by observing reflection: the bottom surface of the film reflects a blurry image when compared to the clear reflection obtained by reflecting fluorescent light from the top film surface. The chemical composition of the different layers that compose this film model is listed in table 3–1. Its effective atomic number calculated by the method shown in McCullough and Holmes [56] gives a value of 6.84 while its density is $1.2 \text{ g}/\text{cm}^2$, values comparable to that of water (effective atomic number 7.42, density $1.00 \text{ g}/\text{cm}^2$) and soft tissue (7.22 and $1.00 \text{ g}/\text{cm}^2$ respectively depending on the type of tissue). [43] Thus one can claim that this film model is near tissue equivalent representing an excellent property for a dosimeter.

3.2.2 Absorption spectrum

Figure 3–2 shows the absorbance spectra of the most recent models of radiochromic films (EBT and EBT-2). From the absorbance spectra (figure 3–2(a))

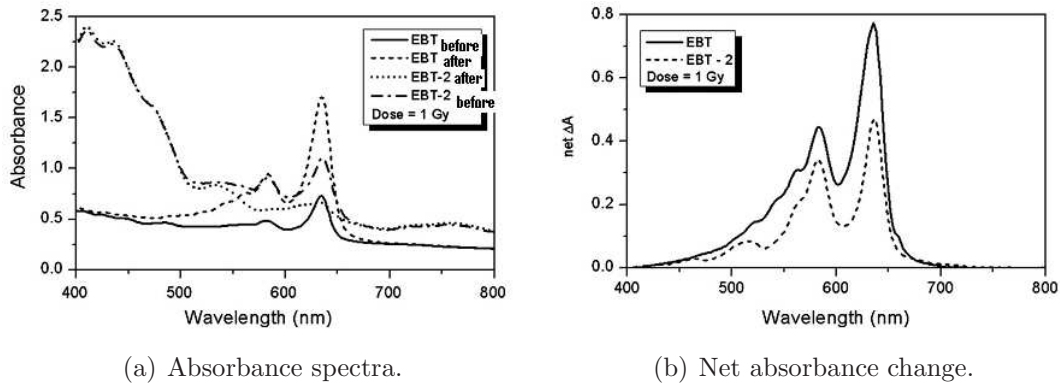


Figure 3-2: This figure shows the absorption spectra of the EBT and EBT-2 film model. (a) Shows the absorbance spectra of both film models prior to irradiation (subscript *before*) and post irradiation (subscript *after*) of a 1 Gy dose. (b) Shows the resultant net absorbance change of the two film models (figures from [26]).

one can see that both models exhibit a sharp absorption peak at a wavelength of 635 nm which is in the red part of the visible light spectrum. This has been proven in the past for the EBT film model [14, 30, 81] and it was also proven recently that the replacement model of EBT (EBT-2) exhibits the same absorbance peak [26]. Also the EBT-2 film model features a pronounced absorption band in the blue part of the spectrum. This is due to the addition of the yellow marker dye in the film composition which is meant to correct for film inhomogeneities. Figure 3-2(b) demonstrates, as the manufacturer claims, that the addition of the yellow marker dye does not affect the dosimetric properties of the film since the absorption peaks are at similar wavelength for both types of films.

One would certainly want to make use of the absorption peak of radiochromic films and it would be quite easy with a densitometer emitting at a single frequency matching the absorbance peak of the films. However most clinical film dosimetry

systems use flatbed document scanners as densitometer. As mentioned in section 3.1.2, a flatbed document scanner used as a densitometer must have the ability to operate in RGB transmission mode. When using this mode and the appropriate file type (see section 3.4.3), one can separate the different color channels of the image and use them separately for analysis. This permits the usage of the red color channel only to obtain transmission values [5, 7, 11, 28, 53, 75]. Note that it has also been shown that using the two other color channels for analysis one could extend the usable dose range of radiochromic films up to 100 Gy [31]. However for clinical dose ranges the red channel part of the image is sufficient to derive an accurate dose measurement. [30]

3.2.3 Post-irradiation coloration of radiochromic films

Due to the nature of the emulsion process, radiochromic films undergo a post-irradiation coloration that can be up to a few percent depending on how much time passes between the irradiation and the digitization process. It has been shown that darkening of the film is of the order of 1% for the first 6 hours post-irradiation [18] and it was not observed to cease for up to 4 months [37]. However, it has been shown that using a calibration curve built with measurements that were performed in the same time window as an unknown measurement, it is possible to obtain results, with a dose error of the order of 1%, for the measured dose. [26]

3.2.4 Linearity

The linearity of a dosimeter is an important feature. Ideally one would want a dosimeter that has a reading that can be linearly related to the measured dose

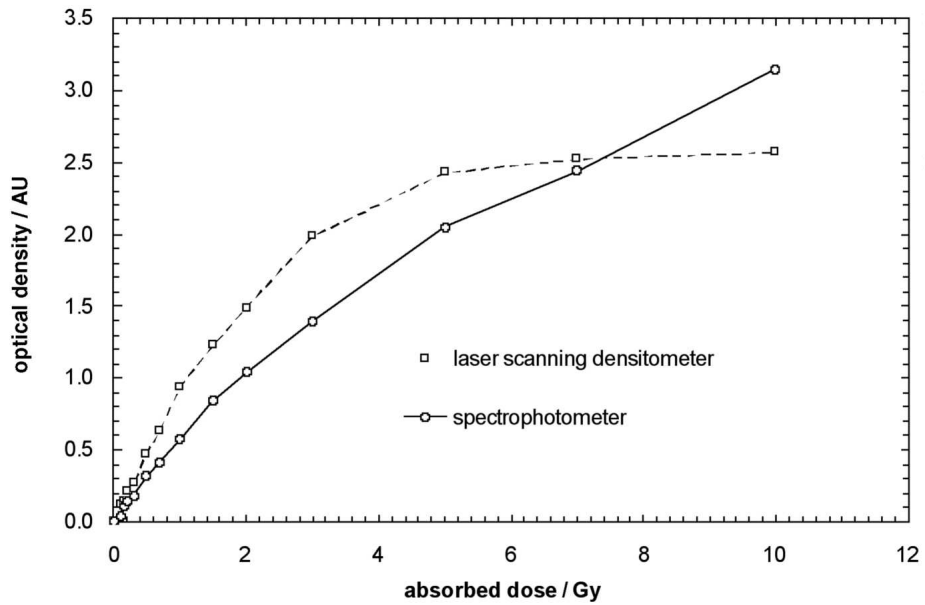


Figure 3-3: Comparison of the response for the EBT film model between a spectrophotometer and a laser scanner (figure from [80]).

that is:

$$D = k \cdot M \tag{3.1}$$

where D is the measured dose, M the reading from the dosimeter, and k a constant that relates the dosimeter reading to the measured dose. Radiochromic films have a fairly linear response when read with a high quality spectrophotometer. However they tend to lose that linearity in the high optical density region (high dose region) when read with lower quality densitometer such as laser scanners and flatbed document scanners (see figure 3-3).

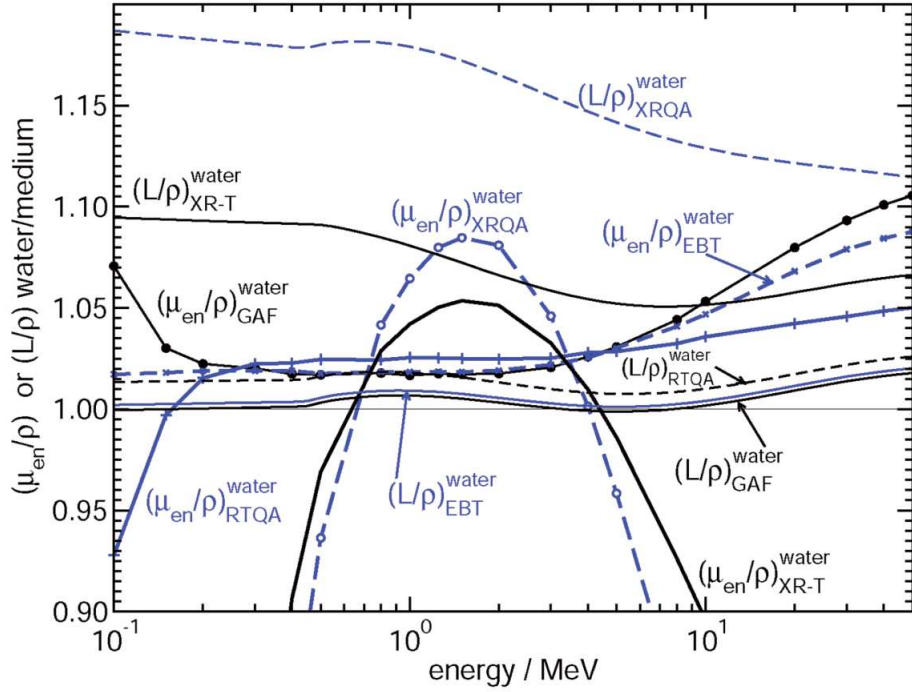


Figure 3-4: Mass collision stopping-power ratios and ratios of mass-energy absorption coefficients for the sensitive materials in radiochromic films relative to water (figure from [80]).

3.2.5 Energy dependance

The energy dependence of a dosimeter is of great concern when considering its particular application. The intrinsic energy dependence of all radiochromic film models are expected to be constant and independent of energy as there is a certain minimum energy required to polymerize the diacetylene molecule (less than 1 keV). As for the absorbed-dose energy dependence, the EBT and EBT-2 film models are supposed to be energy independent when used in the energy range 50 kVp to the MV range. In fact the energy dependence has been shown to be very weak by different studies in the energy range 100 kVp to 18 MV. [15, 22, 76]

Since both EBT and EBT-2 models have the same emulsion layer it is expected that the energy dependence is the same. In fact when calculating the stopping-power ratios and the mass-energy absorption coefficients for the active layer of the film, the results compare well with water as demonstrated in figure 3–4. In the region where the photoelectric effect dominates (photon energies below 100 keV), the effective atomic number (effective Z) is an indicator of water equivalence while in the region where the Compton effect dominates (photon energies greater than 100 keV), the electron density (N_e) is an indicator of water equivalence. As one can see in figure 3–4, the EBT emulsion films are the most water equivalent type as its ratios of mass collision stopping-power and mass energy absorption coefficients are the closest to one throughout the energy spectrum.

3.2.6 Dose-rate dependence

Typically radiochromic films are assumed to be dose-rate independent based on work with ^{60}Co beam irradiations on the MD-55-2 film model by McLaughlin *et al.* [58] In fact it was shown that there is no relevant dose-rate dependence over the clinically relevant dose rate range of 2 Gy/min to 4 Gy/min. [17] This is another advantage of radiochromic films over other dosimetry systems.

3.2.7 Film non-uniformity

The uniformity of the film is the principal common limitation of all radiochromic film models. The films show varying sensitivity from lot to lot and even within the same film lot due to the coating process. This causes the emulsion layer to be varying in thickness and hence the films show varying sensitivity. Several methods to compensate this effect have been proposed such as the double-exposure

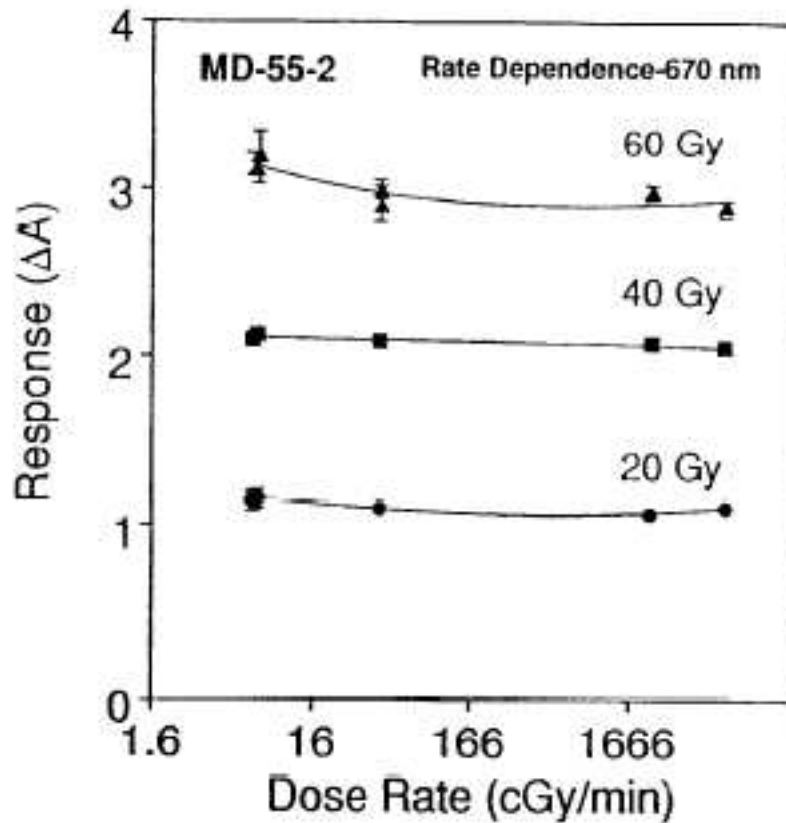


Figure 3-5: The response of the radiochromic film model MD-55-2 for different doses at different dose-rate measured at a wavelength of 670 nm (figure from [58])

method. [96] In this technique, one pre-irradiates the films to a uniform known dose and reads the films to detect uniformity variations. A pixel-by-pixel correction can be determined, if the two images can properly be co-registered, and the films are then used to perform a measurement. This correction is effective if the non-uniformities are greater than the pixel noise of the system. Note that this

correction might actually bring greater errors to the measurements if the film-uniformity is less than the amount of errors implicated by scanning the films twice and co-registering the resultant images.

The improvement in the manufacturing techniques for the EBT model helped reduce the variation in thickness of the emulsion layer. However, with the recently introduced EBT-2 film model the manufacturer claims to have improved the uniformity by adding a yellow marker dye to the sensitive layer of the film and by replacing gelatin as the binder component in the coated layers of the other film models by a synthetic polymer for which the composition can be controlled more thoroughly. The yellow dye is meant to be used with a flatbed document scanner. When scanning the film, the marker dye makes it possible to obtain a signal that is proportional to the thickness of the active layer and thus compensates for small uniformities that could be present. Since the dye is of yellow color, it produces its signal in the blue channel of the image leaving the red channel for the dose analysis. See 3.2.2 for more information on color channels and film analysis.

3.3 Uncertainties in radiochromic film dosimetry systems

There are many sources of uncertainties to consider when performing measurements with radiochromic films. These uncertainties can be summed up in five major categories as presented in 3–2: film manufacturing, film manipulation, irradiation process, digitization process (scanning), and film characterization. They can also be categorized as type A or B uncertainties. Type A uncertainties can be evaluated by a statistical analysis of series of observations while type B uncertainty

Table 3–2: Sources of uncertainties for radiochromic film dosimetry systems

Source	Type	Dependance	
		on OD	on ROI
Film manufacturing			
Emulsion homogeneity	B	no	yes
Perturbation effects and energy dependence	B	no	no
Temperature and humidity dependence	B	no	no
Sensitivity to light	B	no	no
Stabilization of chemical reaction	B	no	no
Film manipulation			
Foreign bodies	B	no	yes
Storage environmental conditions	B	no	no
Irradiation process			
Stochastic nature of dose deposition	B	yes	yes
Measurement setup uncertainty	B	no	no
Linac output reproducibility	A	no	no
Dose variation within region of interest	B	no	no
Digitization process			
Stochastic nature of optical photons detection	B	yes	yes
Scanner homogeneity	B	no	yes
Scanner reproducibility and stability	A/B	no	no
Numerical manipulation	B	no	no
Film characterization			
Calibration curve uncertainty	B	no	yes

can be evaluated by means other than the statistical analysis of series of observations [8]. First there are uncertainties associated with the film manufacturing and intrinsic properties of the films. In this category the emulsion homogeneity is the first one that comes to mind. This uncertainty can be reduced by making use of the yellow marker dye incorporated in the film. Also, increasing the size of the ROI over which one performs the average helps reducing this uncertainty. There are also perturbation effects and energy dependence. These are usually ignored since they are small. However one could consider building a calibration curve if one plans to perform measurements in the low energy range. Then there is the

temperature and humidity dependence of the film during the digitization process. The scanner is warmed up with several pre-scans in order to bring the temperature of the scanner bed to a working (stable) temperature. Humidity in the room should be kept constant. The sensitivity to light is also ignored as films are kept in opaque envelope except when manipulating them. Also the EBT-2 model is 10 times less sensitive to light than its predecessor. The stabilization of the chemical reaction (post-irradiation coloration) error is controlled by scanning the irradiated radiochromic films 24 hours post-irradiation. Note that this is not always practical in a clinical environment and it has been shown that using a different calibration curve for each time window that is used is possible if one is willing to sacrifice a bit of accuracy [26].

The next category of uncertainties to consider is from the film manipulation. One has no choice but to manipulate the films to perform a measurement. In order to reduce the presence of foreign bodies such as dust, scratches, fingerprints, or folded edges, one should always use gloves during manipulation of the films. Films can also be cleaned using alcohol (being careful not to remove the labeling) if they are swiped right away to get rid of dusts and fingerprints. The films should always be cut with a framed paper cutter for the straightest edges possible if the application permits it. When using film pieces in water, one has to limit the exposure to water to a strict minimum to minimize water infiltration. It has been shown for the EBT-2 film model that a prolonged exposition time to water (24h) can lead to water penetration of up to 9 mm within the film edges and affect the measured value if digitization is performed a short time after the exposition.

However an exposition of up to 30 min to water and a sufficient waiting period between the water exposition and digitization (of the same order as the exposition time) should not introduce additional errors. [2] The storage environmental conditions are crucial for radiochromic films. Even though the manufacturer claims that the effects from environmental conditions are very small, it is always recommended to keep the films in a controlled environment (room temperature and low humidity).

The third category is the uncertainties associated with the irradiation process. The stochastic nature of the dose deposition process can be quantified using Monte Carlo methods. It has been shown that using a $1 \times 1 \text{ mm}^2$ minimum size as a region of interest renders this uncertainty negligible compared to the total uncertainty [11]. Then there is the measurement setup uncertainty which can be neglected if the setup is simple enough. It is however to be considered for more complicated applications (setup such as calibration curve measurement is a simple setup while a setup for *in vivo* skin dose measurement is more complicated). The linac output reproducibility which is a type A uncertainty can be reduced by using a monitor ionization chamber during the measurement (whenever possible). The dose variation uncertainty within the region of interest can be reduced by using the flattest dose profile within the region of interest whenever possible.

The fourth category is the digitization process. This category is governed by the stochastic nature of the photon detection process. The uncertainty from this process can be reduced using a large enough ROI (the $1 \times 1 \text{ mm}^2$ minimum ROI is still sufficient). The scanner homogeneity is also an issue but can be

accounted for by using correction curves as explained in section 3.5.2. The scanner reproducibility and stability (dark noise, readout noise, scanner mechanics, lamp stability, Newton rings) is an uncertainty source that can be reduced by taking an average of multiple scans for each reading. It has been shown that a number of 5 scans is what reduces the uncertainty from this source to a minimum and that averaging more (or less) scans increases the uncertainty [29]. The numerical manipulations such as rotation and co-registration are also a source of uncertainty but can be neglected if kept to a minimum. In fact it has been shown that a variation of up to 15% in the measured value can be observed for films that are measured with a rotation (maximum deviation observed is for a rotation of 90°) when compared with a completely straight film position on the scanner bed. [52]

Finally the use of a calibration curve adds to the total uncertainty of the measurement. This source of uncertainty can be kept small by using a large number of points to characterize it. In fact Bouchard *et al* [11] recommends the use of at least 12 points for the characterization of the calibration curve or 35 points for an optimal result (see section 3.4.4). [11, 29, 31, 52, 55, 74, 77]

3.4 Protocols

In the following section the protocols for both obtaining a calibration curve and measurement of an unknown dose will be described. It assumes usage of the most recent film model from International Specialty Products, GAFCHROMIC EBT-2(®), and a high-quality flatbed document scanner such as the Epson Expression 10000XL.

3.4.1 Film preparation

Radiochromic films have the advantage of not being altered very much when cut. Only the edges de-laminate a little so one has to be careful to select a region of interest accordingly. Thus one can use small pieces cut to any shape to adapt to his specific applications. The EBT-2 model is available in sheets of size of 8 inches by 10 inches in box of 25 sheets, or size of 14 inches by 17 inches with 10 sheets per box. Depending on the desired application the user can order the size that fits his needs. One has to first prepare the films by cutting the sheets according to the desired application and labelling them using a permanent marker, preferably at the bottom or in a corner where no measurement will be performed on the film. See section 3.4.5 for information on how to properly handle and store radiochromic films. Note that radiochromic films have preferable polymerization direction due to the needle-like shape of the polymers and thus they must be scanned in the same direction (movement of the scanner light) every time. This scanning direction is chosen during the calibration procedure and must be kept constant throughout every measurement performed using a particular calibration. Thus one either cuts the films in a rectangular shape or draws a sign (such as an arrow) to indicate the scanning direction that must be observed.

3.4.2 Control film piece

As mentioned in section 3.3, different environmental conditions and manipulations affect the film pieces. A simple way to quantify these effects is with the use of a control film piece. This film piece is simply a film of the same lot as the measurement films that is kept in the exact same conditions as the measurement

films. It is also manipulated in the same way and is exposed to the same amount of light as the measurement films. Thus by measuring the net optical density change on the control film piece one can quantify the net optical density change due to the environmental conditions and significantly improve the accuracy of the measurement.

3.4.3 Film scanning

Proper scanning of the radiochromic film is a very important part of the film dosimetry protocol. Note that the scanning technique is the same in either the scanning of the films prior to irradiation or post-irradiation, thus the same scanning protocol applies to both situations. Scans are made before and after exposure and involves manipulating the films (see section 3.4.5 for details). Once the films are cut and labeled, the flatbed document scanner must be warmed up in order to bring the bed temperature to its operating value. It was shown that a warm-up of 7 successive scans of the empty scanner bed was sufficient to bring the temperature to an acceptable level [75]. The film pieces are then positioned in the center of the scanner bed in a manner to be sufficiently far from the edges. Multiple small film pieces can be scanned simultaneously but there must sufficient distance between the films to be able to make a mouse selection (drawing a rectangle around it with a computer mouse) in order to analyze the scans properly (see section 3.5.1). Also one should note that a lateral correction is applied to films that are larger than 5 cm in order to get a proper transmission reading (see section 3.5.2). During the post-irradiation scan one should be careful to reposition the film on the bed with the same position used in the pre-irradiation scan so as to reduce

scanner non-uniformities. Note that films must be positioned on the scanner bed according to the chosen scanning direction in the calibration process. Also the new radiochromic film model is asymmetric and must be scanned on the same side every time. The side can be determined by observing the reflection of light on the film surface (blurry on one side and clear on the other side).

Once the film is properly positioned on the scanner bed it is scanned five consecutive times in order to reduce scanner noise by subsequent averaging of the images [29]. The scans are performed using the flatbed document scanner control software called *Epson Scan* using its transmission mode in 48-bit color. All automatic corrections are turned off and the files are recorded in the tagged image file format³ (**.tiff**). The resolution is typically set to 127 dpi (dot per inch) as this corresponds to 0.2 mm per pixel. The scans are performed and stored for the whole scanner bed surface making it easy to apply a correction matrix whenever necessary. Giving the files descriptive and intuitive names is a good practice to observe as one will end up with at least ten scans (five pre-irradiation and 5 post-irradiation) for each measurement performed.

3.4.4 Calibration curve of the radiochromic film dosimetry system

As a response to irradiation, radiochromic films undergo a change in color. This response can be expressed in terms of net optical density change (*netOD*), which represents the difference in optical densities of the same film piece sampled after and before irradiation. However when using a flatbed document scanner as

³ Adobe Systems Incorporated, San Jose, Ca.

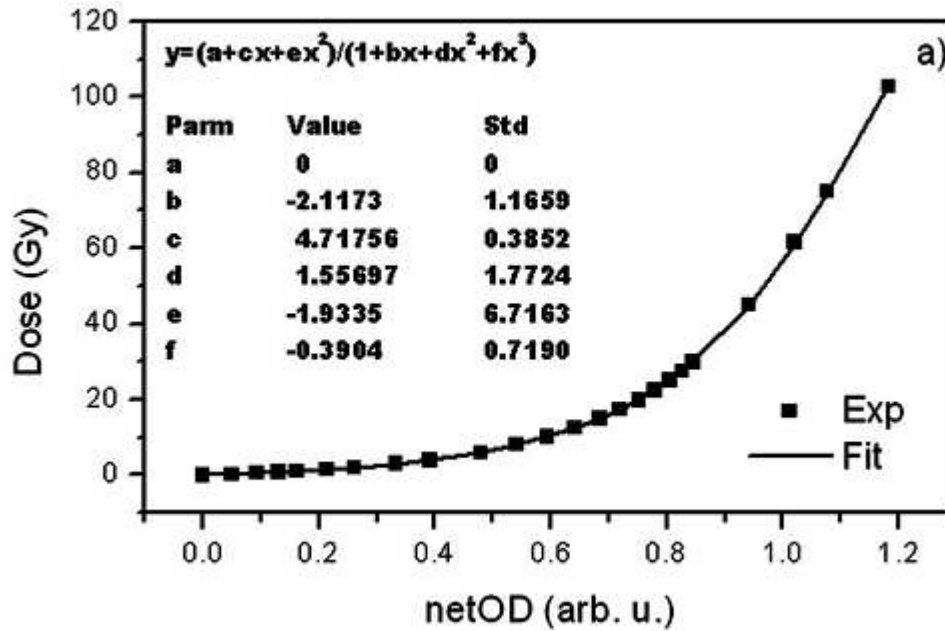


Figure 3-6: A typical calibration curve for the EBT film model (data from [31]).

part of the film dosimetry system, one typically reads pixel values that need to be subsequently converted to optical densities. Optical density is a value that is mainly inherited from the older radiographic film systems and attempts have been made to use a sole pixel value read from the document scanner to characterize the calibration curve of the radiochromic film dosimetry system. However in this document optical densities are used. The optical density is obtained as follows from transmission:

$$OD = \log \left(\frac{1}{T} \right) \quad (3.2)$$

where OD is the optical density and T is the transmission. When radiographic films were in use, the logarithmic conversion of the inverse transmission lead to a

linear relation between the films response (optical density) and dose in a relatively narrow range of doses that were used for most clinical applications. While using optical density to characterize the calibration curve of the radiochromic film dosimetry system, one retains the almost linear behavior of the curve having to add non-linear terms to take into account inherently non-linear response of the film. When using the pixel values only, it results in a pronounced non-linear behavior which will in turn lead to much higher uncertainties of such established radiochromic film dosimetry systems due to larger fitting uncertainty contribution. Also one has to remember that the optical density is a function of the wavelength at which the absorbance was sampled. When one uses densitometers that employ broad band fluoroscopic visible light sources, optical density change (*netOD*) is a rather complex convolution of the film absorption spectrum, the linear CCD array sensitivity spectrum and the emission spectrum of the fluorescent light source of the scanner as shown by the following equation:

$$netOD = \log \left(\frac{I_0}{I} \right) = \log \left(\frac{\int_{-\infty}^{\infty} E(\lambda) \cdot S(\lambda) d\lambda}{\int_{-\infty}^{\infty} E(\lambda) \cdot A(\lambda) \cdot S(\lambda) d\lambda} \right) \quad (3.3)$$

where $E(\lambda)$ is the emission spectrum of the light source, $A(\lambda)$ is the absorption spectrum of the measured film, and $S(\lambda)$ is the sensitivity spectrum of the detectors. Therefore the sensitivity curves for every particular radiochromic film dosimetry will be different from one another even while measuring the same set of calibration films.

The calibration curve for the radiochromic film dosimetry system is obtained by irradiating a set of films to different known doses and fitting a curve through

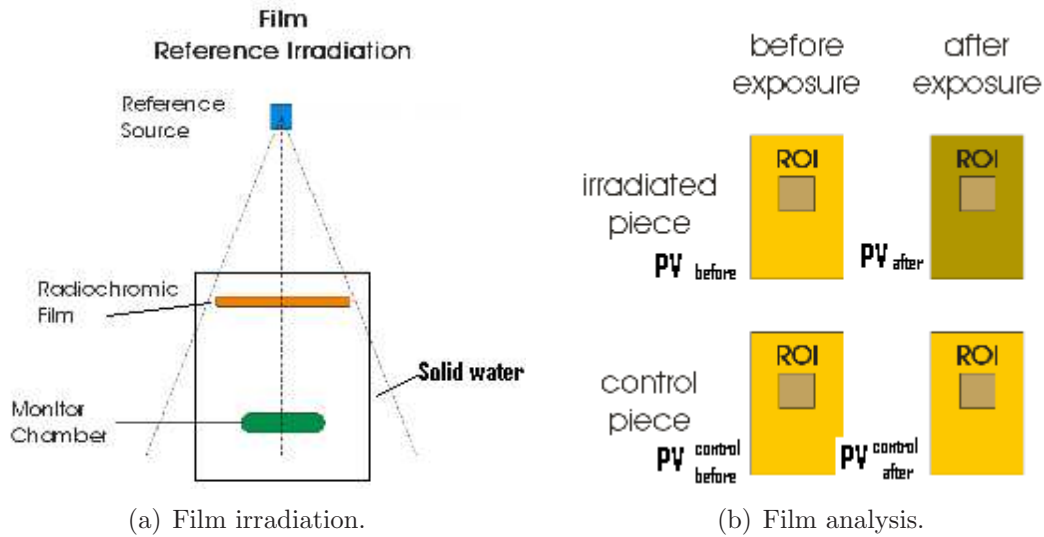


Figure 3-7: The experimental setup for obtaining the calibration curve of the radichromic film dosimetry system. (a) Shows the positioning of the film pieces under a reference beam with the monitor chamber below the film while (b) shows the regions of interest (ROI) on both an irradiated film piece and the control film piece (before and after irradiation, the top film pair being the irradiated film piece and the bottom film pair being the control film piece).

the set of data. The calibration curve needs to be determined for each lot of films due to possible variation in film sensitive layer thickness from lot to lot (see section 3.2.1). Typically the calibration curve is energy independent for megavoltage beams (see section 3.2.5) so the calibration can be performed under any reference beam of such energy. The films are scanned prior to irradiation to obtain the initial optical density reading from each film. Also a control film piece is kept under the same conditions as the other film pieces and will be used to determine a correction for any changes in absorbance due to environmental conditions, e.g., temperature, visible light, humidity, scanning light, etc. The films are then setup for irradiation as shown in figure 3-7(a). The phantom material used is

solid water and the reference dosimeter is typically an ionization chamber. The different film pieces are irradiated to a set of known doses such that the range of doses corresponds to the range of doses of the application that one wants to use the radiochromic films. For clinical purposes a range of doses would be from 0 Gy (unirradiated film piece) to 4 Gy. The reference dosimeter in the setup monitors the delivery of the beam and the correct delivered doses are determined using the reading from the reference dosimeter. The films are then scanned in order to get the optical density of the irradiated film pieces. Note that to get a proper net optical density one has to co-register the non-irradiated film data and the irradiated film data such that the optical density is taken from the same region of interest (ROI) in both scans as shown in figure 3–7(b). This is done by using image processing techniques explained in section 3.5.1. For film pieces with uniform dose distribution such as the calibration film pieces, the transmission data is obtained by averaging the transmission value over a ROI to minimize the error.

When one has digitized the irradiated film pieces and the control film piece the transmission data can be obtained using the unirradiated film pieces previously digitized. The net optical density can be obtained using the transmission data acquired from the unirradiated film piece and the irradiated film piece using:

$$netOD = \log_{10} \left[\frac{I_{unexp} - I_{bckg}}{I_{exp} - I_{bckg}} \right] \quad (3.4)$$

where I_{unexp} is the transmission value of the unexposed film piece, I_{exp} is the transmission value of the exposed film piece, and I_{bckg} is the background reading of the scanner that is the transmission value obtain when scanning a completely

opaque material (dark signal). The net optical density from the control film piece is then subtracted to correct for the environmental conditions and film manipulations. Using the net optical density values of all irradiated films and knowing the doses to which the film pieces were irradiated, one can construct a calibration curve which will allow one to calculate an unknown dose from a net optical density value obtain by irradiating a film piece following the film dosimetry protocol. The mathematical function used to fit the values of the curve should be chosen using the following conditions [11, 95]:

1. The function should cross $(0, 0)$,
2. The function should be strictly increasing,
3. The function should have zero or one point of inflection in the domain of interest, and
4. If the function has a point of inflection, it should occur between $0 \times NOD$ and $0.5 \times NOD$.

Also the function chosen should minimize fitting errors. Bouchard *et al* [11] provides a list of different function types that can be used to characterize the calibration curve.

The uncertainty obtained by using the calibration curve to measure an unknown dose is the minimum uncertainty that one will get when performing a measurement using the radiochromic film dosimetry system. If the application presents additional sources of uncertainties they are added to this minimal uncertainty to obtain a total uncertainty assessment of the measurement. The

uncertainty analysis for the calibration curve obtained for the film dosimetry system at the author's center is presented in the result section on page 71.

3.4.5 Handling precautions and other corrections

Many precautions are to be observed when using radiochromic films for dosimetric purposes. When handling films, gloves need to be used in order to keep fatty substances from human fingers from transferring to the film. Also the films need to be cleaned of any visible dirt or dust particles. This can be achieved using alcohol as a cleaning substance for the film pieces. One also has to minimize film handling to keep the surface from getting scratches. Films should be kept in an environment where the temperature does not fluctuate considerably and where the humidity is not too high. Films are shipped in a cardboard box and inserted in a light opaque envelope. Blank (unirradiated) films are to be kept in that envelope at all times except during manipulations to avoid unnecessary exposure to light even though, according to the manufacturer, this should not be a major concern. Note that when scanning film pieces one has to place them on the surface of the flatbed document scanner. There may be air gaps between the film and the surface which leads to interference patterns (Moiré patterns or Newton rings). Observing the output scan to identify such patterns and replacing the film on the bed if they are found is a good way to avoid such errors.

3.4.6 Summary of radiochromic film measurement protocol

Once a proper protocol is in place, measurements using radiochromic films are performed following rather simple steps. This is a summary of how the measurements have been performed in this work.

1. *Film preparation*: films are cut and labeled and a control piece is kept with the measurement film pieces,
2. *Scanning of pre-irradiated films*: films are scanned prior to irradiation (warm-up of scanner is performed beforehand),
3. *Measurements*: film pieces are irradiated,
4. *Wait time*: the waiting period is determined according to what was done in the calibration process,
5. *Scanning of post-irradiated films*: films are scanned after irradiation (again the warm-up of the scanner is performed beforehand),
6. *Corrections*: the lateral correction is performed,
7. *Image co-registration*: the pre- and post-irradiated film images are co-registered in order to take the same ROI on both scans,
8. *Transmission and environmental correction*: the transmission is found and the transmission from the control film piece is subtracted,
9. *Dose reading*: the calibration curve is used to find the dose from the measured transmission,
10. *Error analysis*: error analysis is performed on the measurement.

Note that as with any reference dosimetry system such as TLD dosimetry system or MOSFET dosimetry system, the radiochromic film dosimetry system comprises a dosimeter (film and scanner) and a procedure that is defined by the user of the dosimetry system which makes the system user dependant.

3.5 Software for analysis of films

The analysis of the films is performed using homemade functions in the Matlab software and programming language along with the *image processing toolbox*⁴. These are designed to perform mostly basic operations and automate many simple tasks. Some functions are explained but thorough descriptions of the codes are not provided in this text.

3.5.1 Film co-registration

Once the films are scanned, the region of interest (ROI) is defined and compared between the post-irradiation film and pre-irradiation film to get the net optical density as described in section 3.4.4. In order to compare the same ROI on both images they are co-registered together using edge detection. By using a Sobel operator and a Hough transform it is possible to detect the edges of the films (square or rectangular piece) with an accuracy of ± 2 pixels. The edges of the films are then used to properly select the ROI on both the unirradiated film piece and the irradiated film piece. These techniques are not discussed in the text as they are part of the Matlab software used for data analysis. Reference on how to use these techniques can be found in Gonzalez *et al* [40, 41]. Also markers (permanent pen marks) can be put on the films to perform the co-registration.

⁴ The Mathworks Inc., Natick, MA; software version R2008b8.

3.5.2 Applied corrections

Wiener filter

Some corrections need to be applied for increased accuracy in the measurement of dose using radiochromic film dosimetry system. For a single dose measurement on a film, one applies a Wiener filter to the ROI after averaging the scans and selecting the desired ROI. This type of filter is applied to decrease the noise caused by the imperfections in the film piece. [29]

Lateral correction

The scanner response to an optical density is not uniform over the whole scanner bed. Along the scanner direction the response stays within an acceptable uniformity difference of less than 1% although one may want to avoid the extreme edges of the scanner bed. In the direction perpendicular to the motion of the scanning light/CCD detectors, variations of up to 6% can be observed depending on the optical density read. However this effect can be accounted for as the discrepancies from the value in the center of the scanner bed presents a quantifiable shape. Thus measurements can be made to obtain the correction curves for different optical densities with respect to the position along the axis perpendicular to the motion of the detecting devices in the scanner (short edge of the scanner bed). This correction is applied for every film piece digitized. This is particularly important for IMRT films as they tend to be of the order of 20 cm on this side of the film. This effect has been quantified for our film dosimetry system and the results can be seen in section 4.1.3. [11, 35, 55, 61, 74]

CHAPTER 4

Results

In this chapter the results for the characterization of the radiochromic film dosimetry system are presented. Different measurements performed using the radiochromic film dosimetry system are also presented such as *in vivo* dose measurements and quality assurance measurements.

4.1 Radiochromic film dosimetry system

4.1.1 Calibration curve

A calibration curve for the GAFCHROMIC EBT-2 film lot# A041510-01B was obtained using the protocol explained in section 3.4. A total of 36 films were used for the characterization of the calibration curve. Table 4–1 on page 72 shows the films along with the planned doses and the corrected doses obtained with the reference ionization chamber. Note that in this table MU delivered represents the number of monitor units delivered by the linear accelerator and $M_{\text{corrected}}$ the reading from the ionization chamber (corrected for temperature and pressure). The measurements were performed using an Elekta Synergy and this accelerator is calibrated using the reference dosimetry protocol TG-51 [3]. It is also the linear accelerator that is used for our IMRT cases and the most stable linear accelerator in our center. The films are positioned at a 5 cm depth in solid water with 10 cm backscatter material (also solid water). Then the ionization chamber is positioned (at a depth of 15 cm) and another 10 cm of solid water is added as backscatter

Table 4-1: Measurements performed for the calibration curve.

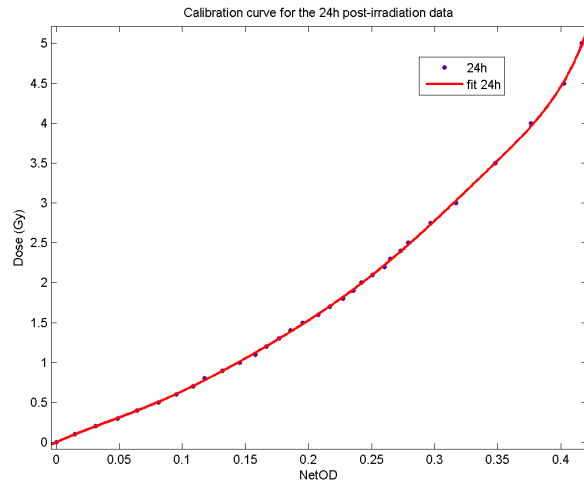
Film #	Planned dose (cGy)	MU delivered	$M_{\text{corrected}}$ (nC)	Corrected dose (cGy)
0	0	(-)	(-)	0
1	10	12	1.3891	0.0985
2	20	24	2.7706	0.1964
3	30	37	4.2718	0.3028
4	40	49	5.6522	0.4006
5	50	61	7.0352	0.4987
6	60	73	8.4210	0.5969
7	70	86	9.9168	0.7029
8	80	98	11.3070	0.8015
9	90	110	12.6936	0.8998
10	100	122	14.0749	0.9977
11	110	135	15.5869	1.1048
12	120	147	16.9565	1.2019
13	130	159	18.3333	1.2995
14	140	171	19.7208	1.3979
15	150	183	21.0726	1.4950
16	160	196	22.5753	1.6016
17	170	208	23.9795	1.7012
18	180	220	25.3569	1.7989
19	190	232	26.7522	1.8979
20	200	245	28.2548	2.0045
21	210	257	29.6502	2.1035
22	220	269	31.0276	2.2012
23	235	281	32.3960	2.2983
24	240	294	33.9076	2.4055
25	250	306	35.2940	2.5039
26	275	336	38.7733	2.7507
27	300	367	42.3599	3.0051
28	350	428	49.4080	3.5051
29	400	489	56.4650	4.0058
30	450	550	63.5041	4.5052
31	500	611	70.5700	5.0064
32 (control)	0	(-)	(-)	0

material for the chamber. The irradiation is performed at a source-surface distance of 100 cm and the film are positioned in the center of a $30 \times 30 \text{ cm}^2$ 6 MV photon field. This part of the field was chosen because it is the flattest and delivers the most uniform dose. The films are then digitized at 7 different time intervals (time between the irradiation of the film and its digitization).

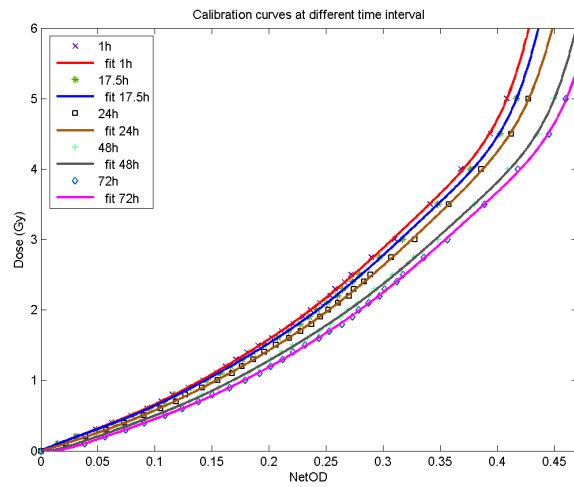
Table 4-2: Difference between the value obtained for a film piece irradiated to 200 cGy and scanned using the same time interval as with the different calibration curves and the value obtained for the film piece used to build the calibration curve.

Digitization from	Calibration curve waiting time						
	1h	2h30	17h30	20h	24h	48h	72h
1h	0.41%	1.61%	4.07%	6.46%	9.31%	17.97%	23.02%
2h30	-0.13%	0.46%	3.55%	5.95%	8.80%	17.51%	22.57%
17h30	-3.01%	-1.94%	0.21%	3.17%	6.05%	15.00%	20.11%
20h	-5.78%	-4.54%	-1.86%	0.22%	3.65%	12.82%	17.97%
24h	-9.60%	-8.34%	-5.52%	2.77%	0.16%	9.66%	14.87%
48h	-21.04%	-19.69%	-16.46%	-13.27%	-10.23%	0.30%	5.67%
72h	-27.60%	-26.21%	-22.74%	-19.28%	-16.16%	-5.03%	0.28

Shown in figure 4-1 are the different calibration curves for the different waiting periods between the irradiation process and the digitization process of the film pieces. Table 4-2 shows the difference in the value obtained for the 200 cGy film piece when using the different curves. As one can see the overall net optical density increases as time between irradiation and digitization increases. This phenomena is expected and explained in section 3.2.3. However, the differences observed when not respecting the time window for digitization are greater than expected. Post-irradiation coloration of the radiochromic films are reported to be about 1% in the first 6 hours and then another 1% from 6 hours to 24 hours. Then the coloration is supposed to increase only very slowly as time passes but



(a) 24h waiting period.



(b) Different waiting period.

Figure 4-1: The calibration curves for GAFCHROMIC EBT-2 lot # A041510-01B. (a) Shows the most used and recommended calibration curve that is the one for a 24h waiting period between irradiation and digitization. (b) Shows the variation in the calibration curves for different waiting periods between irradiation and digitization.

never really stabilizes. This can be observed in figure 4-1(b). As time increase, the net optical density increases and so does the general behavior of the calibration curve. However the results for a 2 Gy film piece (see table 4-2) indicate that using the improper calibration curve can lead to errors of up to 10% on the measured dose in a 24 hours time interval from irradiation to digitization. This is surprising since one expects only a 2% increase in the net optical density in that same time interval. Thus one should be very careful of respecting the time window during which the film should be digitized. Also if the film is digitized one or two days after the 24 hours time interval one can expect errors in the dose measurement in the range of 10% to 20%. From this study it is thus suggested to measure three calibration curves: one 1 hour post-irradiation for quick measurement of dose, one 24 hours post-irradiation for standard measurement of dose, and another 72 hours post-irradiation for problematic measurements (problem with the experiment, forgotten digitization or inaccessibility of the scanner). The calibration curve used for standard measurements for the film lot # A041510-01B is shown in figure 4-1(a). Unless specified, this is the calibration curve used to obtain the dose from net optical density of the films in the measurements presented in this document.

4.1.2 Uncertainty analysis

The uncertainty on the calibration curve, that is uncertainty from conversion of net optical density to dose, or fitting uncertainty, includes both the uncertainty from the digitization and net optical density measurement from the film, and the uncertainty from the conversion of the net optical density to dose itself. As explained in section 3.3, the net optical density measurement uncertainty from

the digitization of the film is optimal when one uses regions of interest (ROIs) that are at least 1 mm². Thus even if the film is digitized using 0.2 mm per pixel (127 dpi) it is subsequently averaged to 1 mm per pixel for analysis, except for certain applications. Also included in this uncertainty characterization is the film manufacturing uncertainties. The type of curve for the parametrization of the calibration curve was chosen such that it minimizes the uncertainty. With all these uncertainties in mind it was estimated that the uncertainty from the conversion of net optical density to dose was 0.35% and the uncertainty from the digitization process and film manufacturing also 0.35%. Thus the total uncertainty from the conversion of net optical density to dose was determined to be a total of 0.5%. This is in fact observed when using the very same setup to irradiate a 2 Gy film piece. This means that we can nearly neglect the uncertainty from the experimental setup as we are in the exact same conditions as when performing the experiment to characterize the calibration curve. As seen in table 4–2, the 2 Gy film piece with net optical density converted to dose using the proper calibration curve has a measured dose that is always within that 0.5% uncertainty (0.41%, 0.46%, 0.21%, 0.22%, 0.16%, 0.30%, 0.28%, for an average of 0.29%). Note that the uncertainty analysis for every case should be estimated separately. In any measurement performed, there will always be an uncertainty associated with the conversion of net optical density to dose as well as an experimental uncertainty (which estimates the uncertainties from the experimental conditions). These uncertainties must be added to each other in quadrature.

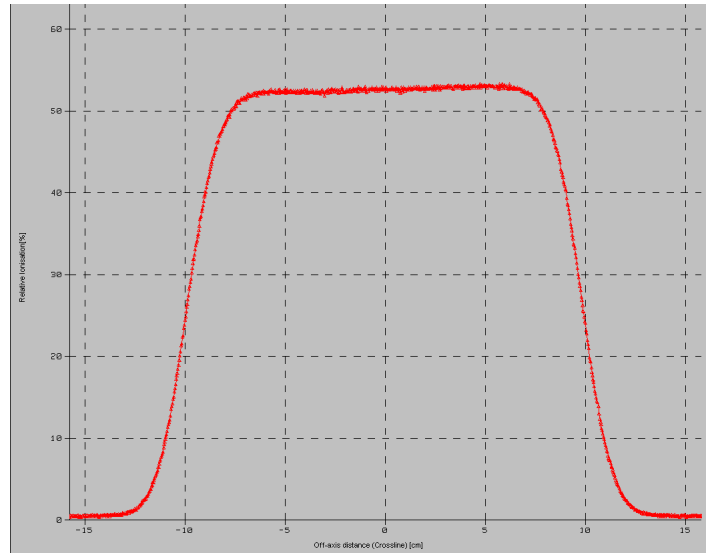


Figure 4–2: The electron beam profile used for the irradiation of the film pieces for the lateral correction measurements.

4.1.3 Scanner corrections

As mentioned in the previous chapter, the scanner has a non-uniform response over its lateral direction (the side perpendicular to the scanner light/CCD array motion). It is thus recommended to perform a correction on the transmission if one plans to use large film pieces. For film pieces small enough one can use the mid-section of the scanner bed and no correction is needed to get an accurate result. In fact scanner non-uniformity was observed to be $\pm 0.5\%$ for a region extending to ± 5 cm from the center of the CCD array detector. In order to have film pieces presenting uniform optical densities, they are irradiated using an electron beam. The setup of the experiment is the same as with the calibration curve except that an electron beam of 12 MeV and a field size of 20×20 cm² was used. The films were positioned at a depth of 5 cm in solid water. An electron

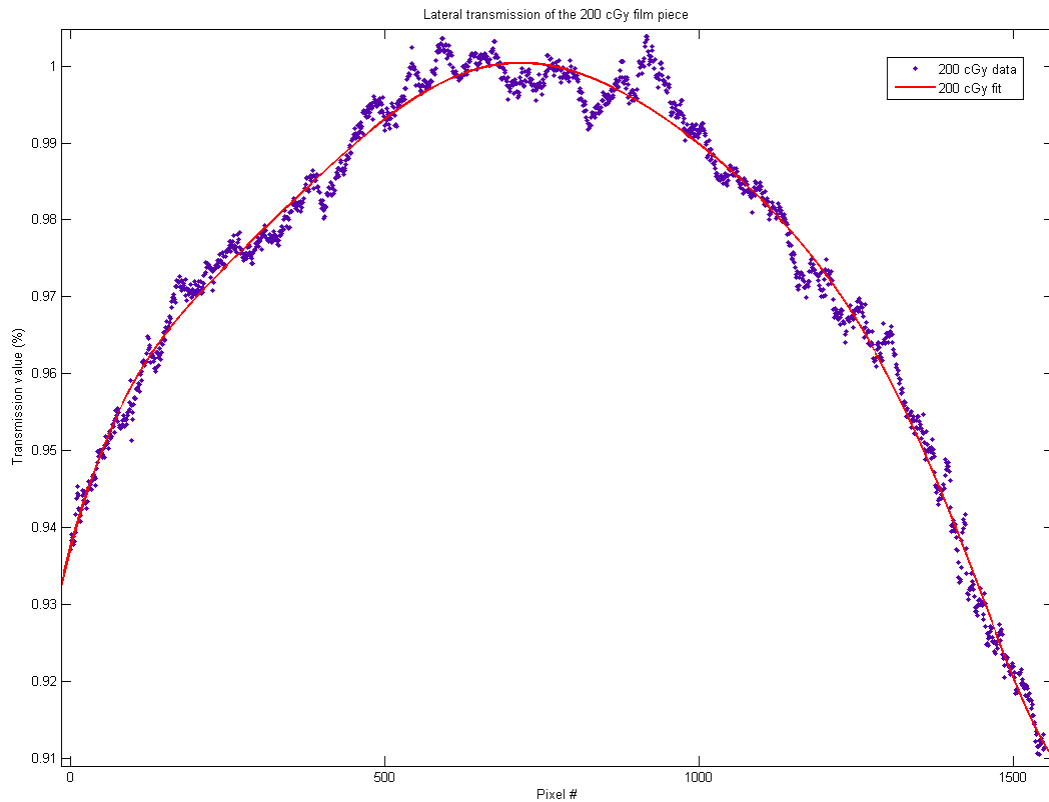


Figure 4-3: Profile of the film irradiated to a dose of 200 cGy and the resulting mathematical fit as ratio of the value for the middle of the scanner bed.

beam is used as it typically possesses a flatter profile than photon beam although this need to be verified for the particular machine used. This can be seen when figure 4-2 is compared with figure 2-10. Both profiles were taken with the same Elekta Synergy machine at CHUS¹. Film pieces of $10 \times 3 \text{ cm}^2$ were used to characterize the profile. They were digitized at 4 different positions to cover the

¹ Centre Hospitalier Universitaire de Sherbrooke

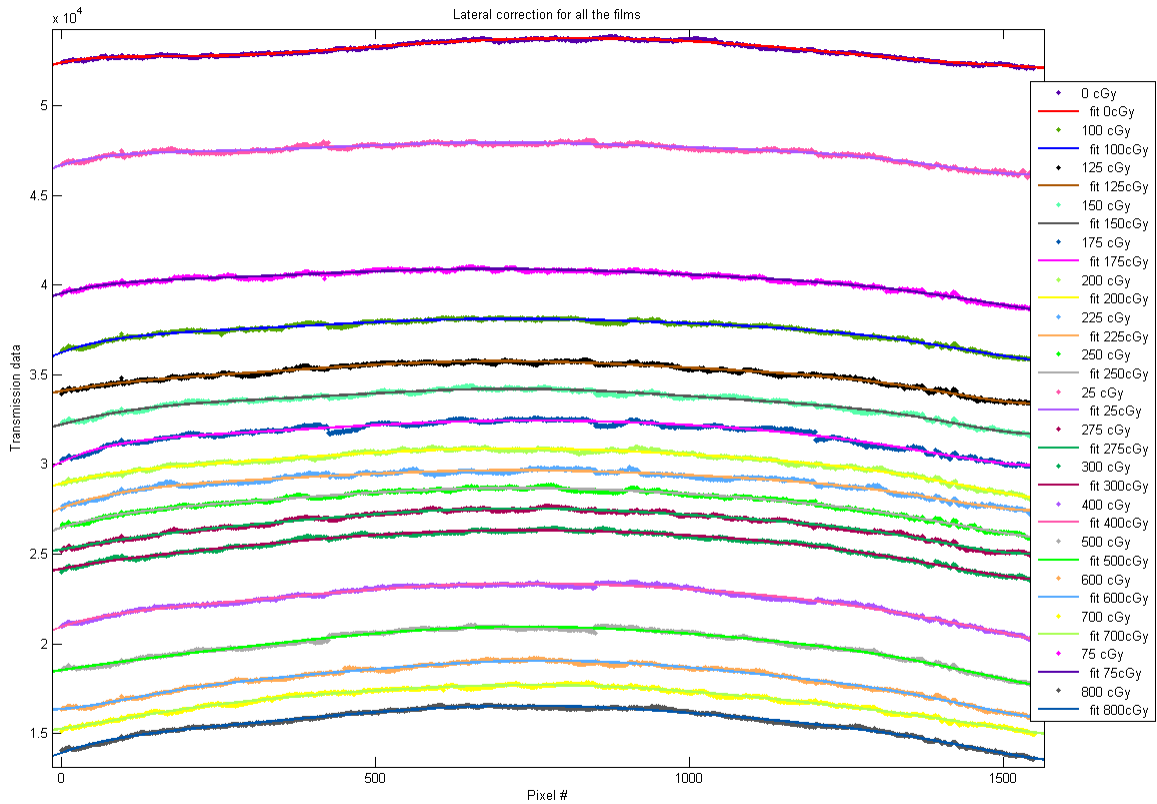


Figure 4-4: Profiles for all the films along the scanner bed with their respective mathematical fit.

whole lateral side of the scanner bed and in the middle of the longitudinal side of the scanner bed. The position of the films on the bed overlap each other by at least 2 cm in so that data from the edge of the film is avoided. The profiles were then build using an average of 1.5 cm (75 pixels) width of the film piece in the longitudinal direction to reduce noise. A ratio was taken for each pixel with respect to the value for the middle pixels of the scanner (average of 0.5 cm on each side of the middle pixel in the lateral direction) and mathematical fits were obtained. The fitted functions are 8th degree polynomials as suggested by

Bouchard *et al* [11] and a typical fit is shown in figure 4–3. This figure shows a typical measurement from all the fitted curves. All the curves are plotted in figure 4–4 along with their respective mathematical fit. A correction matrix was then built using the fitted functions and by linear interpolation between the optical density levels. It is applied to films that are larger than 10 cm on their side parallel with the lateral side of the scanner to limit the effect of scanner non-uniformity on transmission measurements. As one can see, we have found that for a typical clinical dose of 200 cGy the error can be up to 10 percent on the very edge of the profile. This is also increasing for higher doses (lower transmission values) and can be up to 15 percent for doses of the order of 800 cGy. As mentioned earlier no correction is applied in the longitudinal direction of the scanner. The variation in this direction has been found to be of less than 0.5 % and it was not deemed necessary to correct for it as the variation can be considered random when compared with the variation from the lateral side of the scanner. Instead, the edges of the bed in the longitudinal direction (about 2 cm on each side) which are a bit more problematic are simply avoided when scanning a film piece. Whenever a film piece is digitized, the user should position it in the center of the scanner bed in both direction for optimal results.

4.2 Linear accelerator and other equipment QA

As mentioned before, radiochromic films are ideal candidates for the replacement of radiographic films in clinics that are going filmless. Thus the use of radiographic films for quality assurance purposes should be replaced by either a completely different measurement or a similar measurement using radiochromic

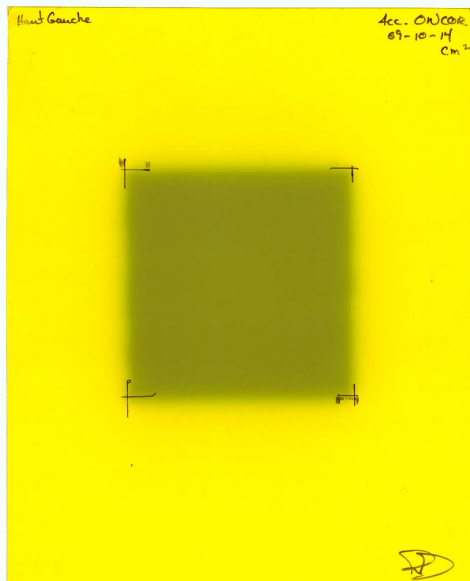


Figure 4-5: Coincidence between the a $10 \times 10 \text{ cm}^2$ light field displayed by the linac versus its measured $10 \times 10 \text{ cm}^2$ radiation field.

films. The later is in most cases the easiest as the procedures are already in place and the validation of the data from the two techniques should be essentially the same. Shown in figure 4-5 is the validation of the coincidence of the light field of a $10 \times 10 \text{ cm}^2$ field as viewed in the treatment room with the actual radiation field produced. The measurement shows that the two agree within acceptable limits set by an accepted quality assurance protocol [47]. The second measurement shown in figure 4-6 shows the validation of the angles of two virtual filter fields delivery. The most pronounced is the 60° filter which has been measured to be 60.1° . The second is the 45° filter which has been measured to be 44.8° . Both show excellent agreement with the expected angle. Now since radiochromic films were used to measure the angle, it is also possible to extract the dose from this

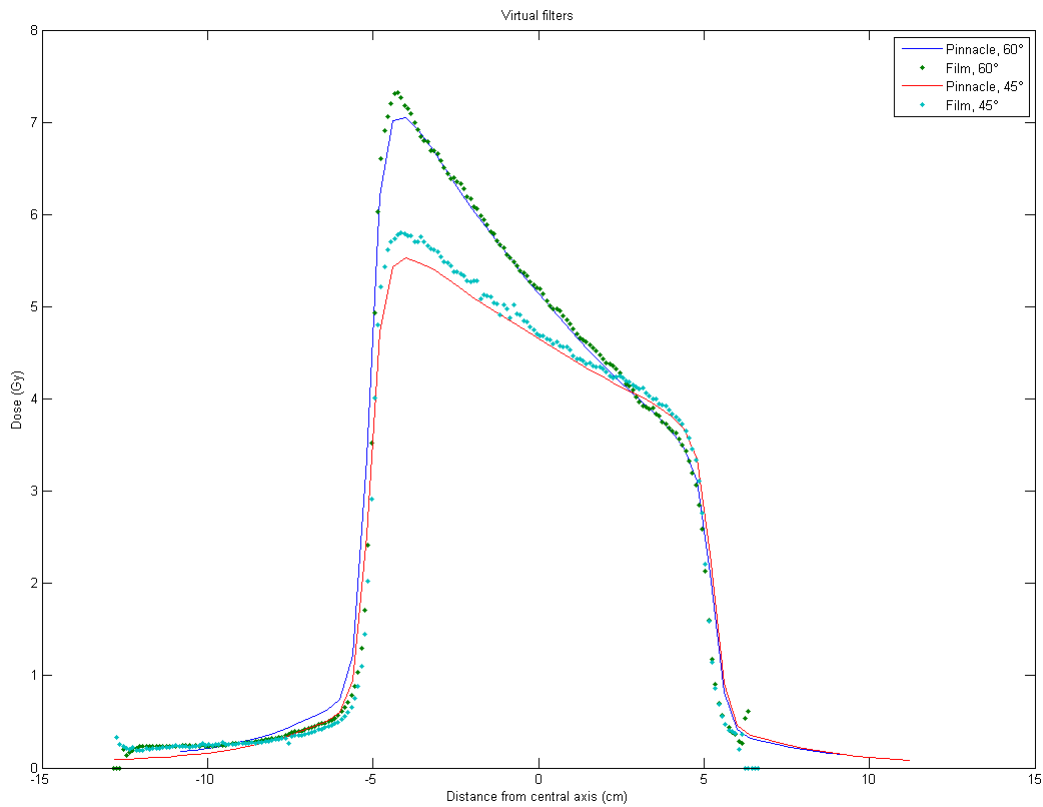


Figure 4–6: Measurement of two virtual filter fields delivery (45 degrees and 60 degrees) using a Siemens Oncor Impression linear accelerator.

measurement and compare it with the value predicted by the treatment planning system. This measurement was performed in a glass cylinder filled with water and immersed in water. The films were irradiated using a Siemens Oncor Impression². This particular setup was chosen because the films in this setup were used for comparison with two other dosimetry techniques which are polymer gel dosimetry

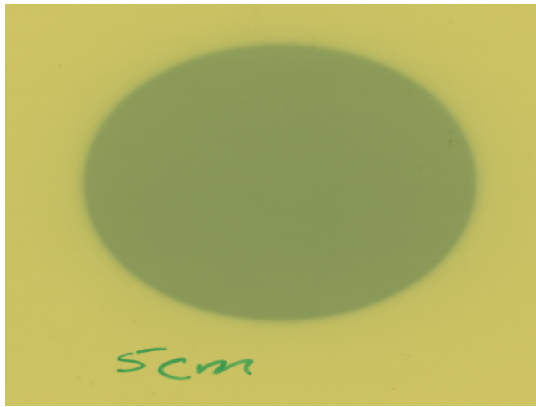
² Siemens AG.

and scintillating fiber dosimetry. These measurements will be published later by N. M. Tremblay³. From the profiles taken, one can see that the agreement between the treatment planning system, PINNACLE3⁴, and the measured dose by the radiochromic films is very good in the central portion of the profiles. Both the 60° and 45° filter doses show an agreement within 1% within the dose profile except for the peak at the edge of the filter. This is a known effect for this treatment planning software and it was also observed with measurements using an ionization chamber [48] during the commissioning process. By careful observation of this figure one can observe a greater discrepancy between the expected and measured dose from the 45° filter than for the 60° filter. This can be explained by the fact that the 45° filter measurement was performed about 1h after the 60° filter measurement (due to the nature of the setup) and that both films were digitized after 24h exposure of the 60° filter film. As it was seen in section 4.1.1 this introduces an error in the measurement which explains this difference.

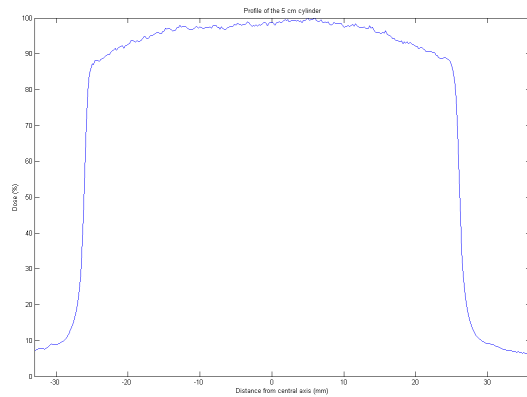
Quality assurance measurements of orthovoltage units require the use of many radiographic films. Since they are meant to be replaced by radiochromic film at the CHUS, simple QA measurements were performed to validate the use of the radiochromic films for this purpose. Shown in table 4–3 are the measured values for the profiles of different cylinder sizes using an orthovoltage unit operating at 150 kVp. The measurements were performed by placing the cylinder directly

³ Nicolas M. Tremblay, Centre Hospitalier Universitaire de Sherbrooke

⁴ PINNACLE³ v8.0m, Koninklijke Philips Electronics NV.



(a) 5 cm cylinder.



(b) 5 cm profile.

Figure 4–7: Measurement of the profile for the cylinders of an orthovoltage unit. (a) Shows the film taken for the 5 cm cylinder at an energy of 150 kVp and (b) shows the dose profile of this cylinder.

Table 4–3: Profile data for different cylinder sizes of the orthovoltage unit. The measured profile have an uncertainty of ± 0.2 mm. The delivered dose is 1.60 Gy.

Cylinder size	x-dir (mm)	Diff	y-dir (mm)	Diff	Dose (Gy)	Diff
10.0 mm	10.2	+2.00%	10.0	0.00%	1.54	-3.75%
15.0 mm	15.2	+1.33%	15.6	+4.00%	1.53	-4.38%
20.0 mm	20.0	0.00%	20.0	0.00%	1.54	-3.75%
25.0 mm	25.2	+0.80%	25.4	+1.60%	1.57	-1.88%
30.0 mm	29.2	-2.67%	28.6	-4.67%	1.56	-2.50%
40.0 mm	41.0	+2.50%	40.4	+1.00%	1.55	-3.13%
50.0 mm	51.0	+2.00%	50.8	+1.60%	1.55	-3.13%

in contact with the radiochromic film piece with a 5 cm solid water thickness as backscatter material. The profile for the 5 cm cylinder is shown in figure 4–7 as well as the digitized film piece. The profile length was taken at the 80% dose value. The measured doses show some discrepancies with the given dose. This is most likely due to the fact that radiochromic films are slightly energy

dependent in this energy region despite what the manufacturer claims. It would be recommended if one wants to use radiochromic films for dose verification to perform a calibration curve measurement (a calibration) for the low energy beams of the orthovoltage unit.

4.3 Percent depth dose of a 6 MV photon beam

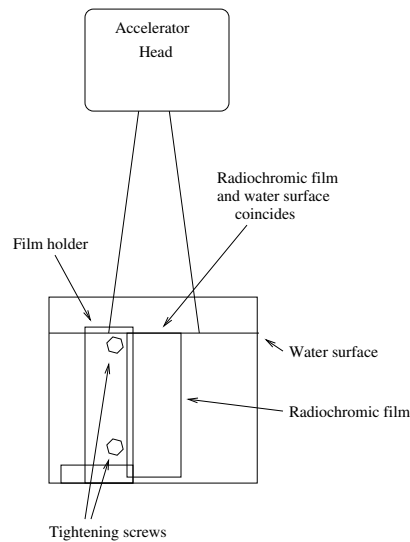


Figure 4–8: Experimental setup for the percent depth dose film measurement. The film is setup parallel to the direction of the beam using a plexiglass film holder.

Radiochromic films have been shown to behave well in the presence of water [2]. Thus it would be normal for a medical physicist to perform a beam characterizing measurement such as a percent depth dose in water. For this measurement a film holder was designed. It is made of plexiglass in order to minimize disturbance to the beam. This holder is meant to keep the film straight in the radiation field, parallel to the direction of the beam (see figure 4–8). The film is positioned in the water tank in order for its top edge to coincide with the

surface of the water. As mentioned in section 3.2.1, EBT-2 radiochromic film model are near tissue-equivalent and thus are near water equivalent. This means that no perturbation to the beam is expected from the presence of the film.

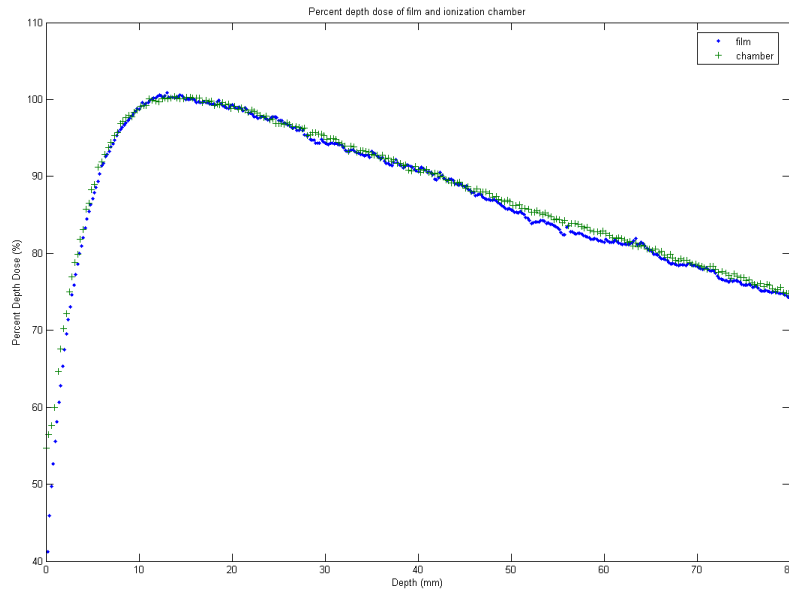


Figure 4-9: Percent depth dose of a 6 MV photon beam in water. Comparison between film measurement and ionization chamber measurement. The ionization chamber used is an Exradin A12 Farmer type and the Percent depth dose curve was shifted 1.83 mm according to the method explained in [3] (chamber shifting technique).

The measurement of the percent depth dose curve is shown in figure 4-9 and is compared with the same measurement performed using an ionization chamber. The coincidence between the two measurements is excellent which prove the validity of the radiochromic film dosimetry system. To measure percent depth dose curve with radiochromic films, one has first to convert the transmission values from the digitization to net optical densities and then the net optical densities

to doses. The ratio of the dose to the maximum dose is taken to obtain the percent depth dose curve. Note that the uncertainty on each point of the curve for the film measurement was calculated to be less than 1% for the majority of the points and less than 1.5% for all the points. The error bars are not shown on the plot for clarity. The depth of dose maximum found using the radiochromic film measurement is 1.45 ± 0.04 cm while it is 1.47 cm from the measurement performed with the ionization chamber. The surface dose was found to be $41.0 \pm 0.5\%$ when using the radiochromic film curve while it is found to be 55.0% when using the ionization chamber measurement. This is explained by the fact that ionization chambers are poor dosimeters when measuring dose prior to the depth of dose maximum because of the lack of electronic equilibrium in the volume of the chamber (see section 2.6.3). Thus radiochromic films are shown to measure percent depth dose curve with an excellent accuracy and make a great tool for the measurement of dose prior to the point of dose maximum such as skin dose measurements.

4.4 *In vivo* measurements

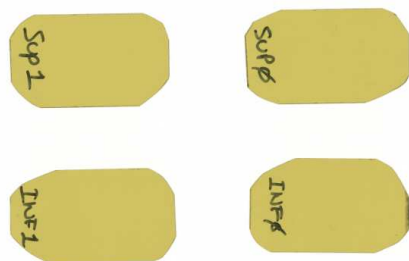
Different *in vivo* dose measurements using gafchromic EBT2 films have been performed following demands by radiation oncologists. Two different cases are presented here.

4.4.1 Seminoma of the testis

For this case the radiation oncologist was particularly concerned by the dose to the testis. The patient was scheduled to receive a dose of 1.80 Gy per fraction. Following the recommendations from Bieri *et al* [9], the radiation oncologist



(a) Gonodal shield.



(b) Unexposed films.



(c) Exposed films.

Figure 4-10: Gonodal shielding setup and results: (a) shows the placement of the films in the gonodal shield prior to each treatment fraction, (b) shows the unexposed films scanned before the first treatment fraction, and (c) shows the exposed films scanned after the last treatment fraction.

asked for the use of a scrotal shielding on the patient for the duration of the treatment. A demand was also made for dose measurement on the scrotum of the patient. Thus a measurement using radiochromic films was performed by a medical physicist. The setup of the experiment is shown in figure 4-10(b). The radiochromic films were taped to the inner wall of the scrotal shielding, and the anterior and posterior position of the films were noted and kept constant for the duration of the treatment in order to characterize the difference in dose (labeled

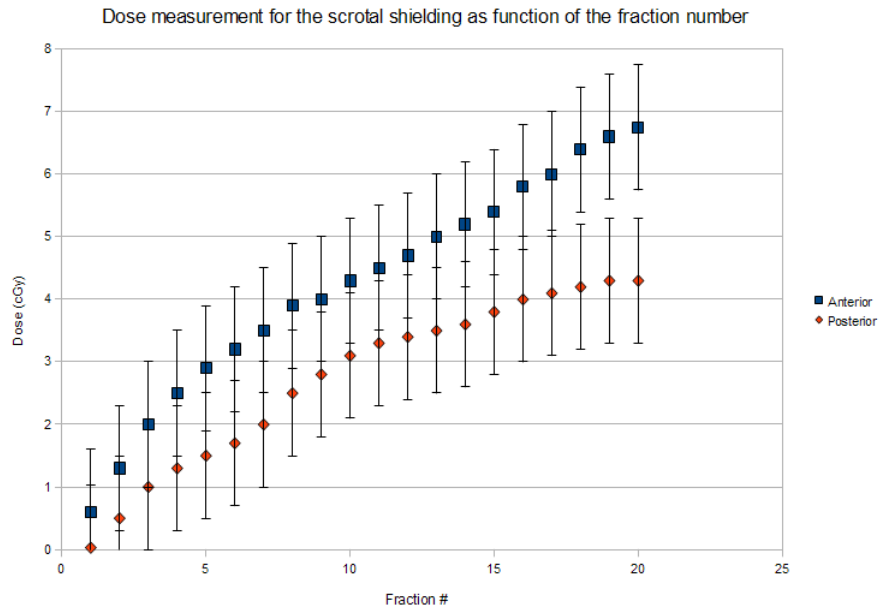


Figure 4–11: Dose measurement for the scrotal shielding as function of the fraction number for the anterior and posterior film.

as *sup1* and *inf1* respectively on the film pieces). The films were removed and digitized after each fraction. A new set of film was used for every fraction as post-irradiation coloration cannot be quantified for multiple irradiations of the same film piece. Control films were kept (labeled *sup0* and *inf0*) in the same conditions as measurement film pieces.

The results from this measurement are shown in figure 4–11. The doses are calculated by summing the doses measured by all the films from the preceding fraction. From the two figures one can see that the posterior film receives less dose than the anterior film. This is consistent with the setup of the experiment as there was more dose delivered from anterior-posterior beams than from posterior-anterior beams. Also on the posterior-anterior direction the patient and treatment table

attenuate the beam more before reaching the film while for the anterior-posterior direction the beam only goes through the scrotal shielding before reaching the film. At the end of the treatment one can see that the anterior-posterior film has received 6.73 ± 1.00 cGy while the posterior-anterior film has received 4.28 ± 1.00 cGy. The uncertainty on the dose measurement is quite large and was estimated from the experimental setup. The sources of uncertainties are the quality of the beam, which is unknown because most of it is scattered radiation and some of it transmission through a thick layer of lead (scrotal shielding), and the heavy manipulation of the film pieces which were inserted and removed in the shielding which requires bending. The effect of the later was however minimized by using a section of the film that showed no visual damage. The uncertainty from the net optical density to dose conversion (fit uncertainty) can be ignored as it is negligible compared to the experimental uncertainty. The measured doses are comparable with the results from Bieri [9] even if they appear to be higher. In fact the dose given for this treatment is higher than the dose given for the experiment in the presented publication.

4.4.2 Skin dose measurement

A skin dose measurement was required by the radiation oncologist. This patient had a superficial lesion that was not reacting as expected and the radiation oncologist wanted to verify the dose given to the skin because he believed the dose to the skin was not what he planned. For the initial treatment a 5 mm bolus was placed over the target. Thus a radiochromic film was taped to the skin of the patient right under the bolus. Figure 4–12 shows the film used for the skin



(a) 10 mm bolus.

(b) Electron beam.

Figure 4–12: Skin dose measurement films. (a) Shows the film for the treatment with 10 mm bolus and (b) shows the electron beam skin dose measurement (no bolus added).

dose measurement of the different treatment setups as decided by the radiation oncologist. The planned dose was 2.5 Gy per fraction to the skin using a 4 MV photon beam. A 2.25 Gy per fraction regime was planned later in the treatment using a 12 MeV electron beam as a boost.

Table 4–4: Results of skin dose measurements for different bolus thicknesses and the electron beam.

Beam type	Bolus thickness mm	Expected Dose Gy	Measured dose %	Uncertainty %	Difference %
4 MV	5	2.50	2.10	2.00	16.00
4 MV	10	2.50	2.27	2.00	9.20
12 MeV	0	2.25	2.26	2.00	0.44

The results from the three skin dose measurements are shown in table 4–4. As one can see the skin dose measured for the 4 MV photon beam was smaller than the expected dose by 16%. Even by adding an additional 5 mm to the bolus material the dose wasn't brought up to what was demanded by the radiation

oncologist. However it was deemed sufficient to treat this particular lesion and thus the treatment was continued using this amount of bolus material. The treatment using the electron beam proved to be exactly what was planned by the radiation oncologist. The uncertainty was determined to be $\pm 2.00\%$ in part because of the uncertainty brought by the conversion from net optical density to dose (0.5%) but also from the measurement setup. The film was taped directly to the skin of the patient that has an irregular surface and air gaps were most likely present between the film and skin. The air gaps led to an uncertainty estimated to be 0.75% because of the lack of attenuating and backscattering material in the vicinity of the film. The irregular surface also led to an uncertainty estimated to be 0.75% because of the difference in source surface distance (the surface irregularity was less than 0.5 cm). Thus an uncertainty of 1.5% was attributed to the experimental part of the measurement for a total of 2.00%.

4.5 IMRT plan QA measurements

Many methods are currently in use for verification of IMRT treatment plans. Among those, there are ion chamber matrix techniques and film dosimetry techniques. At the author's center, the current main technique is the ion chamber matrix technique while the backup technique is film dosimetry. The film dosimetry technique using radiochromic films has been chosen as it agrees well with Monte Carlo based dose calculations and compares well to other film dosimetry techniques such as the EDR2 film technique. These measurements make use of all the measured parameters of the film dosimetry system from the calibration curve to the lateral correction. Successful results from IMRT QA measurements are therefore

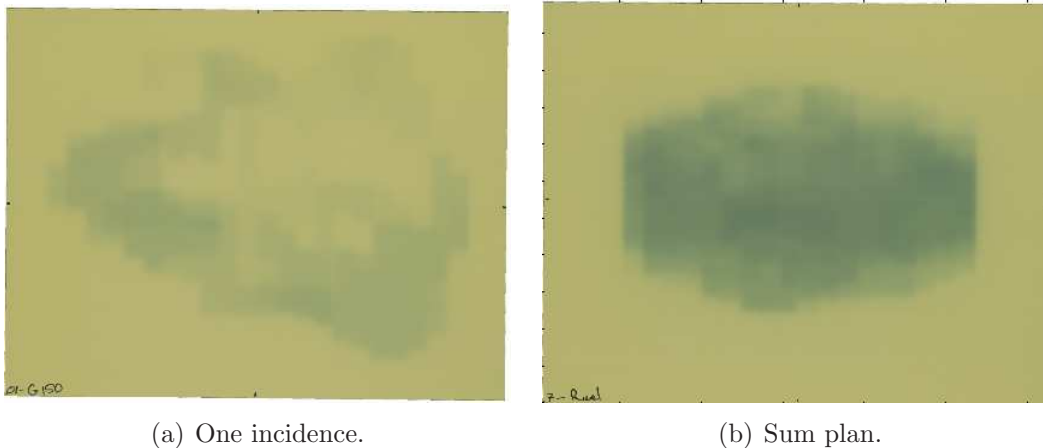


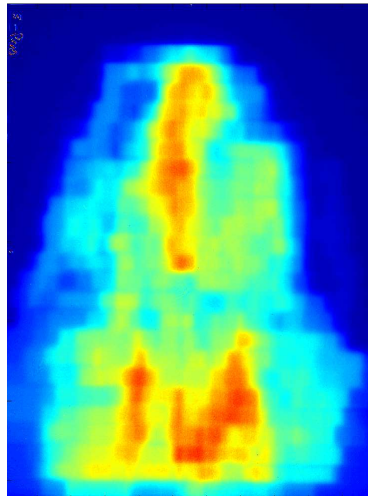
Figure 4–13: IMRT QA film measurements. (a) Shows a film taken for a single incidence of an IMRT treatment plan. (b) Shows a sum plan, that is the sum of all incidences, of an IMRT QA measurement.

a proof that the radiochromic film dosimetry system is properly working. Seven cases are presented and compared. The setup for the IMRT QA measurements using radiochromic films is the same as with the calibration curve measurement except that the film pieces used are larger. The film pieces are positioned at 5 cm depth in solid water with 10 cm solid water as backscatter material. Also fiducial markers are drawn on the film to properly register the film measurement with the expected data from the treatment planning software. Typically film pieces of at least $25 \times 25 \text{ cm}^2$ are necessary to properly perform an IMRT QA. In some cases films were cut to smaller pieces to avoid unnecessary usage of film. In figure 4–13 two radiochromic film measurements are presented. Figure 4–13(a) shows a radiographic film irradiated to a single incidence of the total IMRT treatment plan. However, what one typically measures when performing an IMRT QA measurement is what is shown in figure 4–13(b) which is all the incidences of the IMRT

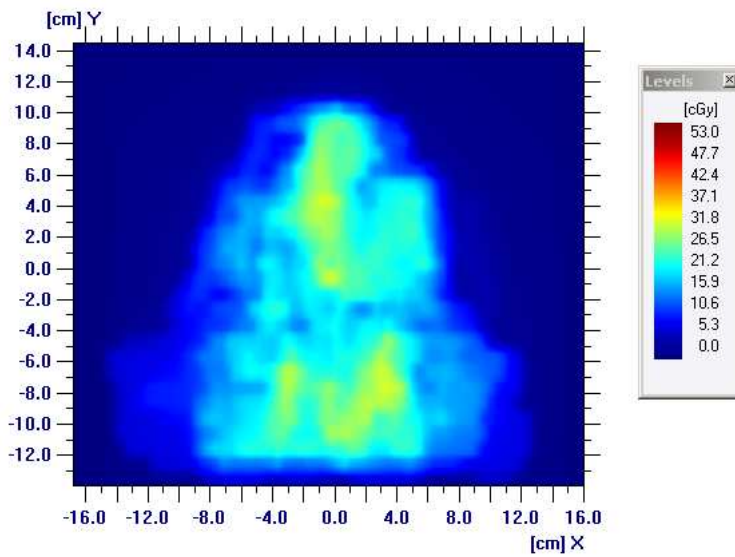
treatment plan irradiated on the same film with the gantry being static at an angle of 0 degree. This summed plan is what is used to calculate the gamma function to determine how good the delivered treatment is compared to the expected treatment plan [51]. The gamma function measures the quality of a plan. In the low-gradient regions of a plan, the accuracy of the computed and measured dose is what matter the most while in the high-gradient regions of the plan the most important criterion is distance to agreement between the same dose value. The gamma function is a method to combine the requirements of achieving either the low-gradient or high-gradient requirements. It will increase with both distance to agreement and dose difference between the calculated plan and measured results. We used a 3%/3 mm acceptance level for the gamma function test. The results for different IMRT QA measurements using radiochromic films are compared with the MatriXX⁵ ionization chamber array and are presented in the next paragraph.

After performing the measurements recommended in the AAPM's IMRT commissioning task group report [34] to ensure that our system was able to perform IMRT quality assurance measurements, different IMRT quality assurance measurements were performed. As explained before, the primary IMRT QA measurement tool at the CHUS is the MatriXX ionization chamber array. Thus radiochromic film measurements were performed after the MatriXX measurements and are simply used as a comparison. The resolution of the MatriXX system is 7.62 mm interpolated to 1 mm. Evidently, the resolution of the radiochromic films

⁵ Iba Dosimetry GmbH, Schwarzenbruck, Germany.

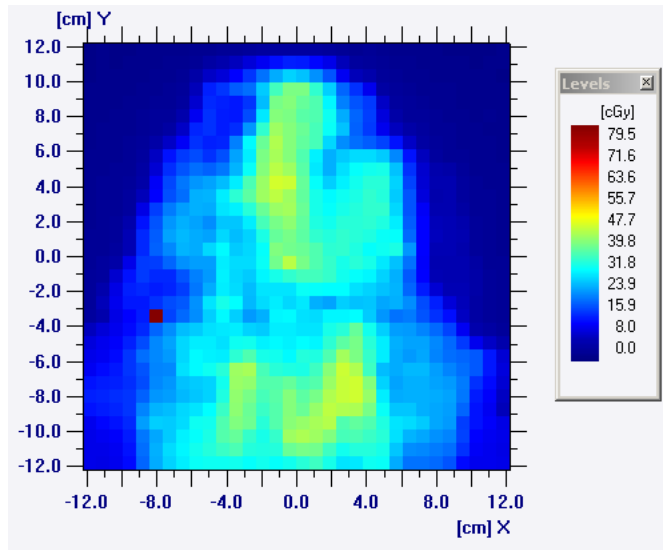


(a) Film dose.

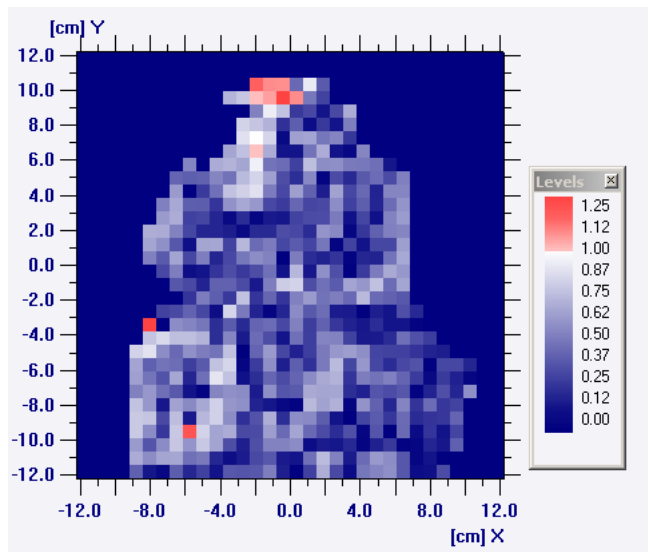


(b) TPS dose map.

Figure 4–14: Typical IMRT QA results using radiochromic films. (a) Shows the dose map measured using the radiographic film and (b) shows the expected dose map as extracted from the treatment planning software (TPS). Note that the film is rotated compared to the TPS image and that the scaling is not the same.

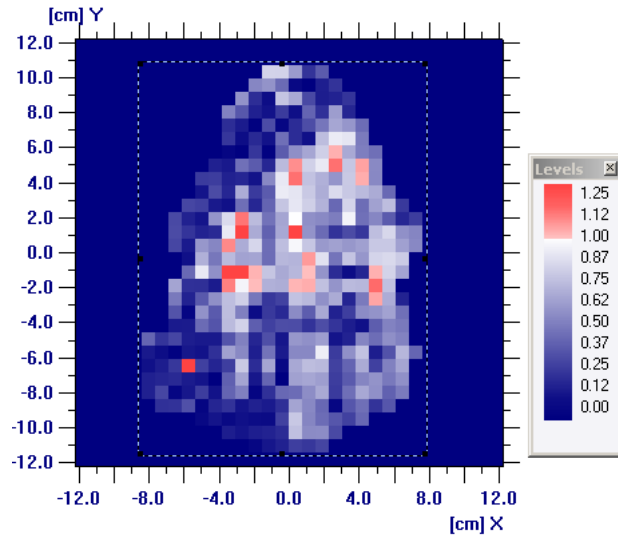


(a) MatriXX dose.

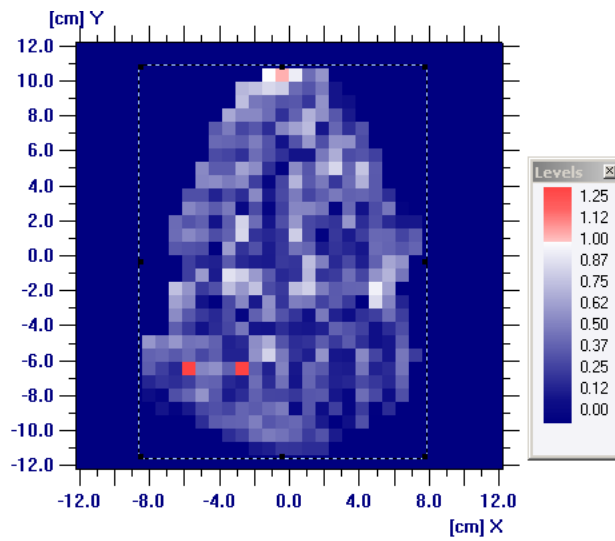


(b) Gamma function.

Figure 4–15: Same IMRT QA measurement than as in figure 4–14 but performed using the MatriXX ionization chambers array. (a) Shows the dose map measured using the MatriXX system and (b) shows the gamma function results of the dose map measured with the MatriXX compared to the expected dose map from the treatment planning software.



(a) MatriXX gamma function.



(b) Film gamma function.

Figure 4-16: Comparison of the gamma function results for the MatriXX ionization chambers array and the radiochromic film. (a) Shows the gamma function results for the MatriXX system and (b) shows the gamma function results for the film. Both dose maps are compared to the treatment planning software expected dose map and converted to the same dose grid.

Table 4–5: Gamma function results for the different IMRT QA measurements performed with radiochromic films and compared with the MatriXX ionization chambers array.

Film #	Film		MatriXX		Difference MatriXX - Film
	Accepted pixels	Rejected pixels	Accepted pixels	Rejected pixels	
1	99.86%	0.14%	99.80%	0.20%	0.06%
2	99.83%	0.17%	99.80%	0.20%	0.03%
3	99.58%	0.42%	99.22%	0.78%	0.36%
4	99.91%	0.09%	99.61%	0.39%	0.30%
5	99.90%	0.10%	99.90%	0.10%	0.00%
6	99.88%	0.12%	99.90%	0.10%	-0.02%
7	99.93%	0.07%	99.90%	0.10%	0.03%

is considerably higher than that of the ionization chamber array. Also ionization chambers are known to be poor dosimeters in regions of high dose gradient. IMRT treatments are known to typically have high dose gradient regions and one expects the radiochromic films to perform better in these regions. However the MatriXX ionization chamber array has the advantage of providing an instantaneous measurement and the ability to easily measure the different gantry incidence separately as well as the sum plan. Table 4–5 shows the comparison of the gamma function result of the sum plans. As one can see from these measurements, the radiochromic film dosimetry system performs as well if not better than the MatriXX ionization chamber array system. The slightly better performance of the radiochromic film dosimetry system is likely due to its better performance in the high dose gradient regions. One can see from figure 4–15 that the pixels not passing the gamma function test (always represented in red) are mostly located in the high dose gradient region when compared with the expected result

from the dose map extracted from the treatment planning software (shown in figure 4–14(b)). This is not the case for the dose map from the radiochromic film dosimetry system. The comparison between a film gamma function result and the MatriXX ionization chamber array is shown in figure 4–16. With the results obtained using the radiochromic film dosimetry system as shown in table 4–5 and from the gamma function results shown in figure 4–16, one can conclude that the radiochromic film dosimetry system has been properly calibrated to use as an IMRT QA measurement technique.

4.6 GammaKnife QA measurements

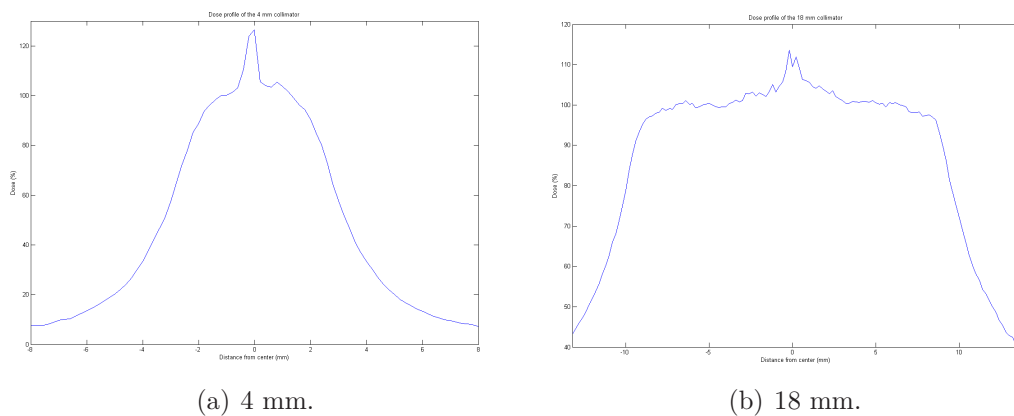


Figure 4–17: Profile of the (a) 4 mm collimator and (b) 18 mm collimator both in the x direction for the Gammaknife 4C.

As explained in section 2.5, the Gammaknife is a very specialized radiosurgery system. As its name implies, it acts as a virtual surgery knife using gamma radiation having great precision. However for a medical physicist, great precision also usually means rigorous quality assurance. In fact many quality assurance tests are performed and some of them involve the use of radiochromic films. Before

Table 4–6: Profile data from the 4 collimator sizes of the Gammaknife. The uncertainty on the profile measurement is ± 0.2 mm.

Collimator size	Profile x	Difference	Profile y	Difference
4 mm	4.2	5.00%	4.0	0.00%
8 mm	8.0	0.00%	8.2	2.50%
14 mm	13.8	1.43%	14.0	0.00%
18 mm	18.4	2.22%	17.8	-1.11%

the implementation of the radiochromic film dosimetry system at the CHUS, these QAs were performed using an older model of radiochromic film, MD-55. All the tests involved were performed using the transmission data from the film. Now that the radiochromic film dosimetry system is in place, the tests can be performed more precisely using either optical densities or dose depending on the measurement. Among the quality assurance tests that are performed at this machine, two are presented here: profile measurements and treatment plan / patient positioning system verification.

4.6.1 Profile measurements

For the Gammaknife 4C model at this institution, four collimator sizes are available: 4 mm, 8 mm, 14 mm, and 18 mm. The profiles are measured using a tool that can be mounted on the machine and designed especially for beam profile verification. The film is embedded in a metal frame and an attached needle is used to mark the center of the beam. Thus it is also possible to correct for misalignment of the beam using this tool by measuring the distance from the middle of the beam using the very high optical density peak produced by puncturing the film with the needle to the edge of the profile defined by the 50 %

OD drop from the average value in the flat region of the profile. As one can see from figure 4-17, the differences in the profile for the two extreme collimators are important. The 18 mm collimator exhibits a large flat region while the 4 mm collimator exhibits a sharp rise and decline of the dose with almost no flat region. This feature is taken into consideration when preparing a treatment plan with the Gammaknife, that is the neurosurgeon/radiation oncologist prescribe the treatment dose at the 50% isodose line in order for the whole planned volume to receive the prescribed dose. The data for the four collimators for two of the three directions (x- and y-direction) are found in table 4-6. The profiles obtained with the new radiochromic film model show that it has effectively replaced the old film model in this QA procedure.

4.6.2 Treatment plan validation and patient positioning system verification

The treatment plan validation and patient positioning system verification is performed using a tool provided by the manufacturer of the GammaKnife. This tool consists of a plexiglass sphere with an insert capable of holding a film. This sphere has been scanned using a magnetic resonance imaging system (MRI) with a special positioning frame also used as part of the patient positioning system. This permits the localization in machine coordinates in the MRI images. The red frame contouring the plexiglass is the definition of the head of the patient but is ignored in this case as we are irradiating a film piece. Again this QA procedures was previously performed using an older radiochromic film model MD-55 and only by using transmission values. Now with the introduction of the calibrated film dosimetry system one can use dose value and compare it directly with the

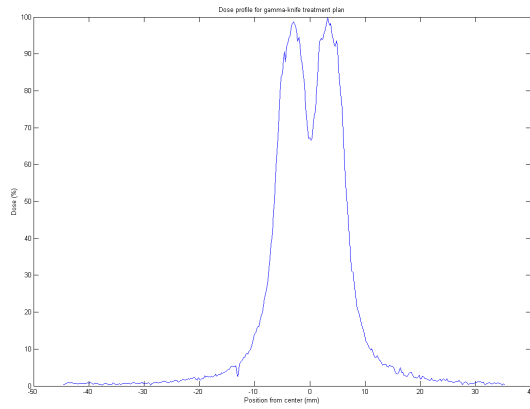
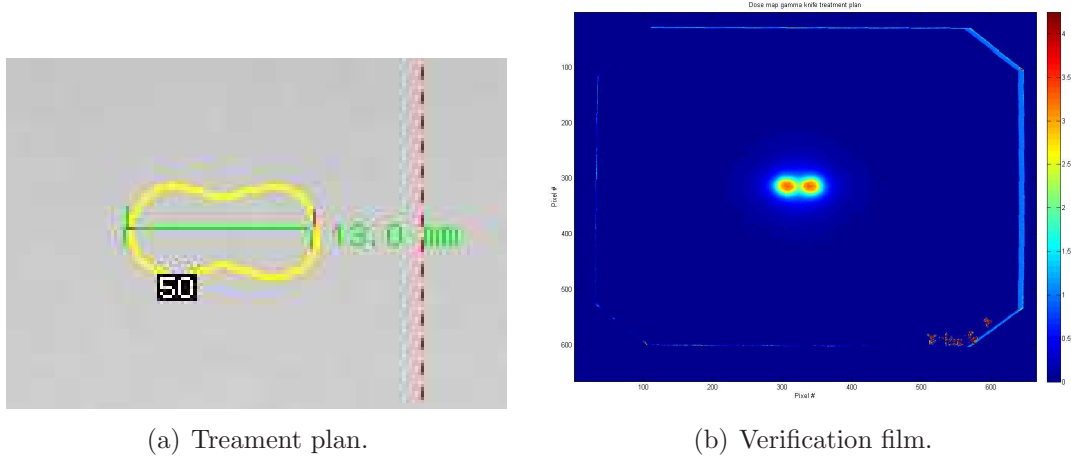


Figure 4-18: Treatment plan validation and patient positioning system validation. (a) Shows the treatment plan as planned with the software for the Gammaknife *GammaPlan version 8.3.1*, (b) shows the verification film converted to dose and (c) shows the dose profile through the middle of the two 4 mm irradiations (called shots).

treatment plan. Also this measurement can be used to verify the dose calibration using a radiochromic film instead of an ionization chamber. Typically dose calibration verification is performed using the same phantom but using a small ionization chamber inserted in the center of the phantom. The results from this

measurement are seen in figure 4–18 and table 4–7. In figure 4–18 the measured plan can be compared with the planned version and one can see that the two agree well with each other. Using a profile we can measure the size of the 50% region. In its longest extent it is measured to be 13.0 ± 0.2 mm from the profile taken from the film. One can see that this agrees very well with the treatment plan shown in figure 4–18(a). Also by comparing directly the verification film and the treatment plan, one can see that the 50% isodose lines agree very well with each other. This has to be done by comparing the distance between the two 50% isodose line in the profile seen in figure 4–18(c) to the length between the two 50% isodose line on the treatment plan shown in figure 4–18(a) since data from the Gammaknife treatment planning software cannot be exported. This is very important because the 50% isodose line is typically isodose that is used to prescribe the treatment dose.

Table 4–7: Patient positioning system verification.

Direction	Measured value (cm)	Expected value (cm)	Difference
x	99.9 ± 0.1	100.0	0.10%
y	100.0 ± 0.1	100.0	0.00%
z	100.8 ± 0.1	100.8	0.00%

The patient positioning system verification measurements are tabulated in table 4–7. From this data one can see that the positions measured agree well with the expected values. This data has been obtained from the distance of the 50% isodose and the position of the film edges. Note that two different films are required to obtain this data because films can only measure two dimensions at a time. The distance between the two peak doses can also be obtained for an

additional verification in one direction. In this case the two peaks were obtained using two 2 Gy irradiations (shots) with the 4 mm collimator separated by 7 mm in the x-direction. Using the profile shown in figure 4-18(c) the distance between the two peaks has been found to be 6.8 ± 0.2 mm confirming that the two shots were effectively treated with the planned separation.

CHAPTER 5

Conclusion

In conclusion, this thesis demonstrates the implementation of a radiochromic film dosimetry system in a clinical environment using a relatively inexpensive flatbed document scanner and simple tools and procedures. A film dosimetry system is typically meant to complement other dosimetry systems such as ion chambers and TLDs. It has been shown that it is a valuable tool especially for 2 dimensional dosimetry applications for techniques such as IMRT and stereotactic radiotherapy. It is also an interesting technique for the replacement of the radiographic films used for different quality assurance applications as many centers are gearing towards a filmless environment. Furthermore, radiochromic film dosimetry systems are excellent for skin dose measurements and *in-vivo* dose verifications. Despite some drawbacks such as post-irradiation darkening and different corrections that need to be applied to obtain a proper dose measurement, radiochromic film dosimetry systems demonstrate many interesting clinical possibilities. It has been shown that using a calibration curve measured from the appropriate time window, one can significantly reduce the error associated with post-irradiation darkening. Moreover, once the corrections to be applied are determined it is rather easy to implement them within the film analysis software. Radiochromic film dosimetry systems have the advantages of having a very high spatial resolution, near tissue equivalence, relatively weak energy dependence and very weak dose-rate

dependence, all this making them ideal candidates for measurements in high dose gradient regions in very small fields. Also their dose measurement point is one of the shallowest of all dosimeters and the small thickness of the film makes it possible to perform *in vivo* dosimetry with very small disturbances in the treatment field. Radiochromic films are also a good candidate for 2 dimensional array measurements by (pseudo 3D) inserting film pieces between slabs of solid water or in human-like phantoms.

The radiochromic film dosimetry system implemented at the CHUS is fairly recent and further developments are planned. Future work includes the development of a film analysis software from the many Matlab routines the author has developed for analysis in this thesis. Also this software will include features to control the scanner directly from the film analysis software such as automatic pre-heating of the scanner and automatic scanning the same film a predefined number of times to make it easier for the user. Another feature that will be investigated is the possibility to use the reflective mode of the scanner as suggested by Kalef-Ezra *et al* [45] to reduce errors in certain applications. Also a technique for *in vivo* quality assurance verifications of IMRT treatment is being investigated motivated by the work of Mans *et al* [54].

Finally the CHUS is on the verge of acquiring a state of the art stereotactic radiosurgery system by the company Elekta and will also be replacing two linear accelerators. A properly calibrated film dosimetry system is surely useful for such tasks and the author predicts an intense use of the system in the coming months.

Finally, the number of requests for *in vivo* dose measurement from the radiation oncologists are increasing now that the system is tested.

REFERENCES

- [1] Elekta AB. Elekta website. <http://www.elekta.com/>, 2010.
- [2] S. Aldelaijan, S. Devic, H. Mohammed, N. Tomic, L. Liang, F. DeBlois, and J. Seuntjens. Evaluation of EBT-2 model Gafchromic film performance in water. *Medical Physics*, 37(7):3687–3693, 2010.
- [3] P. R. Almond, P. J. Biggs, B. M. Coursey, W. F. Hanson, M. S. Huq, R. Nath, and D. W. O. Rogers. AAPM’s TG-51 protocol for clinical reference dosimetry of high-energy photon and electron beams. *Medical Physics*, 26(9):1847–1870, 1999.
- [4] F. H. Attix. *Introduction to Radiological Physics and Radiation Dosimetry*. Wiley, Hoboken, NJ, 1st edition, 1986.
- [5] A. S. Aydarous, P. J. Darley, and M. W. Charles. A wide dynamic range, high-spatial-resolution scanning system for radiochromic dye films. *Physics in Medicine and Biology*, 46(5):1379, 2001.
- [6] J. Baker, T. Telivala, and L. Reinstein. SU-FF-T-466: A single dose calibration method for IMRT QA film dosimetry using Gafchromic EBT film. *Medical Physics*, 33(6):2152–2152, 2006.
- [7] M. Bazioglou and J. Kalef-Ezra. Dosimetry with radiochromic films: a document scanner technique, neutron response, applications. *Applied Radiation and Isotopes*, 55(3):339 – 345, 2001.
- [8] P. R. Bevington and D. K. Robinson. *Data reduction and error analysis for the physical science*. McGraw-Hill, Boston, Ma, 3rd edition, 2003.
- [9] S. Bieri, M. Rouzaud, and R. Miralbell. Seminoma of the testis: is scrotal shielding necessary when radiotherapy is limited to the para-aortic nodes? *Radiotherapy and Oncology*, 50(3):349 – 353, 1999.

- [10] H. Bilge, A. Cakir, M. Okutan, and H. Acar. Surface dose measurements with Gafchromic EBT film for 6 and 18MV photon beams. *Physica Medica*, 25(2):101 – 104, 2009.
- [11] H. Bouchard, F. Lacroix, G. Beaudoin, J. Carrier, and I. Kawrakow. On the characterization and uncertainty analysis of radiochromic film dosimetry. *Medical Physics*, 36(6):1931–1946, 2009.
- [12] M. Boutillon and A. M. Perroche-Roux. Re-evaluation of the W value for electrons in dry air. *Physics in Medicine and Biology*, 32(2):213, 1987.
- [13] A. Bufacchi, A. Carosi, N. Adorante, S. delle Canne, T. Malatesta, R. Caparella, R. Fragomeni, A. Bonanni, M. Leone, L. Marmiroli, and L. Begnozzi. In vivo EBT radiochromic film dosimetry of electron beam for Total Skin Electron Therapy (TSET). *Physica Medica*, 23(2):67 – 72, 2007.
- [14] M. J. Butson, T. Cheung, and P. K. N. Yu. Absorption spectra variations of ebt radiochromic film from radiation exposure. *Physics in Medicine and Biology*, 50(13):N135, 2005.
- [15] M. J. Butson, T. Cheung, and P. K. N. Yu. Weak energy dependence of EBT Gafchromic film dose response in the 50kVp-10MVp X-ray range. *Applied Radiation and Isotopes*, 64(1):60 – 62, 2006.
- [16] M. J. Butson, P. K. N. Yu, and P. E. Metcalfe. Extrapolated surface dose measurements with radiochromic film. *Medical Physics*, 26(3):485–488, 1999.
- [17] A. N. Chair, C. R. Blackwell, B. M. Coursey, K. P. Gall, J. M. Galvin, W. L. McLaughlin, A. S. Meigooni, R. Nath, J. E. Rodgers, and C. G. Soares. Radiochromic film dosimetry: Recommendations of AAPM Radiation Therapy Committee Task Group 55. *Medical Physics*, 25(11):2093–2115, 1998.
- [18] T. Cheung, M. J. Butson, and P. K. N. Yu. Post-irradiation colouration of Gafchromic EBT radiochromic film. *Physics in Medicine and Biology*, 50(20):N281, 2005.
- [19] S. Chiu-Tsao and M. F. Chan. Photon beam dosimetry in the superficial buildup region using radiochromic EBT film stack. *Medical Physics*, 36(6):2074–2083, 2009.

- [20] S. Chiu-Tsao and M. F. Chan. Evaluation of two-dimensional bolus effect of immobilization/support devices on skin doses: A radiochromic EBT film dosimetry study in phantom. *Medical Physics*, 37(7):3611–3620, 2010.
- [21] S. Chiu-Tsao, J. Hanley, J. Napoli, S. Davis, and L. DeWerd. SU-FF-T-147: Determination of TG43 parameters for Cs-131 model CS-132 seed using radiochromic EBT film dosimetry. *Medical Physics*, 34(6):2434–2435, 2007.
- [22] S. Chiu-Tsao, Y. Ho, R. Shankar, L. Wang, and L. B. Harrison. Energy dependence of response of new high sensitivity radiochromic films for megavoltage and kilovoltage radiation energies. *Medical Physics*, 32(11):3350–3354, 2005.
- [23] E. Chung, H. Bouchard, and J. Seuntjens. Investigation of three radiation detectors for accurate measurement of absorbed dose in nonstandard fields. *Medical Physics*, 37(6):2404–2413, 2010.
- [24] G. Ciangaru, J. Yang, P. Oliver, M. Bues, M. Zhu, F. Nakagawa, H. Chiba, S. Nakamura, H. Yoshino, M. Umezawa, and A. Smith. Verification procedure for isocentric alignment of proton beams. *Journal of Applied Clinical Medical Physics*, 8(4), 2007.
- [25] Bureau International des Poids et Mesures. Système international d’unités, Resolution 12 of the 11th meeting of the CGPM. <http://www.bipm.org/en/CGPM/db/11/12/>, 1960.
- [26] S. Devic, S. Aldelaijan, H. Mohammed, N. Tomic, L. Liang, F. DeBlois, and J. Seuntjens. Absorption spectra time evolution of EBT-2 model Gafchromic film. *Medical Physics*, 37(5):2207–2214, 2010.
- [27] S. Devic, J. Seuntjens, W. Abdel-Rahman, M. Evans, M. Olivares, E. B. Podgorsak, T. Vuong, and C. G. Soares. Accurate skin dose measurements using radiochromic film in clinical applications. *Medical Physics*, 33(4):1116–1124, 2006.
- [28] S. Devic, J. Seuntjens, G. Hegyi, E. B. Podgorsak, C. G. Soares, A. S. Kirov, I. Ali, J. F. Williamson, and A. Elizondo. Dosimetric properties of improved Gafchromic films for seven different digitizers. *Medical Physics*, 31(9):2392–2401, 2004.

- [29] S. Devic, J. Seuntjens, E. Sham, E. B. Podgorsak, C. R. Schmidlein, A. S. Kirov, and C. G. Soares. Precise radiochromic film dosimetry using a flat-bed document scanner. *Medical Physics*, 32(7):2245–2253, 2005.
- [30] S. Devic, N. Tomic, Z. Pang, J. Seuntjens, E. B. Podgorsak, and C. G. Soares. Absorption spectroscopy of EBT model Gafchromic film. *Medical Physics*, 34(1):112–118, 2007.
- [31] S. Devic, N. Tomic, C. G. Soares, and E. B. Podgorsak. Optimizing the dynamic range extension of a radiochromic film dosimetry system. *Medical Physics*, 36(2):429–437, 2009.
- [32] L. Ding, M. Urie, and Y. Lo. SU-FF-T-164: Radiochromic EBT film characterization and applicability for IMRT QA verification. *Medical Physics*, 32(6):1987–1987, 2005.
- [33] M. D. C. Evans, S. Devic, and E. B. Podgorsak. High dose-rate brachytherapy source position quality assurance using radiochromic film. *Medical Dosimetry*, 32(1):13 – 15, 2007.
- [34] G. A. Ezzell, J. W. Burmeister, N. Dogan, T. J. LoSasso, J. G. Mechalakos, D. Mihailidis, A. Molineu, J.r R. Palta, C. R. Ramsey, B. J. Salter, J. Shi, P. Xia, N. J. Yue, and Y. Xiao. IMRT commissioning: Multiple institution planning and dosimetry comparisons, a report from AAPM Task Group 119. *Medical Physics*, 36(11):5359–5373, 2009.
- [35] B. C. Ferreira, M. C. Lopes, and M. Capela. Evaluation of an Epson flatbed scanner to read Gafchromic EBT films for radiation dosimetry. *Physics in Medicine and Biology*, 54(4):1073, 2009.
- [36] D. Fontanarosa, L. C. Orlandini, I. Andriani, and L. Bernardi. Commissioning Varian enhanced dynamic wedge in the PINNACLE treatment planning system using Gafchromic EBT film. *Medical Physics*, 36(10):4504–4510, 2009.
- [37] M. Fuss, E. Sturtewagen, C. De Wagter, and D. Georg. Dosimetric characterization of Gafchromic EBT film and its implication on film dosimetry quality assurance. *Physics in Medicine and Biology*, 52(14):4211, 2007.
- [38] A. Garcia-Garduno, M. À. Celis, J. M. Lárraga-Gutiérrez, S. Moreno-Jiménez, A. Martínez-Dávalos, and M. Rodríguez-Villafuerte. Radiation transmission, leakage and beam penumbra measurements of a micro-multileaf collimator

- using Gafchromic EBT film. *Journal of applied clinical medical physics*, 9(3):90 – 98, 2008.
- [39] B. J. Gerbi and E. Y. Han. SU-FF-T-426: The response of radiochromic EBT film in high-energy electron beams. *Medical Physics*, 33(6):2144–2144, 2006.
- [40] R. C. Gonzalez and R. E. Woods. *Digital image processing*. Prentice Hall, Upper Saddle River, NJ, 2nd edition, 2002.
- [41] R. C. Gonzalez, R. E. Woods, and S. L. Eddins. *Digital image processing using MATLAB*. Prentice Hall, Upper Saddle River, NJ, 1st edition, 2002.
- [42] J. H. Hubbell and S. M. Seltzer. Tables of x-ray mass attenuation coefficients and mass energy-absorption coefficients. Technical Report NISTIR 5632, National Institute of Standards and Technology, Gaithersburg, Md, 1996.
- [43] C. A. Jayachandran. Calculated effective atomic number and kerma values for tissue-equivalent and dosimetry materials. *Physics in Medicine and Biology*, 16(4):617, 1971.
- [44] H. E. Johns and J. R. Cunningham. *The physics of radiology*. Charles C Thomas, Springfield, IL, 4th edition, 1983.
- [45] J. Kalef-Ezra and K. Karava. Radiochromic film dosimetry: Reflection vs transmission scanning. *Medical Physics*, 35(6):2308–2311, 2008.
- [46] F. M. Khan. *The physics of radiation therapy*. Lippincott Williams and Wilkins, Philadelphia, PA, 3rd edition, 2003.
- [47] E. E. Klein, J. Hanley, J. Bayouth, F. Yin, W. Simon, S. Dresser, C. Serago, F. Aguirre, L. Ma, B. Arjomandy, C. Liu, C. Sandin, and T. Holmes. Task group 142 report: Quality assurance of medical accelerators. *Medical Physics*, 36(9):4197–4212, 2009.
- [48] C. Lavoie, V. H. Tremblay, and N. M. Tremblay. Virtual filter commissioning with the treatment planning software PINNACLE3. private communications, April 2010.
- [49] Y. Le, E. Armour, and J. Wong. SU-FF-T-214: Evaluation of heterogeneity effect in Intra-Operative HDR (IOHDR) brachytherapy dose calculation using monte carlo simulation and Gafchromic EBT film measurement. *Medical Physics*, 34(6):2450–2450, 2007.

- [50] D. Lightfoot. SU-FF-T-437: Total skin electron beam commissioning with EBT film. *Medical Physics*, 33(6):2146–2146, 2006.
- [51] D. A. Low, W. B. Harms, S. Mutic, and J. A. Purdy. A technique for the quantitative evaluation of dose distributions. *Medical Physics*, 25(5):656–661, 1998.
- [52] B. D. Lynch, J. Kozelka, M. K. Ranade, J. G. Li, W. E. Simon, and J. F. Dempsey. Important considerations for radiochromic film dosimetry with flatbed CCD scanners and EBT Gafchromic film. *Medical Physics*, 33(12):4551–4556, 2006.
- [53] A. Mack, G. Mack, D. Wertz, S. G. Scheib, H. D. Bottcher, and V. Seifert. High precision film dosimetry with Gafchromic films for quality assurance especially when using small fields. *Medical Physics*, 30(9):2399–2409, 2003.
- [54] A. Mans, M. Wendling, L. N. McDermott, J. J. Sonke, R. Tielenburg, R. Vijlbrief, B. Mijnheer, M. van Herk, and J. C. Stroom. Catching errors with in vivo epid dosimetry. *Medical Physics*, 37(6):2638–2644, 2010.
- [55] M. Martisikova, B. Ackermann, and O. Jakel. Analysis of uncertainties in Gafchromic EBT film dosimetry of photon beams. *Physics in Medicine and Biology*, 53(24):7013, 2008.
- [56] E. C. McCullough and T. W. Holmes. Acceptance testing computerized radiation therapy treatment planning systems: Direct utilization of CT scan data. *Medical Physics*, 12(2):237–242, 1985.
- [57] W. L. McLaughlin and M. F. Desrosiers. Dosimetry systems for radiation processing. *Radiation Physics and Chemistry*, 46(4-6, Part 2):1163 – 1174, 1995.
- [58] W. L. McLaughlin, J. M. Puhl, M. Al-Sheikhly, C. A. Christou, A. Miller, A. Kovács, L. Wojnarovits, and D. F. Lewis. Novel radiochromic films for clinical dosimetry. *Radiation Protection Dosimetry*, 66(1-4):263–268, 1996.
- [59] W. L. McLaughlin, C. G. Soares, J. A. Sayeg, E. C. McCullough, R. W. Kline, A. Wu, and A. H. Maitz. The use of a radiochromic detector for the determination of stereotactic radiosurgery dose characteristics. *Medical Physics*, 21(3):379–388, 1994.

- [60] W. L. McLaughlin, C. Yun-Dong, C. G. Soares, A. Miller, G. Van Dyk, and D. F. Lewis. Sensitometry of the response of a new radiochromic film dosimeter to gamma radiation and electron beams. *Nuclear Instruments and Methods in Physics Research Section A: Accelerators, Spectrometers, Detectors and Associated Equipment*, 302(1):165 – 176, 1991.
- [61] L. Menegotti, A. Delana, and A. Martignano. Radiochromic film dosimetry with flatbed scanners: A fast and accurate method for dose calibration and uniformity correction with single film exposure. *Medical Physics*, 35(7):3078–3085, 2008.
- [62] Canadian Organization of Medical Physicists. What is medical physics? <http://www.medphys.ca/>, 2009.
- [63] S. Pai, I. J. Das, J. F. Dempsey, K. L. Lam, T. J. LoSasso, A. J. Olch, J. R. Palta, L. E. Reinstein, D. Ritt, and E. E. Wilcox. Tg-69: Radiographic film for megavoltage beam dosimetry. *Medical Physics*, 34(6):2228–2258, 2007.
- [64] S. Pai, L. E. Reinstein, G. Gluckman, Z. Xu, and T. Weiss. The use of improved radiochromic film for in vivo quality assurance of high dose rate brachytherapy. *Medical Physics*, 25(7):1217–1221, 1998.
- [65] E. B. Podgorsak. Radiation oncology physics: A handbook for teachers and students. Technical report, International Atomic Energy Agency, Vienna, 2005.
- [66] E. B. Podgorsak. *Radiation Physics for Medical Physicists*. Springer-Verlag, Berlin, 1st edition, 2006.
- [67] E. Poon, B. Reniers, S. Devic, T. Vuong, and F. Verhaegen. Dosimetric characterization of a novel intracavitary mold applicator for ^{192}Ir high dose rate endorectal brachytherapy treatment. *Medical Physics*, 33(12):4515–4526, 2006.
- [68] International Specialty Products. Gafchromic EBT self-developing film for radiotherapy dosimetry. Technical report, International Specialty Products, Wayne, NJ, 2007.
- [69] International Specialty Products. Gafchromic EBT-2 self-developing film for radiotherapy dosimetry. Technical report, International Specialty Products, Wayne, NJ, 2009.

- [70] International Specialty Products. Gafchromic HD-810 radiochromic dosimetry film and D-200 pre-formatted dosimeters for high-energy photons: Configuration, specifications and performance data. Technical report, International Specialty Products, Wayne, NJ, 2010.
- [71] International Specialty Products. Gafchromic MD-55 radiochromic dosimetry film for high-energy photons: Configuration, specifications and performance data. Technical report, International Specialty Products, Wayne, NJ, 2010.
- [72] International Specialty Products. ISP website. <http://www.gafchromic.com/>, 2010.
- [73] O. Rampado, E. Garelli, and R. Ropolo. Computed tomography dose measurements with radiochromic films and a flatbed scanner. *Medical Physics*, 37(1):189–196, 2010.
- [74] L. Richley, A. C. John, H. Coomber, and S. Fletcher. Evaluation and optimization of the new EBT2 radiochromic film dosimetry system for patient dose verification in radiotherapy. *Physics in Medicine and Biology*, 55(9):2601, 2010.
- [75] A. Rink, D. F. Lewis, S. Varma, I. A. Vitkin, and D. A. Jaffray. Temperature and hydration effects on absorbance spectra and radiation sensitivity of a radiochromic medium. *Medical Physics*, 35(10):4545–4555, 2008.
- [76] A. Rink, I. A. Vitkin, and D. A. Jaffray. Energy dependence (75 kVp to 18 MV) of radiochromic films assessed using a real-time optical dosimeter. *Medical Physics*, 34(2):458–463, 2007.
- [77] S. Saur and J. Frengen. Gafchromic EBT film dosimetry with flatbed CCD scanner: A novel background correction method and full dose uncertainty analysis. *Medical Physics*, 35(7):3094–3101, 2008.
- [78] M. C. Saylor, T. T. Tamargo, W. L. McLaughlin, H. M. Khan, and D. F. Lewis. A thin film recording medium for use in food irradiation. *Radiation Physics and Chemistry*, 31:529 – 536, 1988.
- [79] C. G. Soares. Calibration of ophthalmic applicators at NIST: A revised approach. *Medical Physics*, 18(4):787–793, 1991.

- [80] C. G. Soares, S. Trichter, and S. Devic. AAPM Summer School 2009 chapter 23: Radiochromic film. Technical report, American Association of Physicists in Medicine, College Park, MD, 2009.
- [81] M. A. Stevens, J. R. Turner, R. P. Hugtenburg, and P. H. Butler. High-resolution dosimetry using radiochromic film and a document scanner. *Physics in Medicine and Biology*, 41(11):2357, 1996.
- [82] E. Sturtewagen, M. Fub, L. Paelinck, C. De Wagter, and D. Georg. Multi-dimensional dosimetric verification of stereotactic radiotherapy for uveal melanoma using radiochromic EBT film. *Zeitschrift fr Medizinische Physik*, 18(1):27 – 36, 2008.
- [83] F. Su, Y. Liu, S. Stathakis, C. Shi, C. Esquivel, and N. Papanikolaou. Dosimetry characteristics of Gafchromic EBT film responding to therapeutic electron beams. *Applied Radiation and Isotopes*, 65(10):1187 – 1192, 2007.
- [84] F. Su, C. Shi, and N. Papanikolaou. Clinical application of Gafchromic EBT film for in vivo dose measurements of total body irradiation radiotherapy. *Applied Radiation and Isotopes*, 66(3):389 – 394, 2008.
- [85] N. Tomic, S. Devic, F. DeBlois, and J. Seuntjens. Reference radiochromic film dosimetry in kilovoltage photon beams during CBCT image acquisition. *Medical Physics*, 37(3):1083–1092, 2010.
- [86] N. Tomic, M. Gosselin, J. F. Wan, U. Saragovi, E. B. Podgorsak, M. Evans, and S. Devic. Verification of cell irradiation dose deposition using a radiochromic film. *Physics in Medicine and Biology*, 52(11):3121, 2007.
- [87] F. Trichter and S. Trichter. TH-C-T-6E-03: CORVUS IMRT film dosimetry using novel Gafchromic EBT film. *Medical Physics*, 32(6):2167–2167, 2005.
- [88] S. M. Vatnitsky. Radiochromic film dosimetry for clinical proton beams. *Applied Radiation and Isotopes*, 48(5):643 – 651, 1997.
- [89] E. Wilcox, G. Daskalov, and L. Nedialkova. Comparison of the Epson Expression 1680 flatbed and the Vidar VXR-16 Dosimetry PRO film scanners for use in IMRT dosimetry using Gafchromic and radiographic film. *Medical Physics*, 34(1):41–48, 2007.

- [90] E. E. Wilcox and G. M. Daskalov. Evaluation of Gafchromic EBT film for CyberKnife dosimetry. *Medical Physics*, 34(6):1967–1974, 2007.
- [91] E. E. Wilcox and G. M. Daskalov. Accuracy of dose measurements and calculations within and beyond heterogeneous tissues for 6 mv photon fields smaller than 4 cm produced by cyberknife. *Medical Physics*, 35(6):2259–2266, 2008.
- [92] L. Xu, M. McEwen, C. Cojocar, and B. Faddegon. SU-FF-T-443: Measurement of lateral dose distributions using Gafchromic EBT films and PTW Starcheck 2-D Array. volume 36, pages 2624–2624. AAPM, 2009.
- [93] O. A. Zeidan, S. A. L. Stephenson, S. L. Meeks, T. H. Wagner, T. R. Willoughby, P. A. Kupelian, and K. M. Langen. Characterization and use of EBT radiochromic film for IMRT dose verification. *Medical Physics*, 33(11):4064–4072, 2006.
- [94] L. Zhao and I. J. Das. Gafchromic EBT film dosimetry in proton beams. *Physics in Medicine and Biology*, 55(10):N291, 2010.
- [95] X. R. Zhu, S. Yoo, P. A. Jursinic, D. F. Grimm, F. Lopez, J. J. Rownd, and M. T. Gillin. Characteristics of sensitometric curves of radiographic films. *Medical Physics*, 30(5):912–919, 2003.
- [96] Y. Zhu, A. S. Kirov, V. Mishra, A. S. Meigooni, and J. F. Williamson. Quantitative evaluation of radiochromic film response for two-dimensional dosimetry. *Medical Physics*, 24(2):223–231, 1997.